Appendix H

Modeling Attainment Demonstration

2016 PLAN FOR THE 2008 8-HOUR OZONE STANDARD

Appendix H: Modeling Attainment Demonstration

[This Appendix is provided by the California Air Resources Board]

MODELING ATTAINMENT DEMONSTRATION

Photochemical Modeling for the 8-Hour Ozone State Implementation Plan in the San Joaquin Valley

Prepared by

California Air Resources Board
San Joaquin Valley Air Pollution Control District

Prepared for

United States Environmental Protection Agency Region IX

May 2, 2016

TABLE OF CONTENTS

LIST OF FIGURES

LIST OF TABLES

ACRONYMS

ARB – Air Resources Board

BCs – Boundary Conditions

CMAQ Model – Community Multi-scale Air Quality Model

CSJV – Central San Joaquin Valley

DV – Design Value

GEOS -5 – Goddard Earth Observing System Model, Version 5

GMAO – Global Modeling and Assimilation Office

ICs – Initial Conditions

MOZART – Model for Ozone and Related chemical Tracers

MDA8 – Maximum Daily Average 8-hour Ozone

NASA – National Aeronautics and Space Administration

NARR - North American Regional Reanalysis

NCAR – National Center for Atmospheric Research

NOAA - National Oceanic and Atmospheric Administration

NSJV – Northern San Joaquin Valley

NO_x – Oxides of nitrogen

OFP - Ozone Forming Potential

ROG – Reactive Organic Gases

RH – Relative Humidity

RRF – Relative Response Factor

SAPRC – Statewide Air Pollution Research Center

SIP – State Implementation Plan

SJV – San Joaquin Valley

SJVAB – San Joaquin Valley Air Basin (SJVAB)

SJVAPCD – San Joaquin Valley Air Pollution Control District

SSJV – Southern San Joaquin Valley

U.S. EPA – United States Environmental Protection Agency

VOCs – Volatile Organic Compounds

WRF Model – Weather and Research Forecast Model

1. INTRODUCTION

The purpose of this document is to summarize the findings of the model attainment demonstration for the 0.075 ppm (or 75 ppb) 8-hour ozone standard in the San Joaquin Valley nonattainment area (SJV or the Valley), which forms the scientific basis for the SJV 2016 8-hour ozone SIP. The 75 ppb standard was promulgated by the U.S. EPA in 2008 and became effective in 2010. Currently, the Valley is designated as an extreme ozone nonattainment area for this standard and is mandated to demonstrate attainment of the standard by 2031.

Findings from the model attainment demonstration are summarized in terms of three sub-regions: 1) Northern SJV (San Joaquin, Stanislaus and Merced counties), 2) Central SJV (Madera, Fresno and King counties), and 3) Southern SJV (Tulare and Western Kern counties). These three sub-regions are characterized by distinct features in terms of geography, meteorology, and air quality. The general approach utilized in the attainment demonstration is described in Section 2, while the remaining sections discuss the meteorological modeling (Section 3), the emissions inventory (Section 4), and the photochemical modeling and results (Sections 5 and 6). A more detailed description of the modeling and development of the model-ready emissions inventory is presented in the Photochemical Modeling Protocol Appendix.

2. APPROACH

This section describes the Air Resources Board's (ARB's) procedures, based on U.S. EPA guidance (U.S. EPA, 2014[1]), for projecting ozone Design Values (DVs) to the future using model output and a Relative Response Factor (RRF) approach in order to show future year 2031 attainment of the 0.075 ppm 8-hour ozone standard.

2.1. METHODOLOGY

The U.S. EPA modeling guidance (U.S. EPA, 2014[1]) outlines the approach for utilizing models to predict future attainment of the 0.075 ppm 8-hour ozone standard. Consistent with the previous modeling guidance (U.S. EPA, 2007[2]), which was utilized in the 2007 SIP for the 0.08 ppm 8-hour ozone standard and informed the methodology used in the 2013 SIP for the 0.12 ppm 1-hour ozone standard, the current guidance recommends utilizing modeling in a relative sense. A brief summary of how models are

[1] U.S. EPA, 2014, Draft Modeling Guidance for Demonstrating Attainment of Air Quality Goals for Ozone, PM2.5 and Regional Haze, available at https://www.epa.gov/ttn/scram/guidance/guide/Draft_O3-PM-RH_Modeling_Guidance-2014.pdf

[2] U.S. EPA, 2007. Guidance on the Use of Models and Other Analyses for Demonstrating Attainment of Air Quality Goals for Ozone, $PM_{2.5}$, and Regional Haze. EPA-454/B07-002, 2007, available at. https://www.epa.gov/ttn/scram/guidance/guide/final-03-pm-rh-guidance.pdf

applied in the attainment demonstration, as prescribed by U.S. EPA modeling guidance (U.S. EPA, 2014[1]), is provided below. A more detailed description of the methodology in this and subsequent sections is provided in the Photochemical Modeling Protocol Appendix.

2.2. MODELING PERIOD

Based on analysis of the conduciveness of recent years' meteorological conditions leading to elevated ozone, as well as the availability of the most detailed emissions inventory, the year 2012 was selected for both baseline modeling and design value calculation in the model attainment test. These baseline design value mixing ratios serve as the anchor point for estimating future year projected design values.
The extreme nonattainment designation for the SJV requires that attainment of the 2008 8-hour ozone standard be demonstrated by 2031. Therefore, 2031 was the future year modeled in this attainment demonstration.

The revised U.S. EPA modeling guidance requires the model attainment demonstration to utilize the top ten modeled days when projecting design values to the future. Peak ozone mixing ratios for a given year at any monitor within the Valley generally occur between June and September. Therefore, the entire ozone season (May – September) was modeled for 2012 and 2031 to ensure that all of the top ozone days were simulated.

2.3. BASELINE DESIGN VALUES

Specifying the baseline design value is a key consideration in the model attainment test, since this value is projected forward and used to test for future attainment at each site. The starting point for the attainment demonstration is with the observational based design value (DV), which represents the three-year average of the annual 4th highest 8-hour ozone mixing ratio observed at a specific monitor for the year in consideration. For example, a DV for 2012 would represent the average of the 4th highest 8-hour ozone mixing ratio from 2010, 2011, and 2012.

The U.S. EPA recommends using an average of three DVs that straddle the baseline year in order to better account for the year-to-year variability inherent in meteorology. Since 2012 was chosen as the base year for projecting DVs to the future, site-specific DVs were calculated for the three three-year periods ending in 2012, 2013, and 2014 and then these three DVs were averaged. This average DV is called a weighted DV (in

[1] U.S. EPA, 2014, Draft Modeling Guidance for Demonstrating Attainment of Air Quality Goals for Ozone, PM2.5 and Regional Haze, available at https://www.epa.gov/ttn/scram/guidance/guide/Draft_O3-PM-RH_Modeling_Guidance-2014.pdf

the context of this SIP, the weighted DV will also be referred to as the reference year DV or DV_R). Table 1 illustrates the observational data from each year that goes into the average DV is calculated.

Table 1. Illustrates the data from each year that are utilized in the Design Value calculation for a specific year (DV Year), and the yearly weighting of data for the average Design Value calculation (or DV_R).

DV Year	Years Averaged for the Design Value (4th highest observed 8-hr O_3)				
2012	2010	2011	2012		
2013		2011	2012	2013	
2014			2012	2013	2014
Yearly Weightings for the Average Design Value Calculation					
2012-2014 Average	$DV_R = \frac{8hrO3_{2010} + (2)8hrO3_{2011} + (3)8hrO3_{2012} + (2)8hrO3_{2013} + 8hrO3_{2014}}{9}$				

Table 2 lists the design values for the sites within the three major sub regions of the Valley that are used in the model attainment demonstration. Note that the DVs are listed in descending order for sites within each subregion. The Clovis monitoring site (highlighted in yellow), and located in Fresno county within the Central SJV, is the Valley's design site (i.e. site with the highest average DV in the SJV non-attainment area) with an average DV of 95.7 ppb. All remaining sites, excluding the Stockton-Hazelton monitor in the Northern SJV, have average DVs that exceed the 75 ppb standard.

Table 2. Year-specific 8-hr ozone design values for 2012, 2013, and 2014, and the average baseline design value (represented as the average of the three year-specific design values) for the monitoring sites located in the SJV.

County	Monitoring Site	8-hr Ozone Design Value (ppb)			
		2012	2013	2014	2012-2014 Average
Northern SJV					
Stanislaus	***Turlock-S Minaret Street***	***88***	***86***	***84***	***86.0***
Merced	Merced-S Coffee Avenue	83	81	81	81.7
San Joaquin	Tracy-Airport	80	79	79	79.3
Stanislaus	Modesto-14th Street	75	75	78	76.0
San Joaquin	Stockton-Hazelton Street	69	67	69	68.3
Central SJV					
Fresno	***Clovis-N Villa Avenue***	***98***	***94***	***95***	***95.7***
Fresno	Fresno-Drummond Street	95	94	88	92.3
Fresno	Parlier	92	92	92	92.0
Fresno	Fresno-Garland	94	89	89	90.7
Fresno	Fresno-Sierra Skypark #2	92	88	87	89.0
Kings	Hanford-S Irwin Street	90	84	84	86.0
Madera	Madera-28261 Avenue 14	86	84	84	84.7
Madera	Madera-Pump Yard	78	79	81	79.3
Fresno	Tranquility	77	77	75	76.3
Southern SJV					
Tulare	***Sequoia and Kings Canyon Natl Park***	***95***	***93***	***91***	***93.0***
Kern	Arvin-Di Giorgio	91	89	88	89.3
Kern	Edison	93	86	84	87.7
Kern	Bakersfield-5558 California Avenue	89	86	85	86.7
Tulare	Porterville-1839 Newcomb Street	90	88	81	86.3
Kern	Oildale-3311 Manor Street	89	84	81	84.7
Tulare	Sequoia Natl Park-Lower Kaweah	81	85	86	84.0
Kern	Maricopa-Stanislaus Street	87	84	79	83.3
Kern	Shafter-Walker Street	86	82	81	83.0
Tulare	Visalia-N Church Street	87	80	80	82.3

2.4. BASE, REFERENCE, AND FUTURE YEARS

The model attainment demonstration consists of the following three primary model simulations, which all utilized the same model inputs, including meteorology, chemical boundary conditions, and biogenic emissions. The only difference between the simulations was in the year represented by the anthropogenic emissions (2012 or 2031) and certain day-specific emissions.

1. Base Year (or Base Case) Simulation

The base year simulation for 2012 was used to assess model performance and includes as much day-specific detail as possible in the emissions inventory such as hourly adjustments to the motor vehicle and biogenic inventories based on observed local meteorological conditions, known wildfire and agricultural burning events, and exceptional events like the Chevron refinery fire in the Bay Area, which occurred over 6 days from August 19-24, 2012.

2. Reference (or Baseline) Year Simulation

The reference year simulation was identical to the base year simulation, except that certain emissions events which are either random and/or cannot be projected to the future were removed from the emissions inventory. For the 2012 reference year modeling there are two categories/emissions sources that were excluded: 1) wildfires, which are difficult to predict in the future and can influence the model response to anthropogenic emissions reductions in regions with large fires, and 2) the Chevron refinery fire mentioned above.

3. Future Year Simulation

The future year simulation is identical to the reference year simulation, except that projected future year (2031) anthropogenic emission levels were used rather than the 2012 emission levels. All other model inputs (e.g., meteorology, chemical boundary conditions, biogenic emissions, and calendar for day-of-week specifications in the inventory) are the same as those used in the reference year simulation.

To summarize (Table 3), the base year 2012 simulation was used for evaluating model performance, while the reference (or baseline) 2012 and future year 2031 simulations were used to project the average DVs to the future as described in the Photochemical Modeling Protocol Appendix and in subsequent sections of this document.

Table 3. Description of CMAQ model simulations.

Simulation	Anthropogenic Emissions	Biogenic Emissions	Meteorology	Chemical Boundary Conditions
Base year (2012)	2012 w/ wildfires and Chevron refinery fire	2012 MEGAN	2012 WRF	2012 MOZART
Reference year (2012)	2012 w/o wildfires and w/o Chevron refinery fire	2012 MEGAN	2012 WRF	2012 MOZART
Future year (2031)	2031 w/o wildfires and w/o Chevron refinery fire	2012 MEGAN	2012 WRF	2012 MOZART

2.5. RELATIVE RESPONSE FACTORS

As part of the model attainment demonstration, the fractional changes in ozone mixing ratios between the model future year and model reference year were calculated at each of the monitors. These ratios, called "relative response factors" (RRFs), were calculated based on the ratio of future year modeled maximum daily average 8-hour (MDA8) ozone to modeled reference year MDA8 ozone (Equation 1).

$$\mathrm{RRF} = \frac{\text{average MDA8 ozone}_{\text{future}}}{\text{average MDA8 ozone}_{\text{reference}}} \quad (1)$$

The MDA8 values, used in calculating the RRF, were based on the maximum simulated ozone within a 3x3 array of cells with the grid cells containing the monitor located at the center of the array (U.S. EPA, 2014). The future and reference year ozone values used in the RRF calculations were paired in space and time (i.e., using the future year MDA8 ozone for the same modeled day and at the same grid cell where the MDA8 ozone for the reference year is located within the 3x3 array of cells).

The modeled days utilized in the RRF calculation were selected based on the following U.S. EPA recommended criteria (U.S EPA, 2014).

- Begin with days that have simulated baseline MDA8 >= 60 ppb and calculate RRFs based on the top 10 high ozone days.

- If there are fewer than 10 days with MDA8 >= 60 ppb then all days >= 60 ppb are used in the RRF calculation, as long as there are at least 5 days used in the calculation.
- If there are fewer than 5 days >= 60 ppb, an RRF is not calculated at that monitor.
- Restrict the simulated days used in the RRF calculation by only including days with reference MDA8 within +/- 20% of the observed value at the monitor. This ensures that only modeled days which are consistent with the observed ozone levels are used in the RRF calculation.

2.6. FUTURE YEAR DESIGN VALUE CALCULATION

Future year design values for each site were calculated by multiplying the corresponding baseline design value (Table 2) by the site-specific RRF (Equation 2).

$$\mathrm{DV_F} = \mathrm{DV_R} \times \mathrm{RRF} \quad (2)$$

where,

DV_F = the future year design value,
DV_R = the reference year design value (from Table 2), and
RRF = the site specific RRF from Equation 1

Future year design values from the model attainment demonstration are discussed in Section 5.3.

3. METEOROLOGICAL MODELING

California's proximity to the ocean, complex terrain, and diverse climate represent a unique challenge for developing meteorological fields that adequately represent the synoptic and mesoscale features of the regional meteorology. In summertime, the majority of the storm tracks are far away to the north of the state and a semi-permanent Pacific high typically sits off the California coast. Interactions between this eastern Pacific subtropical high pressure system and the thermal low pressure further inland over Central Valley or South Coast lead to conditions conducive to pollution buildup (Fosberg and Schroeder, 1966[1]; Bao et al., 2008[2]).

[1] Fosberg, M.A., Schroeder, M.J., Marine air penetration in Central California, Journal of Applied Meteorology, 5, 573-589, 1966.

[2] Bao, J.W., Michelson, S.A., Persson, P.O.G., Djalalova, I.V., Wilczak, J.M., Observed and WRF-simulated low-level winds in a high-ozone episode during the Central California ozone study, Journal of Applied Meteorology and Climatology, 47, 2372-2394, 2008.

In the past, the ARB has utilized both prognostic and diagnostic meteorological models, as well as hybrid approaches in an effort to develop meteorological fields for use in air quality modeling that most accurately represent the meteorological processes that are important to air quality (e.g., Jackson et al., 2006[1]). In this work, the state-of-the-science Weather and Research Forecasting (WRF) prognostic model (Skamarock et al., 2005[2]) version 3.6 was utilized to develop the meteorological fields used in the subsequent photochemical model simulations.

3.1. WRF MODEL SETUP

The WRF meteorological modeling domain consisted of three nested Lambert projection grids of 36-km (D01), 12-km (D02), and 4-km (D03) uniform horizontal grid spacing (Figure 1). WRF was run simultaneously for the three nested domains with two-way feedback between the parent and the nest grids. The D01 and D02 grids were used to resolve the larger scale synoptic weather systems, while the D03 grid resolved the finer details of the atmospheric conditions and was used to drive the air quality model simulations. All three domains utilized 30 vertical sigma layers (defined in Table 4), with the major physics options for each domain listed in Table 5.

Initial and boundary conditions (IC/BCs) for the WRF modeling were based on the 32-km horizontal resolution North American Regional Reanalysis (NARR) data that are archived at the National Center for Atmospheric Research (NCAR). Boundary conditions to WRF were updated at 6-hour intervals for the 36-km grid (D01). In addition, surface and upper air observations obtained from NCAR were used to further refine the analysis data that were used to generate the IC/BCs. Analysis nudging was employed in the outer 36-km grid (D01) to ensure that the simulated meteorological fields were constrained and did not deviate from the observed meteorology. No nudging was used on the two inner domains to allow model physics to work fully without externally imposed forcing (Rogers et al., 2013[3]).

---

[1] Jackson, B.S., Chau, D., Gurer, K., Kaduwela, A.: Comparison of ozone simulations using MM5 and CALMET/MM5 hybrid meteorological fields for the July/August 2000 CCOS episode, *Atmos. Environ.*, 40, 2812-2822, 2006.

[2] Skamarock, W. C., J. B. Klemp, J. Dudhia, D. O. Gill, D. M. Barker, W. Wang, and J. G. Powers, 2005: A description of the Advanced Research WRF Version 2. NCAR Tech Notes-468+STR

[3] Rogers, R.E., Deng, A., Stauffer, D. Gaudet, B.J., Jia, Y., Soong, S.-T., Tanrikulu, S., Application of the Weather Research and Forecasting model for air quality modeling in the San Francisco Bay area, Journal of Applied Meteorology and Climatology, 52, 1953-1973, 2013.

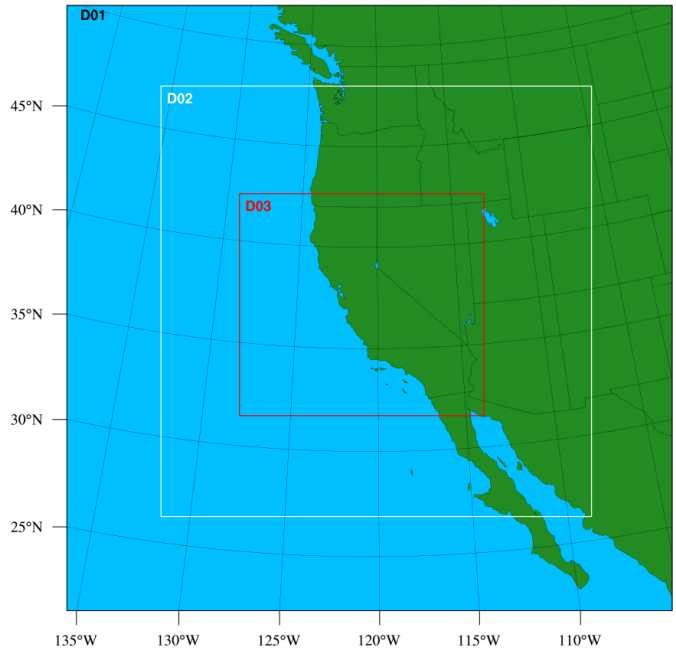

Figure 1. WRF modeling domains (D01 36km; D02 12km; and D03 4km).

Table 4. WRF vertical layer structure.

Layer Number	Height (m)	Layer Thickness (m)	Layer Number	Height (m)	Layer Thickness (m)
30	16082	1192	14	1859	334
29	14890	1134	13	1525	279
28	13756	1081	12	1246	233
27	12675	1032	11	1013	194
26	11643	996	10	819	162
25	10647	970	9	657	135
24	9677	959	8	522	113
23	8719	961	7	409	94
22	7757	978	6	315	79
21	6779	993	5	236	66
20	5786	967	4	170	55
19	4819	815	3	115	46
18	4004	685	2	69	38
17	3319	575	1	31	31
16	2744	482	0	0	0
15	2262	403			

Note: Shaded layers denote the subset of vertical layers used in the CMAQ photochemical model simulations.

Table 5. WRF Physics Options.

Physics Option	Domain		
	D01 (36 km)	D02 (12 km)	D03 (4 km)
Microphysics	WSM 6-class graupel scheme	WSM 6-class graupel scheme	WSM 6-class graupel scheme
Longwave radiation	RRTM	RRTM	RRTM
Shortwave radiation	Dudhia scheme	Dudhia scheme	Dudhia scheme
Surface layer	Revised MM5 Monin-Obukhov	Revised MM5 Monin-Obukhov	Revised MM5 Monin-Obukhov
Land surface	Pleim-Xiu LSM	Pleim-Xiu LSM	Pleim-Xiu LSM
Planetary Boundary Layer	YSU	YSU	YSU
Cumulus Parameterization	Kain-Fritsch scheme	Kain-Fritsch scheme	None

3.2. WRF MODEL RESULTS AND EVALUATION

Simulated surface wind speed, temperature, and relative humidity from the 4 km domain were validated against hourly observations at 55 surface stations in the SJV. Observational data for the surface stations were obtained from the ARB archived meteorological database (http://www.arb.ca.gov/aqmis2/aqmis2.php). Table 6 lists the monitoring stations and which parameters are measured at each station, including wind speed and direction (wind), temperature (T) and relative humidity (RH). The location of each of these sites is shown in Figure 2. Several quantitative performance metrics were used to compare hourly surface observations and modeled estimates: mean bias (MB), mean error (ME) and index of agreement (IOA) based on recommendations from Simon et al. (2012)[1]. A summary of these statistics by performance region is shown in Table 6. The distribution of hourly mean bias and mean error are shown in Figure 3. The spatial distributions of the mean bias and mean error of modeled surface wind, temperature and relatively humidity are shown in Figure 4, while observed vs. modeled scatter plots are shown in Figure 5.

[1] Simon, H., Baker, K. R., and Phillips, S.: Compilation and interpretation of photochemical model performance statistics published between 2006 and 2012, *Atmospheric Environment*, 61, 124-139, 2012.

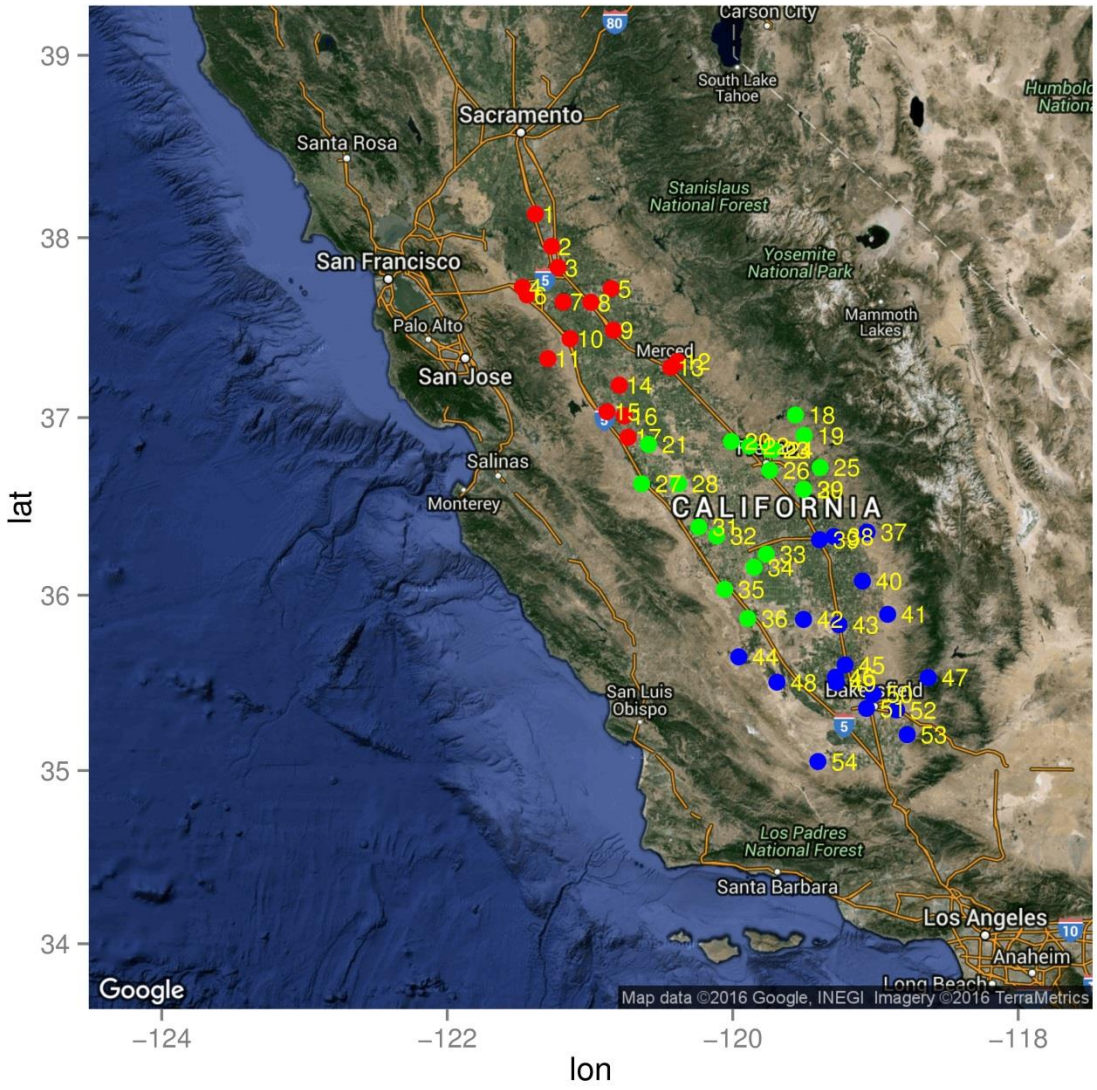

Figure 2. Meteorological monitoring sites in the San Joaquin Valley: red markers represent sites in the Northern SJV; green markers represent sites in the Central SJV, while blue markers represent sites in the Southern SJV. Refer to Table 6 for addition information on sites.

Table 6. Meteorological site location and parameter measured

Site	Site ID	Site Name	Region	Parameter observed
1	5809	Lodi West	NSJV	T, RH
2	2094	Stockton-Hazelton Street	NSJV	Wind, T, RH
3	5736	Manteca	NSJV	T, RH
4	5810	Tracy	NSJV	T, RH
5	5831	Oakdale #2	NSJV	T, RH
6	3696	Tracy-Airport	NSJV	Wind, T
7	5737	Modesto #3	NSJV	T, RH
8	2833	Modesto-14th Street	NSJV	Wind, T
9	2996	Turlock-S Minaret Street	NSJV	Wind, T
10	5805	Patterson #2	NSJV	T, RH
11	3526	Diablo Grande	NSJV	Wind, T, RH
12	5793	Merced	NSJV	T, RH
13	3022	Merced-S Coffee Avenue	NSJV	Wind, T
14	3647	San Luis National Wildlife Refuge	NSJV	Wind, T, RH
15	5752	Kesterson	NSJV	T, RH
16	5730	Los Banos #2	NSJV	T, RH
17	5770	Panoche	NSJV	T, RH
18	3522	Hurley 1	CSJV	T, RH
19	3346	Fancher Creek	CSJV	T, RH
20	3211	Madera-Pump Yard	CSJV	Wind, T, RH
21	5711	Firebaugh - Telles	CSJV	T, RH
22	2844	Fresno-Sierra Skypark #2	CSJV	Wind, T
23	5741	Fresno State #2	CSJV	T, RH
24	3026	Clovis-N Villa Avenue	CSJV	Wind, T, RH
25	5787	Orange Cove	CSJV	T, RH
26	2013	Fresno-Drummond Street	CSJV	Wind, T
27	3309	Panoche Road	CSJV	T, RH
28	5757	Westlands	CSJV	T, RH
29	5723	Parlier #2	CSJV	T, RH
30	2114	Parlier	CSJV	Wind, T, RH
31	5828	Five Points SW	CSJV	T, RH
32	5708	Five Points #2	CSJV	T, RH
33	3712	Santa Rosa Rancheria-17225 Jersey	CSJV	T
34	5715	Stratford #2	CSJV	T, RH
35	3330	Kettleman Hills	CSJV	T, RH
36	5717	Kettleman	CSJV	T, RH
37	5746	Lindcove	SSJV	T, RH
38	2032	Visalia-N Church Street	SSJV	Wind, T
39	3250	Visalia-Airport	SSJV	Wind, T, RH
40	5812	Porterville #3	SSJV	T, RH
41	3350	Fountain Springs	SSJV	Wind, T, RH
42	6813	Alpaugh	SSJV	T, RH
43	5823	Delano #2	SSJV	T, RH
44	5729	Blackwells Corner	SSJV	T, RH
45	5783	Famoso	SSJV	T, RH
46	5709	Shafter - USDA	SSJV	T, RH
47	5879	Democrat #2	SSJV	Wind, T, RH
48	5791	Belridge	SSJV	T, RH
49	2981	Shafter-Walker Street	SSJV	Wind, T, RH
50	2772	Oildale-3311 Manor Street	SSJV	Wind, T
51	3146	Bakersfield-5558 California Avenue	SSJV	Wind, T, RH
52	2312	Edison	SSJV	Wind, T
53	5771	Arvin-Edison	SSJV	T, RH
54	2919	Maricopa-Stanislaus Street	SSJV	Wind, T

Wind Speed biases are positive in each of the three regions, with the smallest bias occurring in Southern SJV (SSJV) (0.49 m/s) and the largest bias occurring in the Central SJV (CSJV) (0.65 m/s). Temperature bias is relatively small in the SSJV and Northern SJV (NSJV), -0.87 ˚K and -0.41 ˚K, respectively, and higher in the NSJV (0.41 ˚K). Temperature generally shows very good agreement between the observations and simulation in all regions with IOA values above 0.90. Relative humidity biases range from -3.87% to 12.99%, with the largest bias occurring in the SSJV. These results are comparable to other recent WRF modeling efforts in California investigating ozone formation in Central California (e.g., Hu et al., 2012[1]) and modeling analysis for the CalNex and CARES field studies (e.g., Fast et al., 2014[2]; Baker et al., 2013[3]; Kelly et al., 2014[4]; Angevine et al., 2012[5]). Detailed hourly time-series of surface temperature, relative humidity, wind speed, and wind direction for each sub-region can be found in the supplementary material.

[1] Hu, J., Howard, C. J., Mitloehner, F., Green, P. G., and Kleeman, M. J.: Mobile Source and Livestock Feed Contributions to Regional Ozone Formation in Central California, *Environmental Science & Technology*, 46, 2781-2789, 2012.

[2]Fast, J. D., Gustafson Jr, W. I., Berg, L. K., Shaw, W. J., Pekour, M., Shrivastava, M., Barnard, J. C., Ferrare, R. A., Hostetler, C. A., Hair, J. A., Erickson, M., Jobson, B. T., Flowers, B., Dubey, M. K., Springston, S., Pierce, R. B., Dolislager, L., Pederson, J., and Zaveri, R. A.: Transport and mixing patterns over Central California during the carbonaceous aerosol and radiative effects study (CARES), *Atmos. Chem. Phys.,* 12, 1759-1783, 2012, doi:10.5194/acp-12-1759-2012.

[3]Baker, K. R., Misenis, C., Obland, M. D., Ferrare, R. A., Scarino, A. J., and Kelly, J. T.: Evaluation of surface and upper air fine scale WRF meteorological modeling of the May and June 2010 CalNex period in California, *Atmos. Environ.*, 80, 299-309, 2013.

[4] Kelly, J. T., Baker, K. R., Nowak, J. B., Murphy, J. G., Milos, Z. M., VandenBoer, T. C., Ellis, R. A., Neuman, J. A., Weber, R. J., Roberts, J. M., Veres, P. R., de Gouw, J. A., Beaver, M. R., Newman, S., and Misenis, C.: Fine-scale simulation of ammonium and nitrate over the South Coast Air Basin and San Joaquin Valley of California during CalNex-2010, *J. Geophysical Research,* 119, 3600-3614, doi:10.1002/2013JD021290.

[5] Angevine, W. M., Eddington, L., Durkee, K., Fairall, C., Bianco, L., Brioude, J.: Meteorological model evaluation for CalNex 2010, *Monthly Weather Review*, 140, 3885-3906, 2012.

Table 7. Hourly surface wind speed, temperature and relative humidity statistics by region for May-September 2012.

Region	Observed Mean	Modeled Mean	Mean Bias	Mean Error	IOA
		Wind Speed (m/s)			
SSJV	1.87	2.36	0.49	0.99	0.64
CSJV	2.06	2.70	0.65	1.06	0.68
NSJV	2.42	3.05	0.64	1.24	0.71
		Temperature (˚K)			
SSJV	298.40	297.53	-0.87	2.91	0.90
CSJV	297.99	297.34	-0.65	2.78	0.91
NSJV	295.57	295.97	0.41	2.41	0.94
		Relative Humidity (%)			
SSJV	41.95	54.95	12.99	17.99	0.63
CSJV	39.63	49.80	10.17	16.85	0.60
NSJV	50.36	46.49	-3.86	12.35	0.79

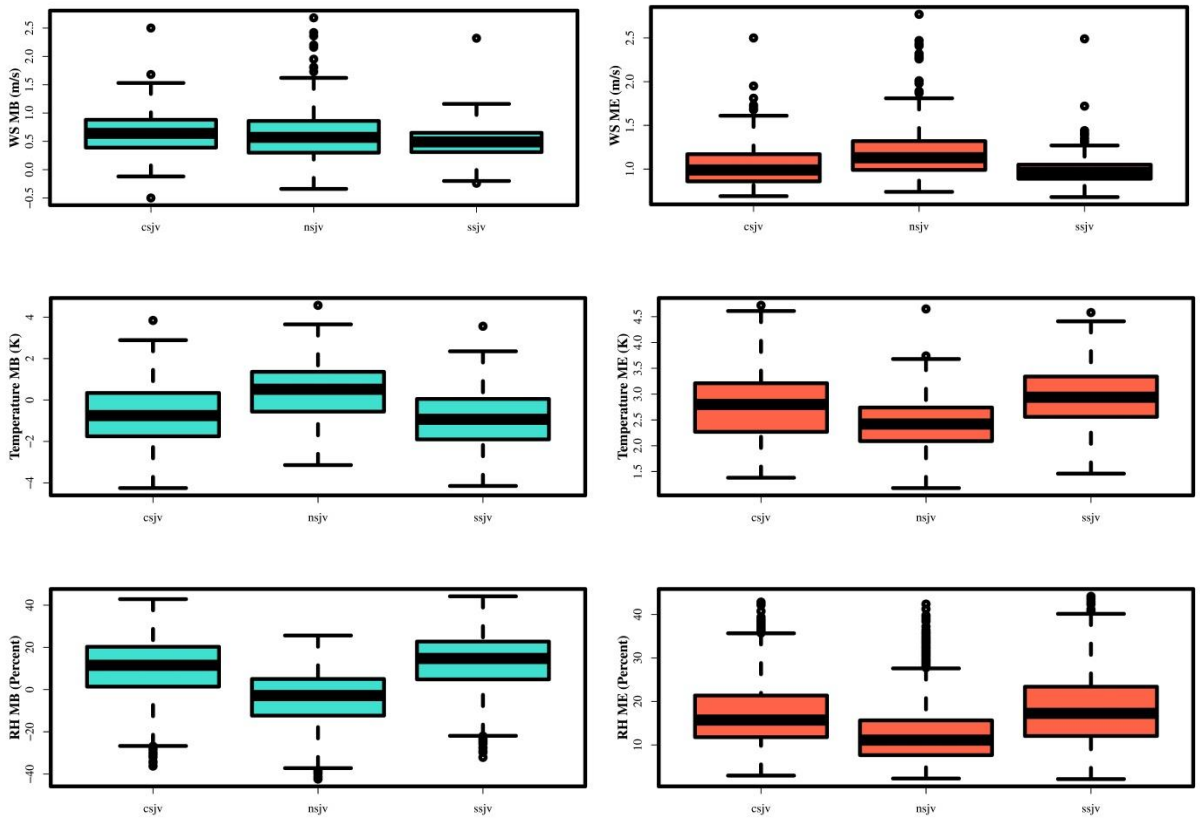

Figure 3. Distribution of hourly mean bias (left) and mean error (right) for May-September 2012. Results are shown for wind speed (top), temperature (middle), and Relative Humidity (bottom).

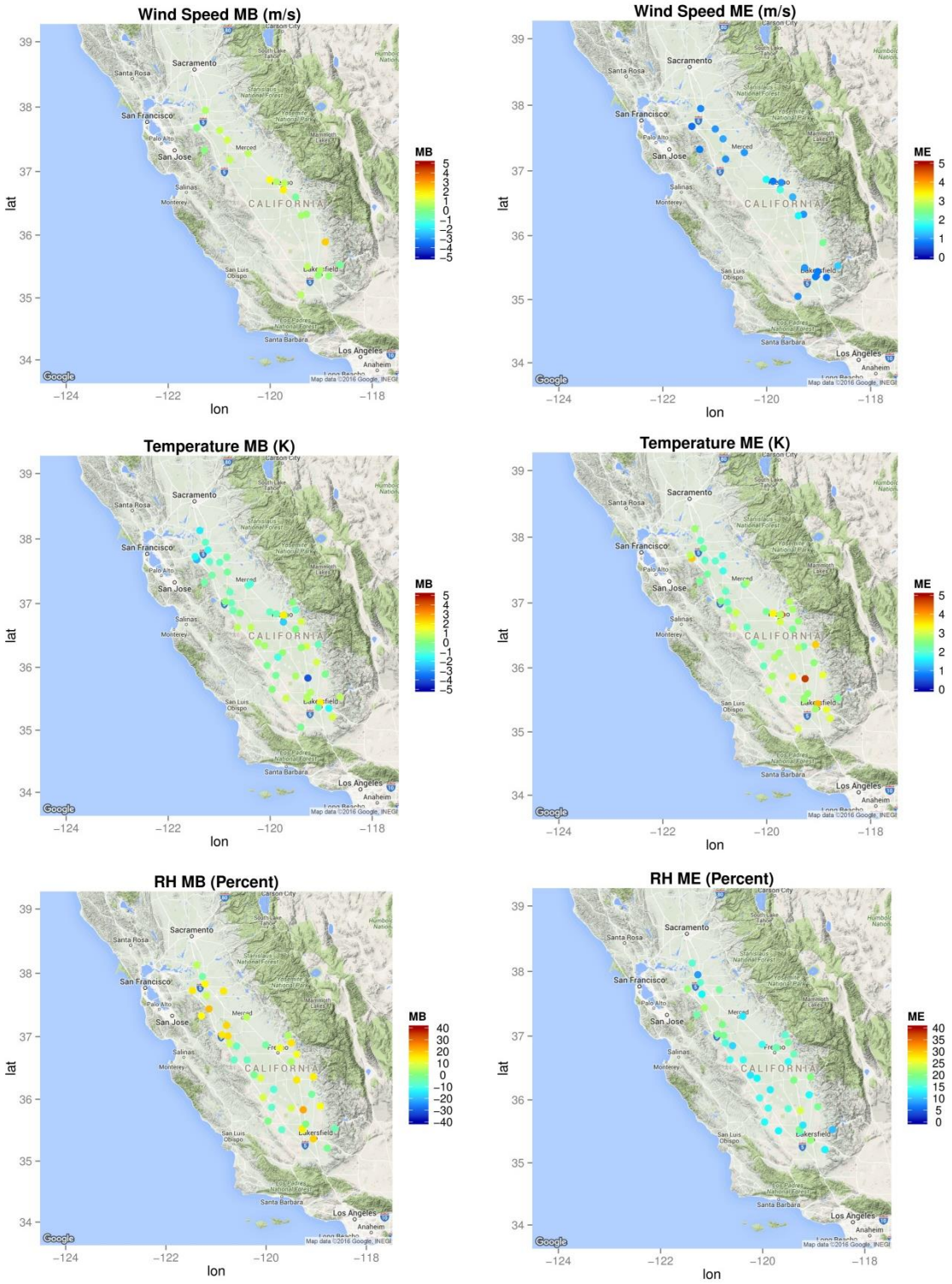

Figure 4. Spatial distribution of mean bias (left) and mean error (right) for May-September 2012. Results are shown for wind speed (top), temperature (middle), and Relative Humidity (bottom).

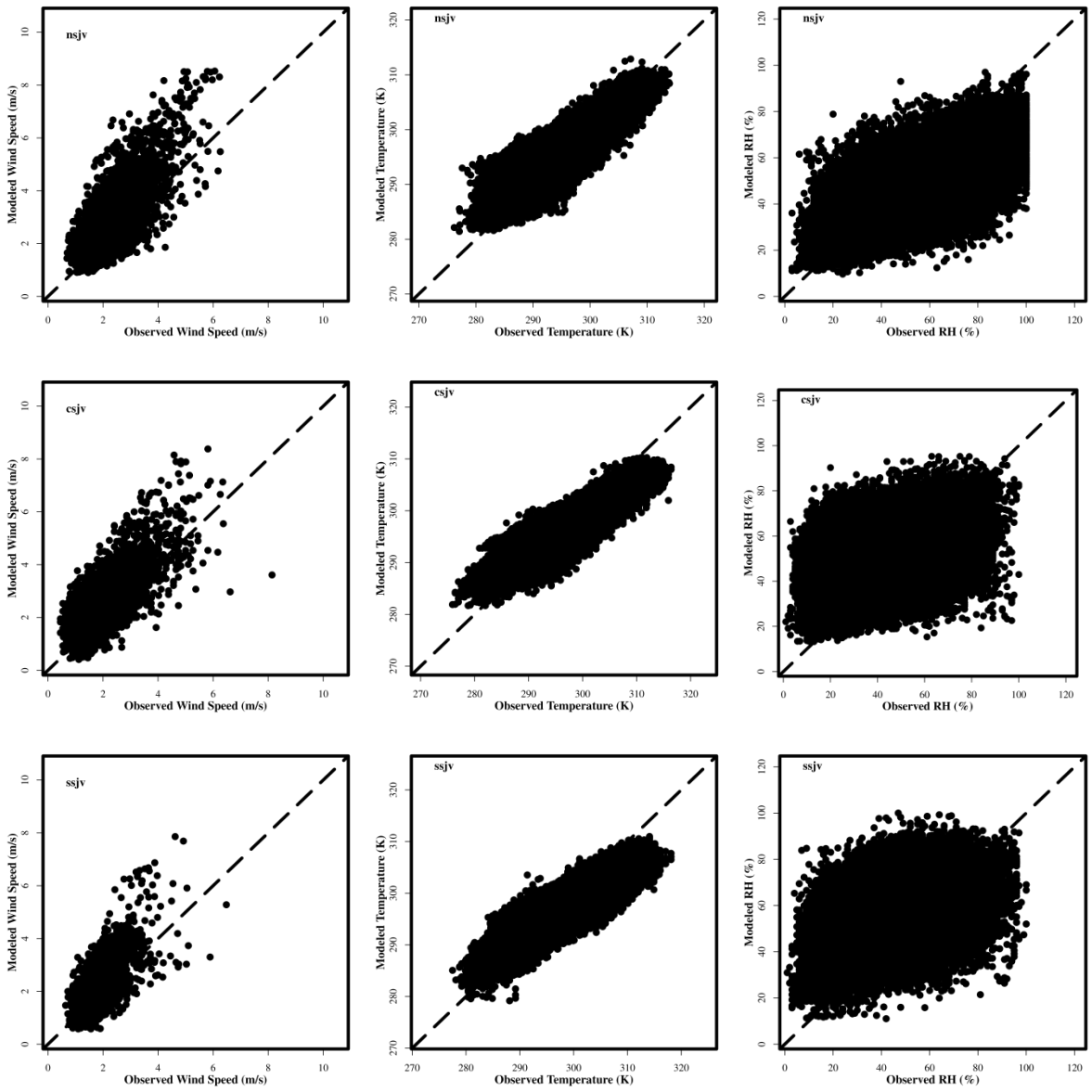

Figure 5. Comparison of modeled and observed hourly wind speed (left column), 2-meter temperature (middle column), and relative humidity (right column). Results for the Northern SJV are shown in the top row, Central SJV in the middle row, and Southern SJV in the bottom row.

3.2.1 PHENOMENOLOGICAL EVALUATION

Conducting a detailed phenomenological evaluation for all modeled days can be resource intensive given that the entire ozone season was modeled. However, some insight and confidence that the model is able to reproduce the meteorological conditions leading to elevated ozone can be gained by investigating the meteorological conditions during a period of peak ozone within the Valley in more detail. The highest-ozone-conducive meteorological conditions in the Valley occurred on or around July 10, 2012. Surface weather analysis shows the SJV was in between a high pressure center off the California coast and a large high pressure system over the areas spanning from the Rockies to the Midwest. The surface wind distributions (Figure 6, 7, 8) indicate the model was able to capture many of the important features of the meteorological fields in the SJV. The winds in the area of the San Joaquin delta split into flows going up towards the Sacramento Valley and down towards SJV. The westerly winds also penetrated into SJV via Pacheco pass. However, wind direction over Tehachapi pass varies, depending on the relative strength of the valley floor winds and the slope winds over the Tehachapi Mountains. The up-slope (Figure 7) and down-slope wind (Figure 8) changes are well reproduced in the model, both over the eastern slope of the Coastal Ranges and western slope of the Sierra.

4. EMISSIONS

The emissions inventory used in this modeling was based on the most recent inventory submitted to the U.S. EPA, with base year 2012 (http://www.arb.ca.gov/planning/sip/2012iv/2012iv.htm). For a detailed description of the emissions inventory, updates to the inventory, and how it was processed from the planning totals to a gridded inventory for modeling, see Modeling Emissions Inventory Appendix.

4.1 EMISSIONS SUMMARIES

Table 7 summarizes the 2012 and 2031 SJV anthropogenic emissions used in this work. Overall, anthropogenic NO_x was projected to decrease by ~60% between 2012 and 2031 from 339.5 tpd to 131.9 tpd. In contrast, anthropogenic ROG was projected to decrease by ~12% from 337.2 tpd to 296.7 tpd. Monthly biogenic ROG totals for 2012 within the Valley are shown in Figure 9 (note that the same biogenic emissions were used in 2012 and 2031 modeling). Throughout the summer, biogenic ROG emission ranged from ~800 tpd in September to nearly 1600 tpd in July and August, with the difference in emissions primarily due to differences in temperature and leaf area from month-to-month.

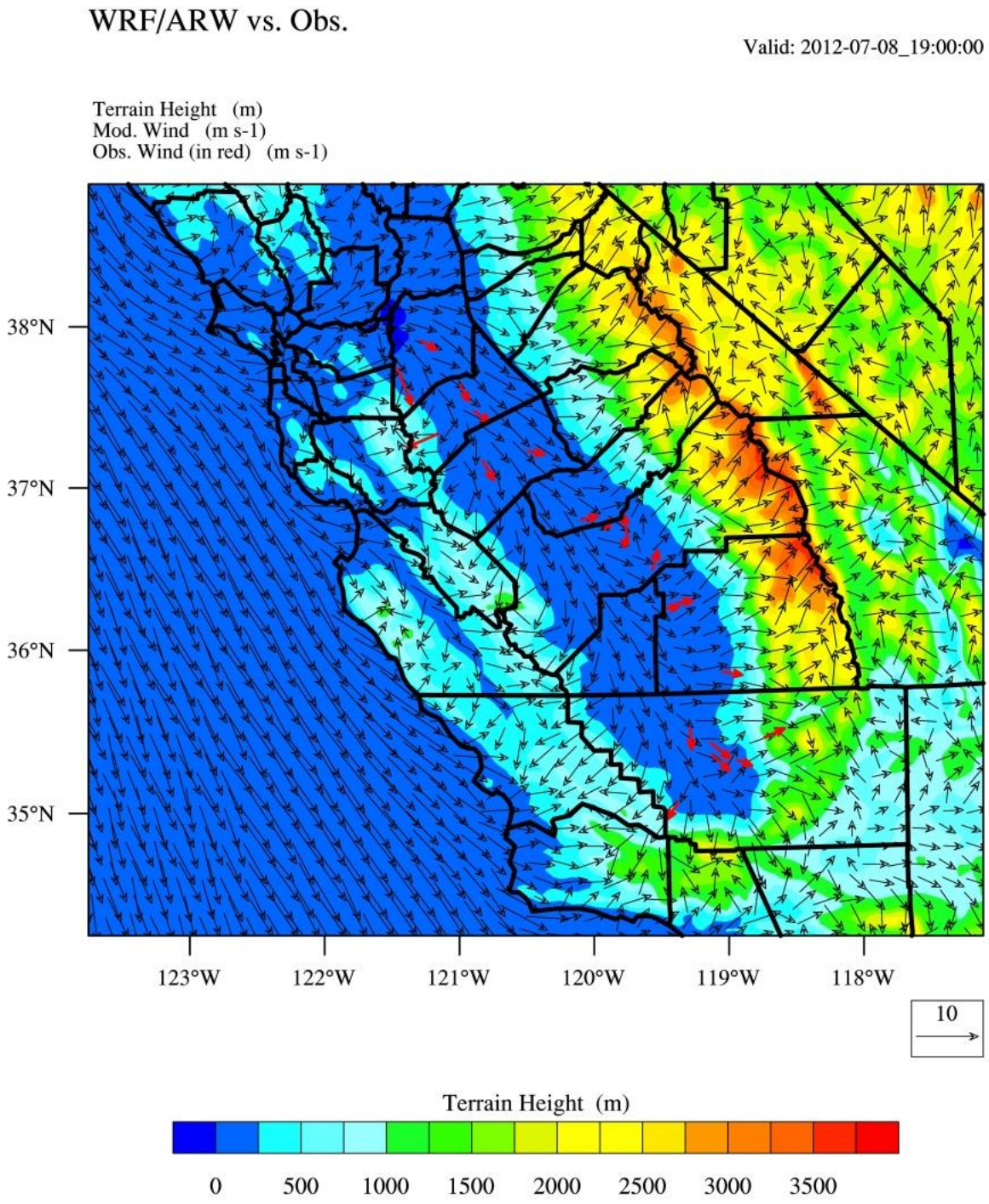

Figure 6. Surface wind field at 11:00 PST July 08, 2012.

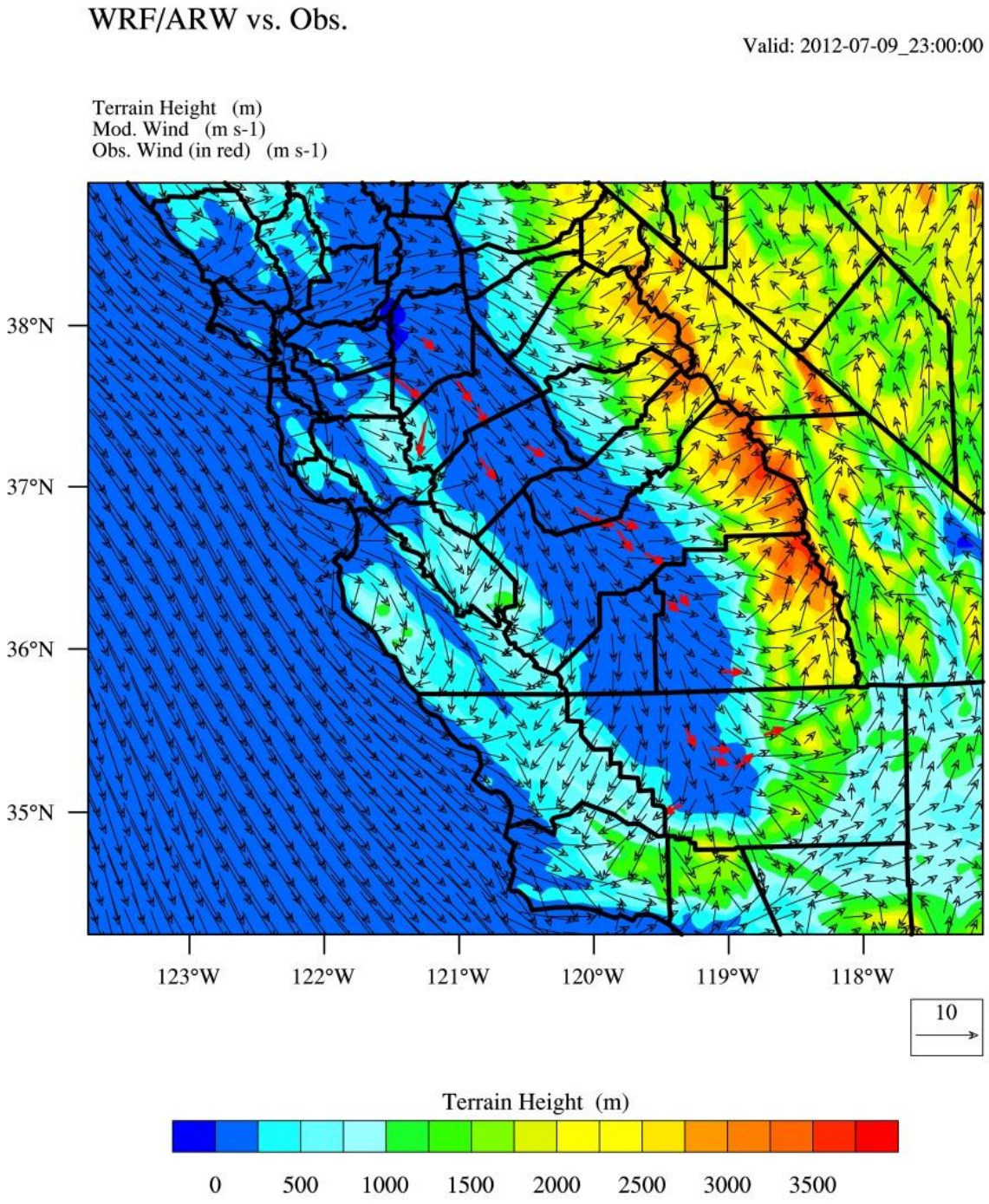

Figure 7. Surface wind field at 15:00 PST July 09, 2012.

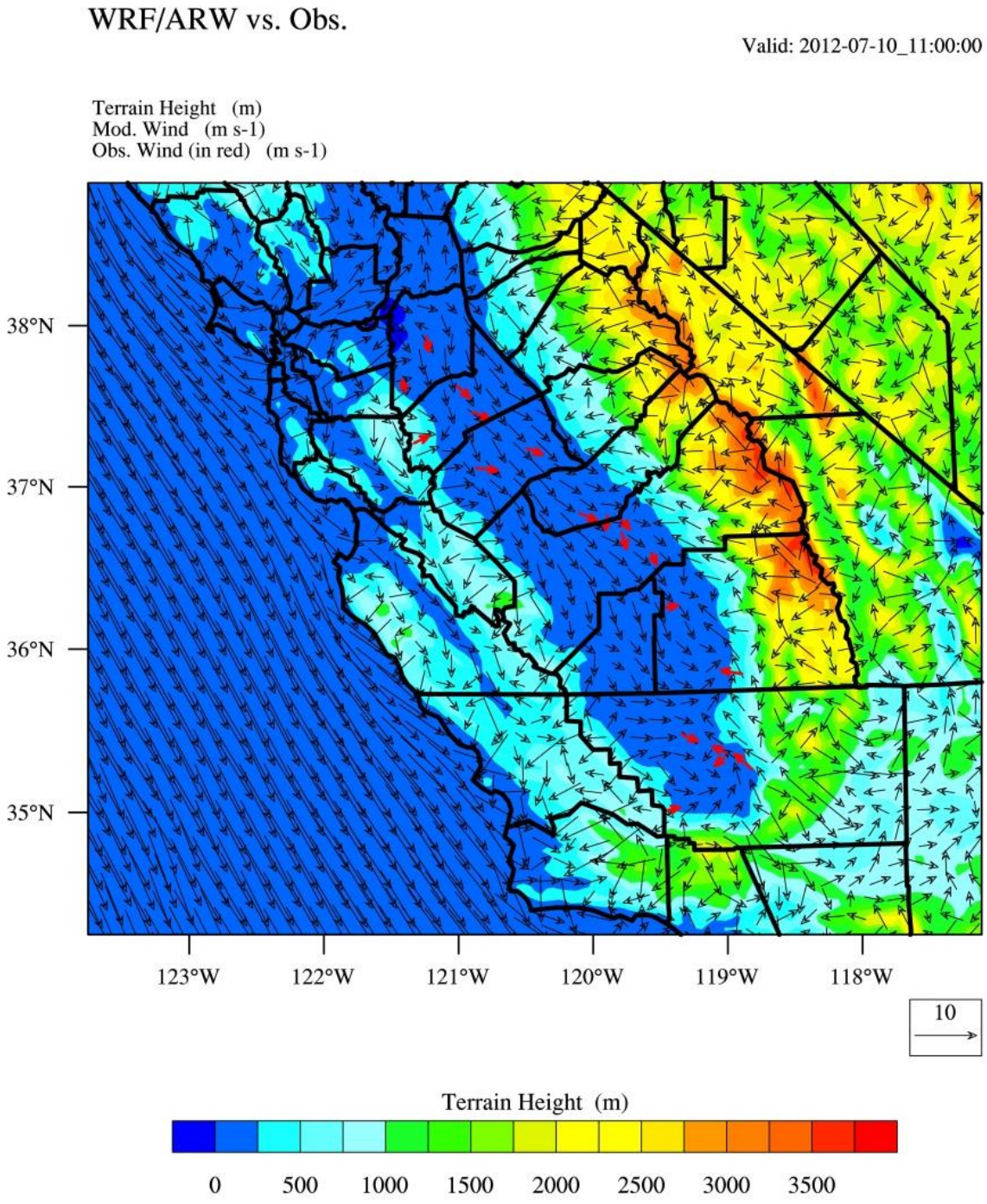

Figure 8. Surface wind field at 03:00 PST July 10, 2012.

Table 8. SJV Summer Planning Emissions for 2012 and 2031 (tons/day).

Source Category	2012		2031	
	NO_x [tons/day]	ROG [tons/day]	NO_x [tons/day]	ROG [tons/day]
Stationary	42.4	85.3	29.5	100.0
Area	4.7	147.0	4.9	152.7
On-Road Mobile	187.7	60.4	45.1	18.3
Other Mobile	104.7	44.5	52.4	25.7
Total	339.5	337.2	131.9	296.7

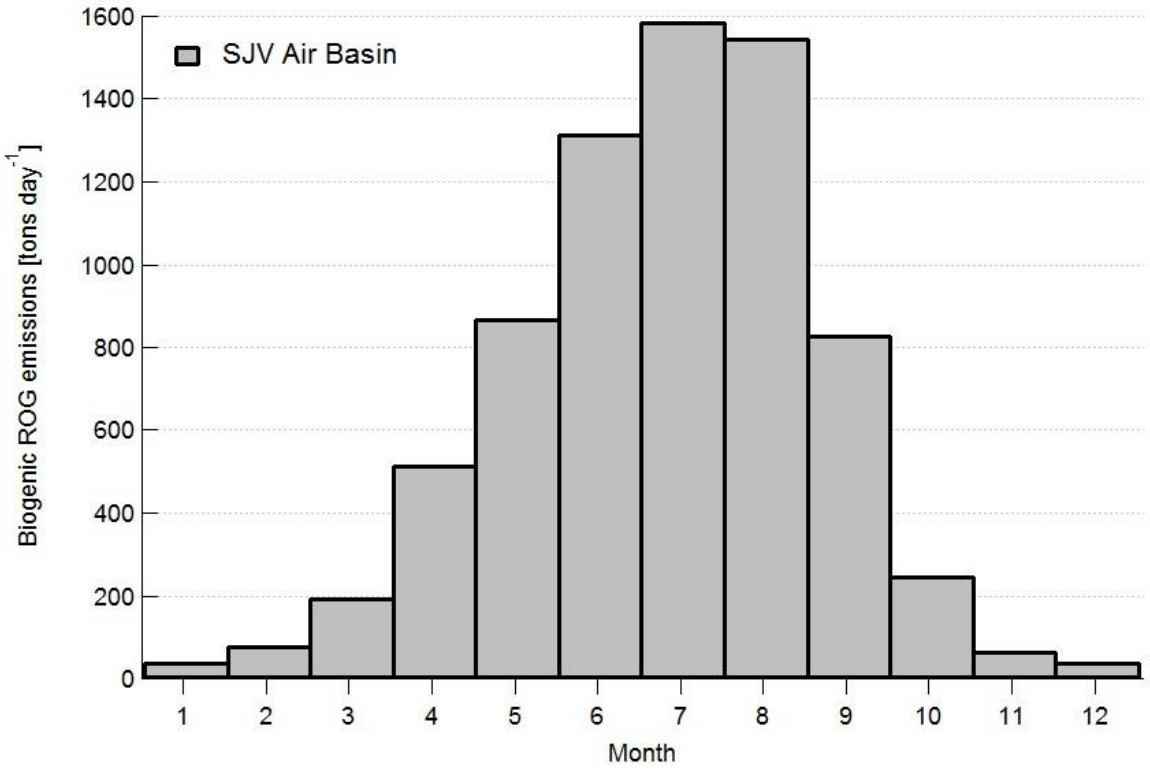

Figure 9. Monthly average biogenic ROG emissions for 2012.

5. OZONE MODELING

5.1. CMAQ MODEL SETUP

Figure 10 shows the CMAQ modeling domains used in this work. The larger domain covering all of California has a horizontal grid size resolution of 12 km with 107x97 lateral grid cells for each vertical layer and extends from the Pacific Ocean in the west to Eastern Nevada in the east and runs from the U.S.-Mexico border in the south to the California-Oregon border in the north. The smaller nested domain covering the SJV region has a finer scale 4km grid resolution and includes 192x192 lateral grid cells. The 12km and 4km domains are based on a Lambert Conformal Conic projection with reference longitude at -120.5°W, reference latitude at 37°N, and two standard parallels at 30°N and 60°N, which is consistent with WRF domain settings. The 30 vertical layers from WRF were mapped onto 18 vertical layers for CMAQ extending from the surface to 100 mb such that majority of the vertical layers fall within the planetary boundary layer. This vertical layer structure is based on the WRF sigma-pressure coordinates and the exact layer structure used can be found in Table 4.

The photochemical modeling for this attainment demonstration utilized CMAQ version 5.0.2, released by the U.S. EPA (https://www.cmascenter.org/cmaq/) in May 2014. The SAPRC07 mechanism was selected as the photochemical mechanism for the CMAQ simulations. Further details of the CMAQ configuration used in this work are summarized in Table 9 and in the Photochemical Modeling Protocol Appendix. The same configuration has been used for all simulations including the base, reference, and future years. CMAQ was compiled using the Intel FORTRAN compiler version 12.

The entire ozone season (May – September 2012) was simulated through parallel individual monthly simulations. For each month, the CMAQ simulations included a seven day spin-up period (i.e., the last seven days of the previous month) for the outer 12 km domain where initial conditions for the beginning day were set to the default initial conditions included with the CMAQ release. The 4 km inner domain simulations utilized a three day spin-up period, where the initial conditions for the starting day were based on output from the corresponding day of the 12 km domain simulation.

Chemical boundary conditions for the outer 12 km domain were extracted from the global chemical transport Model for Ozone and Related chemical Tracers, version 4 (MOZART-4; Emmons et al., 2010[1]). The MOZART-4 data for 2012 was obtained from the National Center for Atmospheric Research (NCAR; http://www.acom.ucar.edu/wrf-chem/mozart.shtml) for the simulations driven by meteorological fields from the NASA GMAO GEOS-5 model. The same MOZART derived BCs for the 12 km outer domain, were used for all simulations (e.g., Base, Reference, Future, and any sensitivity simulation). The inner 4 km domain simulations utilized BCs that were based on the output from the corresponding day of the 12 km domain simulation.

[1] Emmons, L. K., Walters, S., Hess, P. G., Lamarque, J.-F., Pfister, G. G., Fillmore, D., Granier, C., Guenther, A., Kinnison, D., Laepple, T., Orlando, J., Tie, X., Tyndall, G., Wiedinmyer, C., Baughcum, S. L., and Kloster, S.: Description and evaluation of the Model for Ozone and Related chemical Tracers, version 4 (MOZART-4), Geosci. Model Dev., 3, 43-67, doi:10.5194/gmd-3-43-2010, 2010.

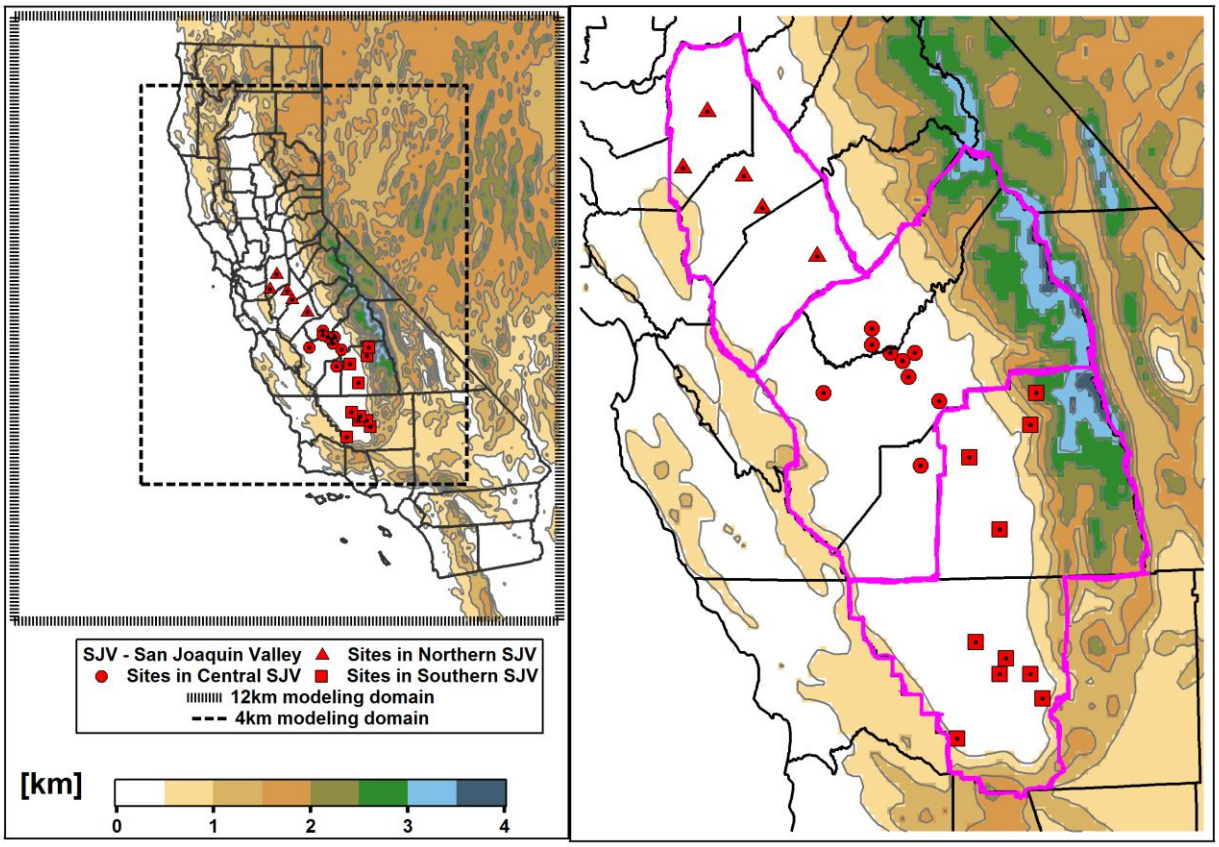

Figure 10. The CMAQ modeling domains used in this SIP modeling. The outer box of the left panel is the California statewide 12 km modeling domain, while the inner box shows the 4km modeling domain covering Central California. The shaded and gray line contours denote the gradients in topography (km). The insert on the right shows the zoomed-in view of the spatial extent (magenta lines) and the location of sites in the Northern (red triangle markers), Central (red circle makers) and Southern (red square markers) sub regions in the Valley that have been used in evaluating model performance for ozone. (Figure adapted from Kulkarni et al., 2014[1])

[1] Kulkarni, S., Kaduwela, A. P., Avise, J. C., DaMassa, J. A., and Chau, D.: An extended approach to calculate the ozone relative response factors used in the attainment demonstration for the National Ambient Air Quality Standards, *J. Air & Waste Management Association,* 64(10), 1204-1213, 2014, doi:10.1080/10962247.2014.936984.

Table 9. CMAQ configuration and settings.

Process	Scheme
Horizontal advection	Yamo (Yamartino scheme for mass-conserving advection)
Vertical advection	WRF-based scheme for mass-conserving advection
Horizontal diffusion	Multi-scale
Vertical diffusion	ACM2 (Asymmetric Convective Model version 2)
Gas-phase chemical mechanism	SAPRC-07 gas-phase mechanism with version “C” toluene updates
Chemical solver	EBI (Euler Backward Iterative solver)
Aerosol module	Aero6 (the sixth-generation CMAQ aerosol mechanism with extensions for sea salt emissions and thermodynamics; includes a new formulation for secondary organic aerosol yields)
Cloud module	ACM_AE6 (ACM cloud processor that uses the ACM methodology to compute convective mixing with heterogeneous chemistry for AERO6)
Photolysis rate	phot_inline (calculate photolysis rates in-line using simulated aerosols and ozone concentrations)

5.2. CMAQ MODEL EVALUATION

Observed ozone data from the Air Quality and Meteorological Information System (AQMIS) database (www.arb.ca.gov/airqualitytoday/) was used to evaluate the accuracy of the 4 km CMAQ modeling for all ozone monitors listed in Table 2 and Figure 10. The U.S. EPA modeling guidance (U.S. EPA, 2014[1]) recommends using the grid cell value where the monitor is located, to pair observations with simulated values in operational evaluation of model predictions. However, the future year design value calculations (discussed in Sections 2.5 and 2.6) are based on simulated values > 60ppb near the monitor (i.e. the maximum simulated ozone within a 3x3 array of cells with the grid cell containing the monitor located at the center of the array). Hence, model performance was evaluated at each monitor by comparing observations against the simulated values using only data above the 60 ppb threshold at the monitored grid cell as well as the peak grid cell within the 3x3 grid array centered on the monitor (i.e., the 3x3 maximum). Model performance is further summarized separately for the three sub-regions in the Valley due to their distinct geographical, meteorological and air quality patterns.

As recommended by U.S. EPA, a number of statistical metrics have been used to evaluate the model performance for ozone. These metrics include mean bias (MB), mean error (ME), mean fractional bias (MFB), mean fractional error (MFE), normalized mean bias (NMB), normalized mean error (NME), root mean square error (RMSE), and correlation coefficient (R^2). In addition, the following plots were used in evaluating the modeling: time-series plots comparing the predictions and observations, scatter plots for comparing the magnitude of the simulated and observed mixing ratios, box plots to summarize the time series data across different regions and averaging times, as well as frequency distributions.

The model performance evaluation is presented for the entire SJV region and also disaggregated for the three sub regions. Performance statistics for data above 60 ppb are reported separately for different ozone metrics including 8-hour daily maximum ozone, 1-hour daily maximum ozone, and hourly ozone (all hours of the day) for the monitored grid cell as well as the 3x3 maximum.

Performance statistics for Maximum Daily Average 8-hour ozone (MDA8) are shown in Table 10. Overall, when simulated data extracted at the grid cell is used for comparison with observations, the model shows a slight negative bias in MDA8 ozone greater than

[1] U.S. EPA, 2014, Draft Modeling Guidance for Demonstrating Attainment of Air Quality Goals for Ozone, PM2.5 and Regional Haze, available at https://www.epa.gov/ttn/scram/guidance/guide/Draft_O3-PM-RH_Modeling_Guidance-2014.pdf

60 ppb in all regions, with the smallest bias occurring in the Southern SJV (-4.3 ppb) and the largest bias occurring in the Central SJV (-6.9 ppb). However, when the 3x3 maximum is used instead, the bias reduces to -2.1 ppb in Southern SJV and to -5 ppb in the Central SJV. Mean error shows a consistent trend with the error getting smaller from 7.9 ppb to 7.2 ppb for the entire SJV when the 3x3 maximum is considered. Similar statistics for daily maximum 1-hour ozone and hourly ozone can be found in Table 11 and Table 12, respectively.

Model performance statistics within the range of values shown in Tables 10, 11 and 12 are consistent with previous studies in the SJV and studies elsewhere in the U.S. Hu et al. (2012)[1], simulated an ozone episode in the SJV (July 27 – August 2, 2000) using a different chemical mechanisms and found that modeled bias ranged from -0.5 to -12.6 ppb for daily maximum 8-hour ozone (compared to -5.2 and -3.2 ppb for the entire SJV in this work) and -0.2 to -15.3 ppb for daily maximum 1-hour ozone in the SJV (compared to -7.5 and -4.7 ppb in this work). Similarly, Shearer et al. (2012)[2] compared model performance in Central California during two episodes in 2000 (July 24 – 26 and July 31 – August 2) for two different chemical mechanisms and found that normalized bias for daily maximum 8-hour ozone ranged from -7% to -14% with hourly peak ozone showing a slightly larger range from -7% to -18%. These are also consistent with the statistics found in this work, which were calculated as -4.3 % (8-hour) and -5.9 % (1-hour). Jin et al. (2010)[3] conducted a longer term simulation over Central California (summer 2000) and found a RMSE for daily maximum 8-hour ozone of 13 ppb, which is greater than the 9.2 ppb found in this work, but Jin et al. (2010) also showed a smaller overall bias of -1 ppb, compared to -3.2 ppb in this work.

[1] Hu, J., Howard, C. J., Mitloehner, F., Green, P. G., and Kleeman, M. J.: Mobile Source and Livestock Feed Contributions to Regional Ozone Formation in Central California, *Environmental Science & Technology*, 46, 2781-2789, 2012.

[2] Shearer, S. M., Harley, R. A., Jin, L., and Brown, N. J.: Comparison of SAPRC99 and SAPRC07 mechanisms in photochemical modeling for central California, *Atmos. Environ.*, 46, 205-216, 2012.

[3] Jin, L., Brown, N. J., Harley, R. A., Bao, J.-W., Michelson, S. A., and Wilczak, J. M.: Seasonal versus episodic performance evaluation for an Eulerian photochemical air quality model, *J. Geophys. Res.*, 115, D09302, doi:10.1029/2009JD012680, 2010.

Table 10. Daily maximum 8-hour ozone performance statistics by modeling subregions and entire SJV region for May-September 2012.

Daily Maximum 8-hour ozone > 60 ppb with simulated data extracted at grid cell where the monitor is located				
Parameter	**NSJV**	**CSJV**	**SSJV**	**Entire SJV**
Number of data points	172	494	944	1610
Mean obs (ppb)	72.4	75.6	75.8	75.4
Standard Deviation obs (ppb)	8.8	9.5	8	8.7
Mean Bias (ppb)	-5.2	-6.9	-4.3	-5.2
Mean Error (ppb)	7.1	8.4	7.8	7.9
RMSE (ppb)	9.6	10.7	9.6	10
Normalized Mean Bias (%)	-7.2	-9.1	-5.7	-6.9
Normal Mean Error (%)	9.9	11.1	10.3	10.5
R-squared	0.18	0.28	0.19	0.21
Index of Agreement	0.58	0.63	0.64	0.64

Daily Maximum 8-hour ozone > 60 ppb with simulated data extracted from the 3x3 grid cell array maximum centered at the monitor				
Parameter	**NSJV**	**CSJV**	**SSJV**	**Entire SJV**
Number of data points	197	557	1009	1763
Mean obs (ppb)	71.9	75.1	75.4	74.9
Standard Deviation obs (ppb)	8.6	9.4	8.1	8.7
Mean Bias (ppb)	-3.7	-5	-2.1	-3.2
Mean Error (ppb)	6.7	7.6	7.1	7.2
RMSE (ppb)	9	9.6	8.9	9.2
Normalized Mean Bias (%)	-5.2	-6.6	-2.8	-4.3
Normal Mean Error (%)	9.4	10.1	9.5	9.6
R-squared	0.18	0.31	0.22	0.24
Index of Agreement	0.62	0.69	0.68	0.69

Table 11. Daily maximum 1-hour ozone performance statistics by modeling subregions and entire SJV region for May-September 2012.

Daily Maximum 1-hour ozone > 60 ppb with simulated data extracted at grid cell where the monitor is located				
Parameter	**NSJV**	**CSJV**	**SSJV**	**Entire SJV**
Number of data points	310	714	1094	2118
Mean obs (ppb)	76.1	81.3	82.1	81
Standard Deviation obs (ppb)	11.1	13.3	10.5	11.8
Mean Bias (ppb)	-4.9	-9.9	-6.7	-7.5
Mean Error (ppb)	8.4	11.5	10.3	10.4
RMSE (ppb)	10.9	14.7	12.6	13.1
Normalized Mean Bias (%)	-6.4	-12.2	-8.2	-9.3
Normal Mean Error (%)	11	14.1	12.6	12.9
R-squared	0.25	0.35	0.24	0.27
Index of Agreement	0.65	0.65	0.65	0.66

Daily Maximum 1-hour ozone > 60 ppb with simulated data extracted from the 3x3 grid cell array maximum centered at the monitor				
Parameter	**NSJV**	**CSJV**	**SSJV**	**Entire SJV**
Number of data points	333	789	1164	2286
Mean obs (ppb)	75.5	80.5	81.5	80.3
Standard Deviation obs (ppb)	11	13.1	10.6	11.8
Mean Bias (ppb)	-2.9	-6.8	-3.8	-4.7
Mean Error (ppb)	7.6	9.6	9.1	9.1
RMSE (ppb)	10	12.4	11.4	11.5
Normalized Mean Bias (%)	-3.8	-8.5	-4.6	-5.9
Normal Mean Error (%)	10.1	12	11.2	11.3
R-squared	0.28	0.42	0.29	0.34
Index of Agreement	0.7	0.74	0.71	0.73

Table 12. Hourly ozone performance statistics by modeling subregions and entire SJV region for May-September 2012. Note that only statistics for the grid cell in which the monitor is located were calculated for hourly ozone.

Hourly ozone > 60 ppb with simulated data extracted at grid cell where the monitor is located				
Parameter	**NSJV**	**CSJV**	**SSJV**	**Entire SJV**
Number of data points	1421	3999	8180	13600
Mean obs (ppb)	74.3	77.1	75.9	76.1
Standard Deviation obs (ppb)	9.8	11	9.6	10.1
Mean Bias (ppb)	-5	-7.7	-4.2	-5.3
Mean Error (ppb)	8	9.8	8.3	8.8
RMSE (ppb)	10.6	12.8	10.6	11.3
Normalized Mean Bias (%)	-6.7	-10	-5.5	-7
Normal Mean Error (%)	10.8	12.8	11	11.5
R-squared	0.16	0.2	0.2	0.18
Index of Agreement	0.59	0.59	0.65	0.62

Simon et al. (2012)[1] conducted a review of photochemical model performance statistics published between 2006 and 2012 for North America (from 69 peer-reviewed articles). In Figure 11, the statistical evaluation of this model attainment demonstration is compared to the model performance summary presented in Simon et al. (2012) by overlaying the various summary statistics from the attainment demonstration onto the Simon et al. (2012) model performance summary. Note that the box-whisker plot (colored in gray) shown in Figure 11 is reproduced using data from Figure 4 of Simon et al. (2012). The blue and red colored horizontal line markers in each of the panels of Figure 11 denote the model performance statistics calculated using simulated data at the grid cell and the 3x3 maximum from the current modeling work. Figure 11 clearly shows that the modeling performance statistical metrics for hourly, daily maximum 8-hr and daily maximum 1-hr ozone from this work are consistent with and fall within the range of values reported by other studies in the literature. In particular, the Simon et. al. (2012) study found that mean bias for daily maximum 8-hour ozone ranged from approximately -7 ppb to 13 ppb, while mean error ranged from around 4 ppb to 22 ppb, and RMSE ranged from approximately 8 ppb to 23 ppb; all of which are similar in magnitude to the statistics presented in Table 10. Time series, scatter plots, box plots of mean bias (grouped into 10 ppb bins based on observed values) and frequency distributions of the hourly, 1-hr daily maximum and 8-hour daily maximum ozone data used to generate Tables 10, 11 and 12 can be found in the supplementary material.

[1] Simon, H., Baker, K. R., and Phillips, S.: Compilation and interpretation of photochemical model performance statistics published between 2006 and 2012, *Atmospheric Environment*, 61, 124-139, 2012.

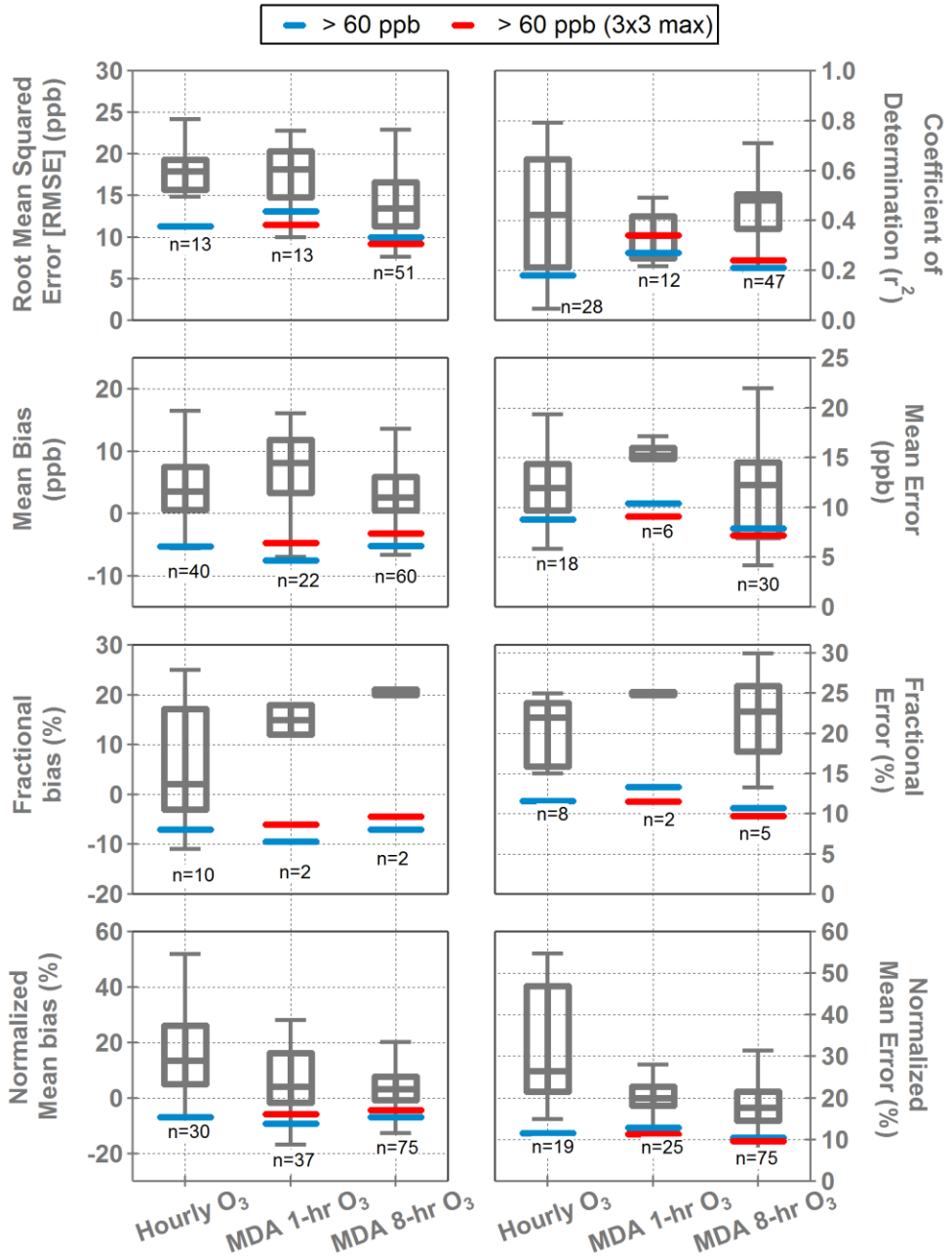

Figure 11. Comparison of various statistical metrics from the model attainment demonstration modeling to the range of statistics from the 69 peer-reviewed studies summarized in Simon et al. (2012)[1]. (MDA denotes Maximum Daily Average)

[1] Simon, H., Baker, K. R., and Phillips, S.: Compilation and interpretation of photochemical model performance statistics published between 2006 and 2012, *Atmospheric Environment*, 61, 124-139, 2012.

5.2.1 DIAGNOSITC EVALUATION

In addition to the statistical evaluation presented above, since the modeling is utilized in a relative sense, it is also useful to consider whether the model is able to reproduce observable relationships between changes in emissions and ozone. One approach to this would be to conduct a retrospective analysis where additional years are modeled (e.g., 2000 or 2005) and the ability of the modeling system to reproduce the observed change in ozone over time is investigated. However, this approach is extremely time consuming. Another approach to investigating the ozone response to changes in emissions is through the so called "weekend effect".

The weekend effect is a well-known phenomenon in some major urbanized areas where emissions of NO_x are substantially lower on weekends than on weekdays, but measured levels of ozone are higher on weekends than on weekdays. This is due to the complex and non-linear relationship between NO_x and ROG precursors and ozone (Swamy et al., 2012)[1]. Ozone formation exhibits a nonlinear dependence to NO_x and ROG precursors in the atmosphere. In general terms, under ambient conditions of high-NO_x and low-ROG (NO_x-disbenefit region in Figure 12), ozone formation tends to exhibit a disbenefit to reductions in NO_x emissions (i.e., ozone increases with decreases in NO_x) and a benefit to reductions in ROG emissions (i.e., ozone decreases with decreases in ROG). In contrast, under ambient conditions of low-NO_x and high-ROG (NO_x-limited region in Figure 12), ozone formation shows a benefit to reductions in NO_x emissions, while changes in ROG emissions result in only minor decreases in ozone. These two distinct "ozone chemical regimes" are illustrated in Figure 12 along with a transitional regime that can exhibit characteristics of both the NO_x-disbenefit and NOx-limited regimes. Note that Figure 12 is shown for illustrative purposes only, and does not represent the actual ozone sensitivity within the SJV for a given combination of NO_x and VOC (ROG) emissions.

In this context, the prevalence of weekend effect in a region suggests that the region is in a NO_x-disbenefit regime (Heuss et al., 2003)[2]. A lack of a weekend effect (i.e., no pronounced high O_3 occurrences during weekends) would suggest that the region is in a transition regime and moving between being NO_x-limited and exhibiting a NO_x-

[1] Swamy, Y.V., Venkanna, R.,Nikhil, G.N., Chitanya, D.N.S.K., Sinha, P.R., Ramakrishna, M., and Rao, A.G., 2012. Impact of Nitrogen Oxides, Volatile Organic Compounds and Black Carbon on
Atmospheric Ozone Levels at a Semi Arid Urban Site in Hyderabad. Aerosol and Air Quality Research 12, 662–671.

[2] Heuss, J.M., Kahlbaum, D.F., and Wolff, G.T., 2003. Weekday/weekend ozone differences: What can we learn from them? Journal of the Air & Waste Management Association 53(7), 772-788

disbenefit. A reversed weekend effect (i.e., lower O_3 during weekends) would suggest that the region is NO_x-limited.

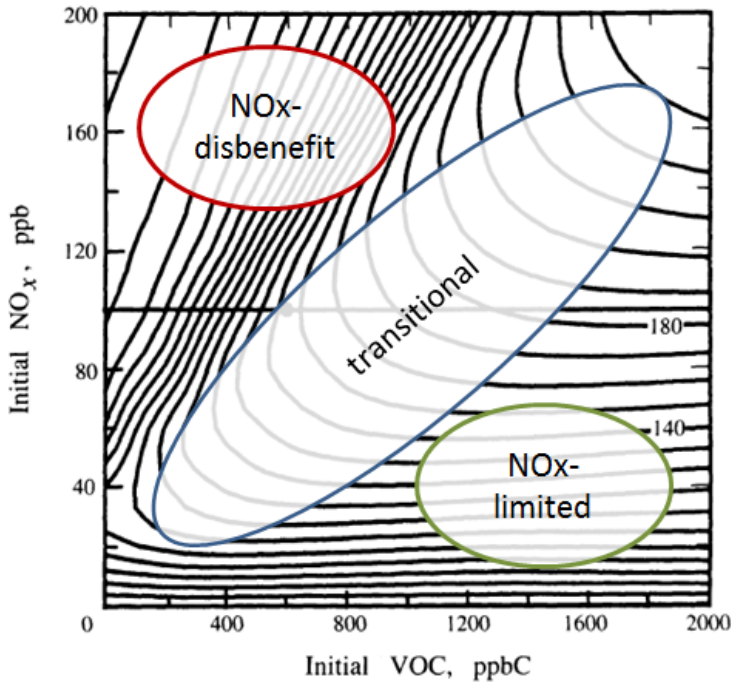

Figure 12. Illustrates a typical ozone isopleth plot, where each line represents ozone mixing ratio, in 10 ppb increments, as a function of initial NO_x and VOC (or ROG) mixing ratio (adapted from Seinfeld and Pandis, 1998[1], Figure 5.15). General chemical regimes for ozone formation are shown as NO_x-disbenefit (red circle), transitional (blue circle), and NO_x-limited (green circle).

Investigating the "weekend effect" and how it has changed over time is a useful real world metric for evaluating the ozone chemistry regime in the SJV and how well it is represented in the modeling. The trend in day-of-week dependence of the Valley's sub-regional observed ozone levels between 2000 and 2014 is shown in Figure 13. The three-panel scatter plot compares the average site-specific weekday (Wednesday and Thursday) and weekend (Sunday) observed summertime (June through September) daily maximum 8-hr ozone value by year (2000 to 2014) and separated into three sub-regions: Northern SJV (top), Central SJV (middle), and Southern SJV (bottom). The light grey triangle and dark gray square markers denote the predicted baseline (2012) and future (2031) average site-specific weekday and weekend ozone values from the attainment demonstration modeling. (Different definitions of weekday and weekend

[1] Seinfeld J. H. and Pandis S. N. (1998) Atmospheric Chemistry and Physics: From Air Pollution to Climate Change, 1st edition, J. Wiley, New York.

days were also investigated and did not show appreciable differences from the Wednesday/Thursday and Sunday definitions.)

From Figure 13 it can be seen that ozone levels are highest in the Southern (i.e. Bakersfield area) and Central (i.e. Fresno area) SJV regions, with the lowest levels seen in the Northern SJV region. A key observation in Figure 13 is that the summertime average weekday and weekend ozone levels have steadily declined between 2000 and 2014.

Along with the declining ozone, there is a pattern shift in the weekday and weekend ozone between 2000 and 2014. In the early 2000's, the central and southern regions of the SJV exhibited roughly an equal number of sites with weekend ozone greater and less than weekday ozone, which suggests that the regions may have been in the transitional chemical regime for ozone formation. By the mid-2000's, the majority of the sites were showing weekday ozone greater than weekend ozone, which is consistent with a shift into complete NO_x-limited chemistry. By 2014, however, some of the sites had shifted back towards a more equal distribution between weekday and weekend ozone, likely due to variability in the biogenic emissions and meteorology. In contrast to the central and southern portions of the SJV, the northern region clearly experienced a greater NO_x-disbenefit in the early 2000's and then moved into a transitional chemical regime in the mid-2000's and is yet to move fully into the NO_x-limited regime.

The simulated baseline 2012 weekday/weekend values (light gray triangle markers) fall above the 1:1 dashed line for central and southern portions, while the values in the northern fall close to the 1:1 dashed line. These predicted values are consistent with observed findings that show a shift into NO_x limited chemistry in the Central and Southern SJV regions and prevalence of transitional chemical regime in Northern SJV.

These findings are consistent with an independent analysis by UC Berkeley researchers on the observed response of ozone from 1995 to 2010 in the SJV to emission reductions in NO_x and VOC reactivity (Pusede et al., 2012[1]). The Pusede et al. study concluded that NO_x emission reductions have been effective at reducing ozone levels and have successfully transitioned the southern and central portions of the SJV into a NO_x-limited chemistry regime, while the northern portion of the SJV is currently in the process of transitioning to the same chemical regime.

[1] Pusede, S. E., and R. C. Cohen, 2012, On the observed response of ozone to NOx and VOC reactivity reductions in San Joaquin Valley California 1995–present, *Atmos. Chem. Phys.*, *12*, 8323–8339.

The predicted future 2031 values (dark gray square markers) clearly show that weekday and weekend ozone decline significantly (all values are below 60 ppb) and all three sub regions show a shift to a NO_x-limited regime with all values falling above the 1:1 dashed line. This modeling-based finding of 2031 NO_x limitation has been corroborated by a study from the UC Berkeley researchers that analyzed the impacts of future emissions controls using an analytical model constrained by CalNex 2010 measurements in the Valley (Pusede et. al., 2014[1]) and concluded that the NO_x controls will be immediately and incrementally more effective than the corresponding ROG controls in lowering the Valley's ozone levels.

[1] Pusede, S. E., Gentner, D. R., Wooldridge, P. J., Browne, E. C., Rollins, A. W., Min, K.-E., Russell, A. R., Thomas, J., Zhang, L., Brune, W. H., Henry, S. B., DiGangi, J. P., Keutsch, F. N., Harrold, S. A., Thornton, J. A., Beaver, M. R., St. Clair, J. M., Wennberg, P. O., Sanders, J., Ren, X., VandenBoer, T. C., Markovic, M. Z., Guha, A., Weber, R., Goldstein, A. H., and Cohen, R. C.: On the temperature dependence of organic reactivity, nitrogen oxides, ozone production, and the impact of emission controls in San Joaquin Valley, California, Atmos. Chem. Phys., 14, 3373-3395, doi:10.5194/acp-14-3373-2014, 2014.

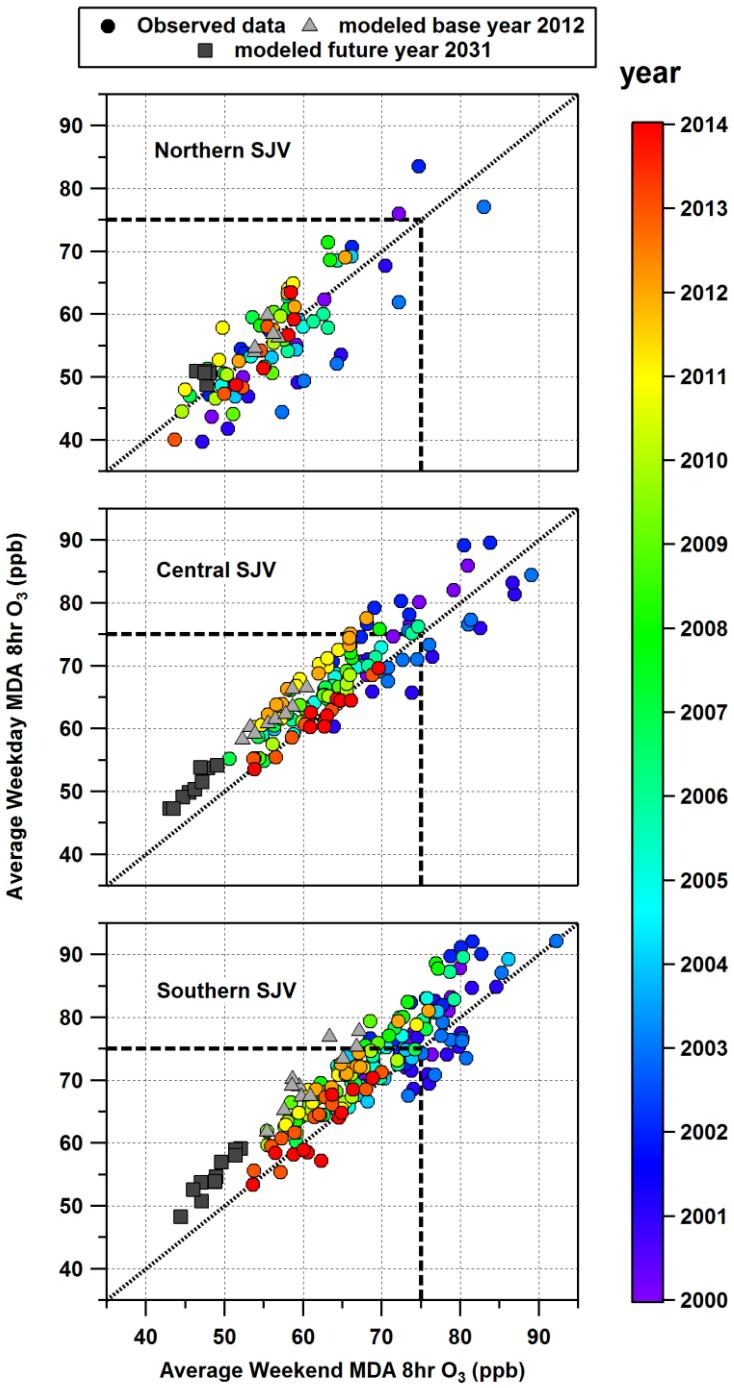

Figure 13. Site-specific average weekday and weekend maximum daily average 8-hour ozone for each year from 2000 to 2014 for the Northern SJV (top), Central SJV (middle), and Southern SJV (bottom). The colored circle markers denote observed values while the light gray triangle and dark gray square markers denote the simulated baseline 2012 and future 2031 values. Points falling below the 1:1 dashed line represent a NO_x-disbenefit regime, those on the 1:1 dashed line represent a transitional regime, and those above the 1:1 dashed line represent a NO_x-limited regime.

5.3. RELATIVE RESPONSE FACTORS AND FUTURE YEAR DESIGN VALUES

The RRFs (Section 2.5) and the future 2031 design values (Section 2.6) for the representative sites in the northern, central and southern regions of the Valley were calculated using the procedures outlined in the corresponding sections, respectively, and are summarized in Table 13. Note that the results shown in Table 13 are ordered by each sub region in descending order of the average reference year 2012 DVs.

The results in Table 13 show that all monitoring sites in the Valley have a future DV less than 75 ppb based on the 2031 emissions inventory, with the Clovis monitor in Central SJV having the highest predicted future design of 74 ppb in 2031 (Note that Clovis is also the valley's design site for base year 2012). Therefore, the air quality simulations predict that the entire Valley will attain the 75 ppb 8-hour O_3 standard by 2031.

The three sub regions show varied response to emission controls as evident from the RRF values shown in Table 13. The Southern SJV shows the greatest response followed by Central SJV as seen from the low values of the site-specific RRF and the 2031 DVs, which is consistent with the prevalence of NO_x-limited ozone formation regimes (Section 5.2) in those regions. The Northern SJV shows the lowest response (relatively higher RRF values), which is expected as this region is still transitioning to the NO_x-limited chemical regime (section 5.2).

Table 13. Summary of key parameters related to the future year 2031 design value (DV) calculation.

County	Site	Average Reference Year 2012 DV (ppb)	RRF	Average Future Year 2031 DV (ppb)
Northern SJV				
Stanislaus	***Turlock-S Minaret Street***	***86.0***	***0.8019***	***69***
Merced	Merced-S Coffee Avenue	81.7	0.8009	65
San Joaquin	Tracy-Airport	79.3	0.8428	66
Stanislaus	Modesto-14th Street	76.0	0.8100	61
San Joaquin	Stockton-Hazelton Street	68.3	0.8444	57
Central SJV				
Fresno	***Clovis-N Villa Avenue***	***95.7***	***0.7729***	***74***
Fresno	Fresno-Drummond Street	92.3	0.7712	71
Fresno	Parlier	92.0	0.7513	69
Fresno	Fresno-Garland	90.7	0.7812	70
Fresno	Fresno-Sierra Skypark #2	89.0	0.7684	68
Kings	Hanford-S Irwin Street	86.0	0.7537	64
Madera	Madera-28261 Avenue 14	84.7	0.7746	65
Madera	Madera-Pump Yard	79.3	0.7789	61
Fresno	Tranquility	76.3	0.7943	60
Southern SJV				
Tulare	***Sequoia and Kings Canyon Natl Park***	***93.0***	***0.7037***	***65***
Kern	Arvin-Di Giorgio	89.3	0.7242	64
Kern	Edison	87.7	0.7397	64
Kern	Bakersfield-5558 California Avenue	86.7	0.7573	65
Tulare	Porterville-1839 Newcomb Street	86.3	0.7327	63
Kern	Oildale-3311 Manor Street	84.7	0.7772	65
Tulare	Sequoia Natl Park-Lower Kaweah	84.0	0.7302	61
Kern	Maricopa-Stanislaus Street	83.3	0.7561	63
Kern	Shafter-Walker Street	83.0	0.7556	62
Tulare	Visalia-N Church Street	82.3	0.7391	60

5.4. UNMONITORED AREA ANALYSIS

The unmonitored area analysis is used to ensure that there are no regions outside of the existing monitoring network that would exceed the NAAQS if a monitor was present (U.S. EPA, 2014[1]). U.S. EPA recommends combining spatially interpolated design value fields with modeled ozone gradients and grid-specific RRFs in order to generate gridded future year gradient adjusted design values. This analysis can be done using the Model Attainment Test Software (MATS) (Abt , 2014[2]). However, this software is not open source and comes as a precompiled software package. To maintain transparency and flexibility in the analysis, in-house R codes (https://www.r-project.org/) developed at ARB, were utilized in this analysis.

The unmonitored area analysis was conducted using the 8-hr O_3 weighted DVs from all the available sites that fall within the 4km inner modeling domain along with the reference year 2012 and future year 2031 4 km CMAQ model output. The steps followed in the unmonitored area analysis are as follows:

Step 1: For each grid cell, calculate the average of the top-10 modeled maximum daily average 8-hour ozone concentrations from the reference year simulation.

Step 2: Interpolate the monitor-specific weighted base-year DVs to an unmonitored grid cell using normalized inverse distance squared weightings for all monitors within a grid cell's Voronoi Region (calculated with the R tripack library; https://cran.r-project.org/web/packages/tripack/README), and adjusted based on the ozone gradient between the grid cell and the corresponding monitor from Step 1. Interpolation is done only within the geographic region constrained by the monitoring network, since extrapolating to outside of the monitoring network is inherently uncertain.

Step 3: For each grid cell, calculate an RRF based on the reference- and future-year modeling following the same approach outlined in Section 2.5, except that the +/- 20% limitation on the simulated and observed maximum daily average 8-

[1] U.S. EPA, 2014, Draft Modeling Guidance for Demonstrating Attainment of Air Quality Goals for Ozone, PM2.5 and Regional Haze, available at https://www.epa.gov/ttn/scram/guidance/guide/Draft_O3-PM-RH_Modeling_Guidance-2014.pdf

[2] Abt, 2014. Modeled Attainment Test Software: User's Manual. MATS available at: http://www.epa.gov/scram001/modelingapps_mats.htm

hour ozone is not applicable because observed data do not exist for grid cells in unmonitored areas.

Step 4: Multiply the gradient-adjusted interpolated DVs from Step 2 by the gridded RRFs from Step 3 to calculated future-year gridded DVs.

Step 5: Examine the future-year gridded DVs to determine if there are peak values higher than those at the monitors, which could cause violations of the 8-hour ozone NAAQS.

Figure 14 shows the spatial distribution of gridded DVs for the SJV non-attainment area based on the unmonitored area analysis (described above). The black colored triangle markers denote the monitoring sites, which had valid reference year 2012 DVs and were used in the analysis. The entire valley shows gridded DVs that are below the 75 ppb standard. The gridded DVs falling between 71 and 75 ppb can be found near the Tracy monitoring site in the northern region and to the east of Fresno in the Central region, but are below the 75 ppb standard. Therefore, the unmonitored area analysis predicts that all unmonitored regions within the Valley will attain the 75 ppb 8-hour O_3 standard by 2031.

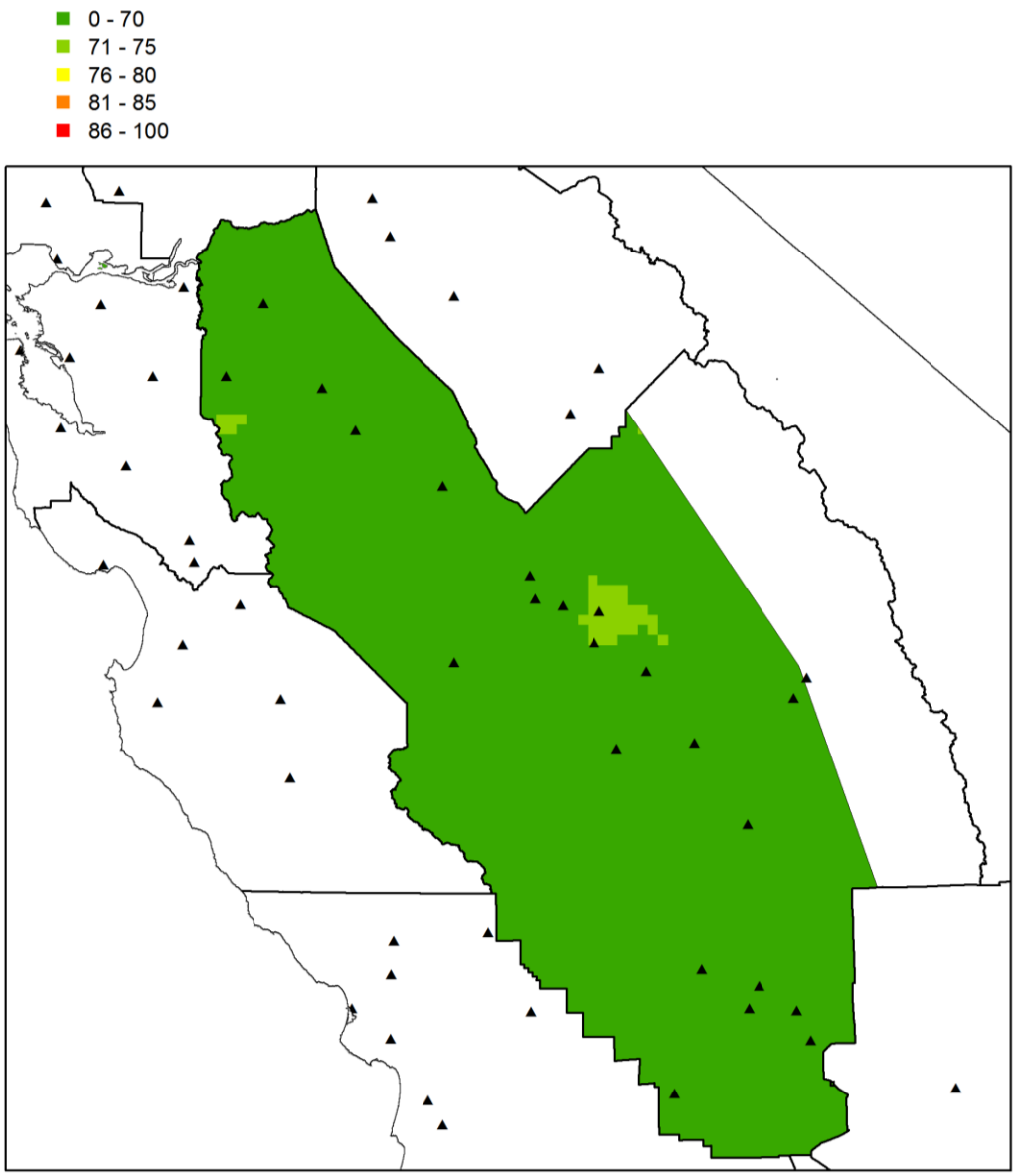

Figure 14. Spatial distribution of the future 2031 DVs based on the unmonitored area analysis in the Valley. Color scale is in ppb of ozone.

5.5. "BANDED" RELATIVE RESPONSE FACTORS AND FUTURE YEAR DESIGN VALUES

The "Band-RRF" approach expands upon the standard "Single-RRF" (Section 5.3) approach to account for differences in model response to emissions controls at varying ozone levels. The most recent U.S. EPA modeling guidance (U. S. EPA 2014[1]) accounts for some of these differences by focusing on the top ten modeled days, but even the top ten days may contain a significant range of ozone mixing ratios. The Band-RRF approach accounts for these differences more explicitly by grouping the simulated ozone into bands of lower, medium, and higher ozone mixing ratios.

In this work, the banded RRFs were calculated to project the future year 2031 DVs. The inherent data used for this analysis is consistent with the data used in the single RRF calculations (Sections 2.5 and 5.3). The various steps involved in the calculation of banded RRFs are as follows:

1. MDA 8-hour ozone mixing ratios for all days that are above 60 ppb and that fall within +/- 20% of observations are stratified into 5 ppb increments in the 60 -100 ppb range. (All days above 100 ppb are grouped into a single bin)

2. A separate RRF is calculated for each ozone band following a similar approach as the standard Single-RRF. A linear regression is then fit to the data resulting in an equation relating RRF to ozone band as long as there are at least 3 bands (without missing data). The band RRF calculations were not available for sites that had fewer than 3 bands of valid RRFs. Similar to the Single-RRF; this equation is unique to each monitor/location.

3. The top ten days for each monitor, based on observed 8-hour ozone for each year of the 5 years that is utilized in the design value calculation (see Table 1), are then projected to the future using the appropriate RRF for the corresponding ozone band.

4. The top ten future days for each individual year are then re-sorted, the fourth highest 8-hour ozone is selected, and the future year design value is calculated

[1] U.S. EPA, 2014, Draft Modeling Guidance for Demonstrating Attainment of Air Quality Goals for Ozone, PM2.5 and Regional Haze, available at https://www.epa.gov/ttn/scram/guidance/guide/Draft_O3-PM-RH_Modeling_Guidance-2014.pdf

in a manner consistent with the base/reference year design value calculation.

5. The future Design Values was then compared with the 75 ppb 8-hour O_3 standard to determine the attainment status for each monitor.

More detailed information on the Band-RRF approach can be found in Kulkarni et al. (2014)[1] and the SJV 2013 1-Hour Ozone SIP[2].

The banded RRFs and the corresponding future 2031 design values for the representative sites in the northern, central and southern regions of the Valley were calculated using the procedure outlined above, and are summarized in Table 14. Note that the results shown in Table 14 are ordered by each sub region in the descending order of average reference year 2012 DVs.

The results in Table 14 show that all the monitoring sites in the Valley have a future DV less than 75 ppb, with the Clovis monitoring site in Central SJV having the highest predicted future design with an estimated future design value of 72 ppb in 2031, which is 2 ppb lower than the corresponding single-RRF value (Table 13). (Note that Clovis is also the valley's design site for base year 2012).

[1] Kulkarni, S., Kaduwela, A. P., Avise, J. C., DaMassa, J. A., and Chau, D.: An extended approach to calculate the ozone relative response factors used in the attainment demonstration for the National Ambient Air Quality Standards, *J. Air & Waste Management Association,* 64(10), 1204-1213, 2014, doi:10.1080/10962247.2014.936984.

[2] http://www.valleyair.org/Air_Quality_Plans/Ozone-OneHourPlan-2013.htm

Table 14. Summary of banded RRF calculation along with the future year 2031 design values projected from the average reference year 2012 design value

County	Site	Average Reference Year 2012 Design Value (ppb)	Average Future Year 2031 Design Value using banded "RRF"(ppb)
Northern SJV			
Stanislaus	***Turlock-S Minaret Street***	***86.0***	65
Merced	Merced-S Coffee Avenue	81.7	64
San Joaquin	Tracy-Airport	79.3	66
Stanislaus	Modesto-14th Street	76.0	61
San Joaquin	Stockton-Hazelton Street	68.3	--
Central SJV			
Fresno	***Clovis-N Villa Avenue***	***95.7***	72
Fresno	Fresno-Drummond Street	92.3	67
Fresno	Parlier	92.0	66
Fresno	Fresno-Garland	90.7	--
Fresno	Fresno-Sierra Skypark #2	89.0	63
Kings	Hanford-S Irwin Street	86.0	--
Madera	Madera-28261 Avenue 14	84.7	62
Madera	Madera-Pump Yard	79.3	60
Fresno	Tranquility	76.3	--
Southern SJV			
Tulare	***Sequoia and Kings Canyon Natl Park***	***93.0***	65
Kern	Arvin-Di Giorgio	89.3	65
Kern	Edison	87.7	66
Kern	Bakersfield-5558 California Avenue	86.7	65
Tulare	Porterville-1839 Newcomb Street	86.3	62
Kern	Oildale-3311 Manor Street	84.7	65
Tulare	Sequoia Natl Park-Lower Kaweah	84.0	62
Kern	Maricopa-Stanislaus Street	83.3	61
Kern	Shafter-Walker Street	83.0	60
Tulare	Visalia-N Church Street	82.3	61

6. OZONE ISOPLETHS

Since the entire Valley is projected to be in attainment for 2008 75 ppb 8-hour O_3 standard, no additional emission reductions beyond what is currently being implemented through the current control program will be necessary. However, the U.S. EPA revised the 8-hr O_3 standard to a level of 0.070 ppm (70 ppb) on October 1, 2015 (80 FR 65292), for which the final designations are due in late 2017.

Hence, it is important to know the precursor limitation in the future to assess the level of emissions controls needed to attain the 2015 8-hr O_3 standard of 0.070 ppm (70 ppb) and ensure that emissions controls that could be needed for other standards (e.g., 1-hour O_3, 24-hour $PM_{2.5}$, annual $PM_{2.5}$, and 1-hour NO_x) support attainment of the revised standard. Looking at the future DVs in Table 13, it can be seen that the majority of sites in the Valley are predicted to attain the 70 ppb standard by 2031, with exception of the Clovis and Fresno Drummond monitoring sites.

In order to identify what combinations of precursor emissions reductions (including which precursors are most effective at reducing ozone as well as the magnitude of reductions needed) might lead to attainment, modeling sensitivity simulations with varying degrees of precursor reductions from anthropogenic sources are typically performed. The results of these sensitivity simulations are plotted on ozone isopleth diagrams, which are also referred to as carrying capacity diagrams (see Figure 12 for isopleth example). The isopleths provide an estimate of the level of emissions needed to demonstrate attainment and thereby inform the development of a corresponding control strategy.

To examine the future ozone sensitivity within the SJV for different combinations of NO_x and VOC (ROG) emissions in the Valley, modeling sensitivity simulations were conducted to generate the 8-hr ozone isopleths. These sensitivity simulations are identical to the future year 2031 simulation discussed earlier in Section 2.4 and Table 3, except that domain-wide fractional reductions were applied to future year 2031 anthropogenic NO_x and ROG emission levels. Each sensitivity simulation was run for the entire ozone season (May – September 2012) and included statewide 12 km simulations nested down to 4 km. The inner 4 km domain sensitivity simulations utilized BCs based on output from the corresponding 12 km sensitivity simulation, while the 12 km simulations all utilized the same MOZART derived BCs. The RRF methodology described in Section 2.5 was then applied to the inner 4 km domain output of each fractional ROG and NO_x sensitivity simulation to calculate the future DV (for that specific NO_x-ROG combination) at each monitoring site in the Valley.

Figures 15 and 16 show the 2031 8-hour ozone isopleths for the Clovis and Fresno Drummond monitoring sites (isopleths for other sites are not shown since their projected DVs are below 70 ppb). In each figure, the bottom and top axes represent the domain-wide fractional ROG emissions and the corresponding SJV basin emission totals (tons per day) in 2031, respectively. Likewise, the left and right axes represent the domain-wide fractional NO_x emissions and the corresponding SJV basin emission totals (tons per day) in 2031, respectively. The top right point on each diagram represents the projected DV for the attainment demonstration (listed in Table 13).

The shape of the ozone isopleths shown in Figures 15 and 16 indicates that they fall in the bottom right corner of the Figure 12, where the NO_x-limited regime is prevalent. It is evident from these diagrams that the future O_3 mixing ratios throughout the San Joaquin Valley are predicted to be in the NO_x-limited regime and that the sensitivity to ROG emissions controls will be much lower when compared to NO_x. Since NO_x is the limiting precursor, modest additional NO_x reductions are needed to attain the 70 ppb standard in the Valley.

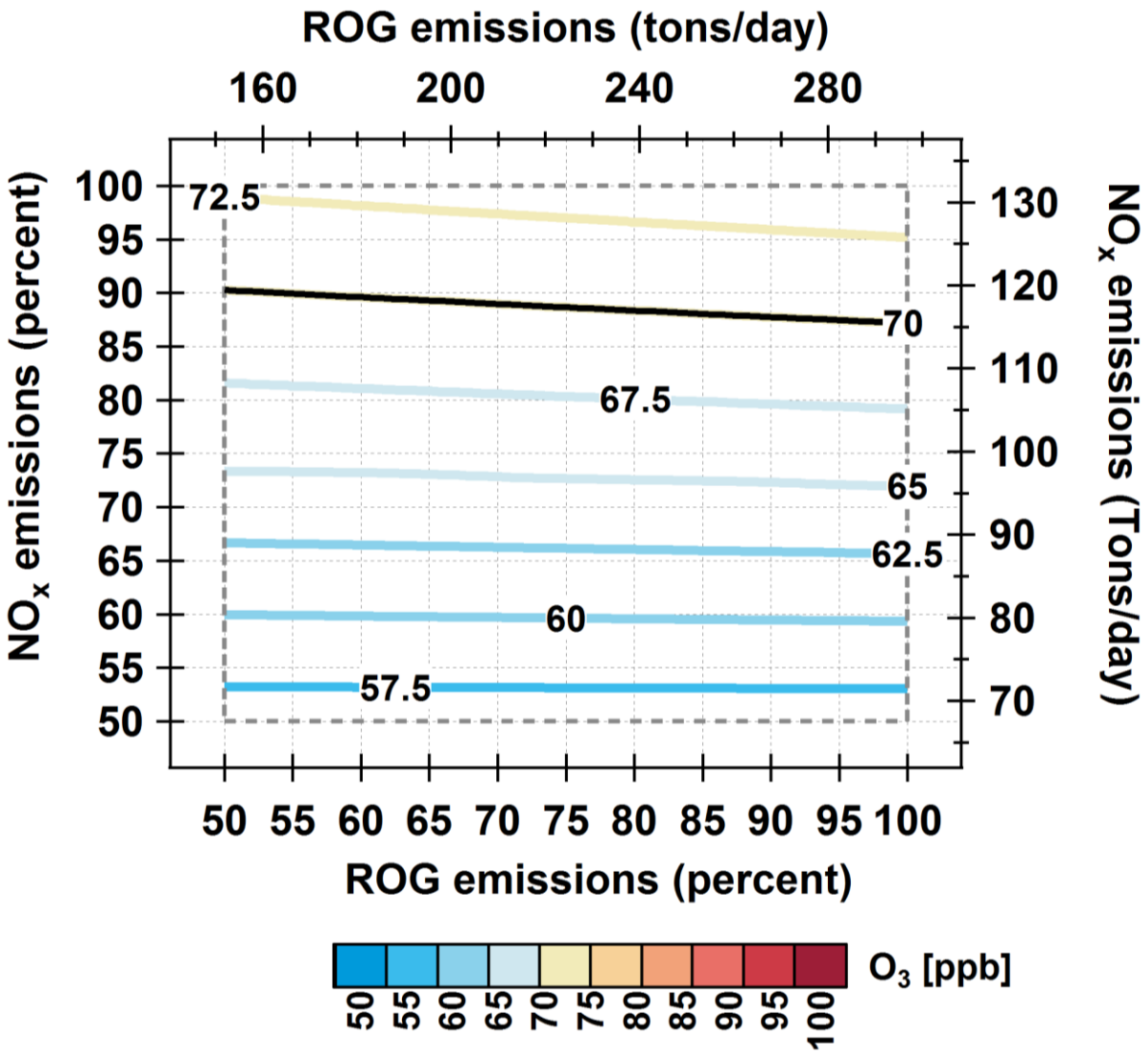

Figure 15. The 8-hr ozone isopleth based on 2031 emission levels at the Clovis site located in Central SJV.

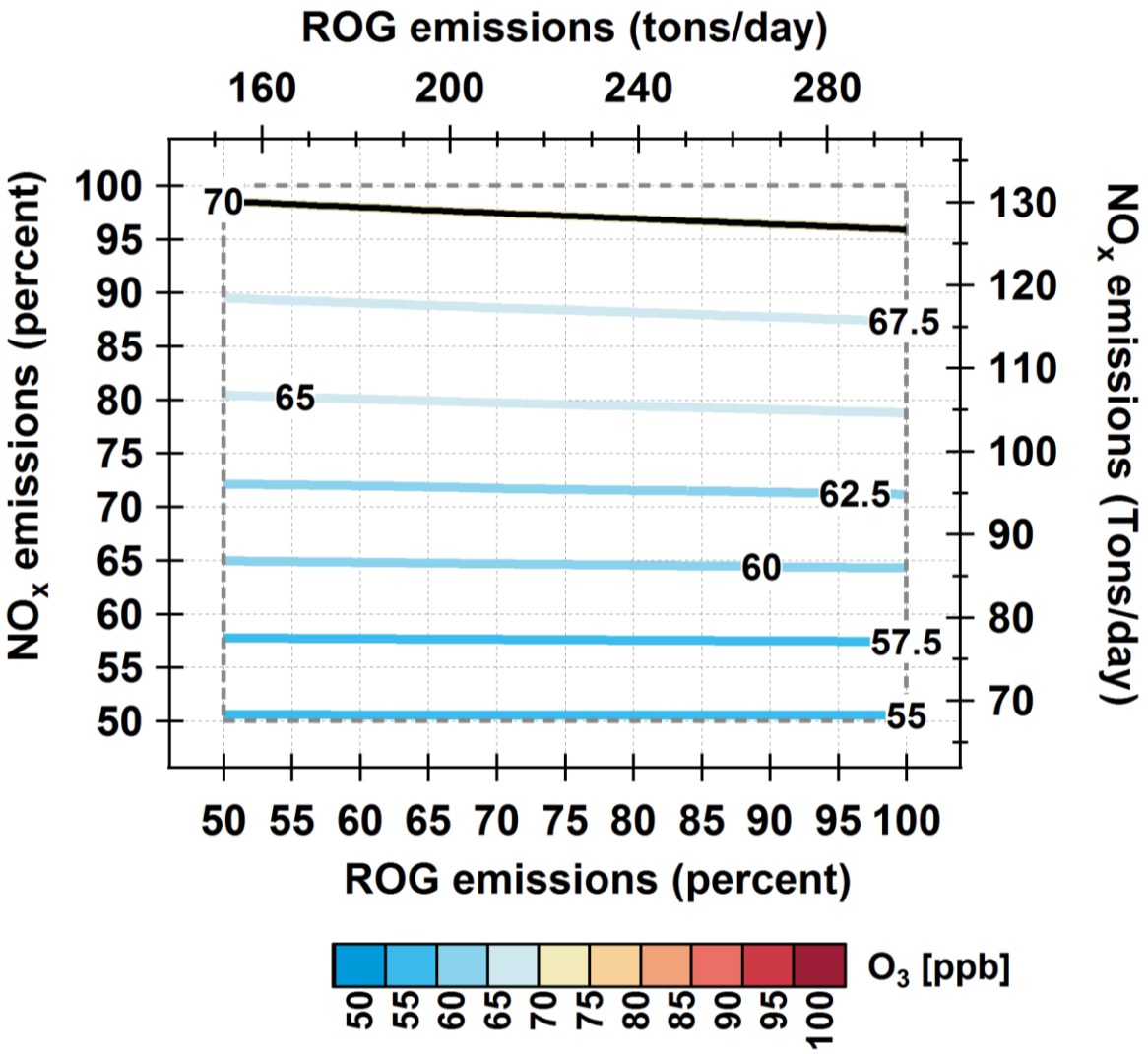

Figure 16. The 8-hr ozone isopleth based on 2031 emission levels at the Fresno Drummond site located in Central SJV.

SUPPLEMENTAL MATERIALS

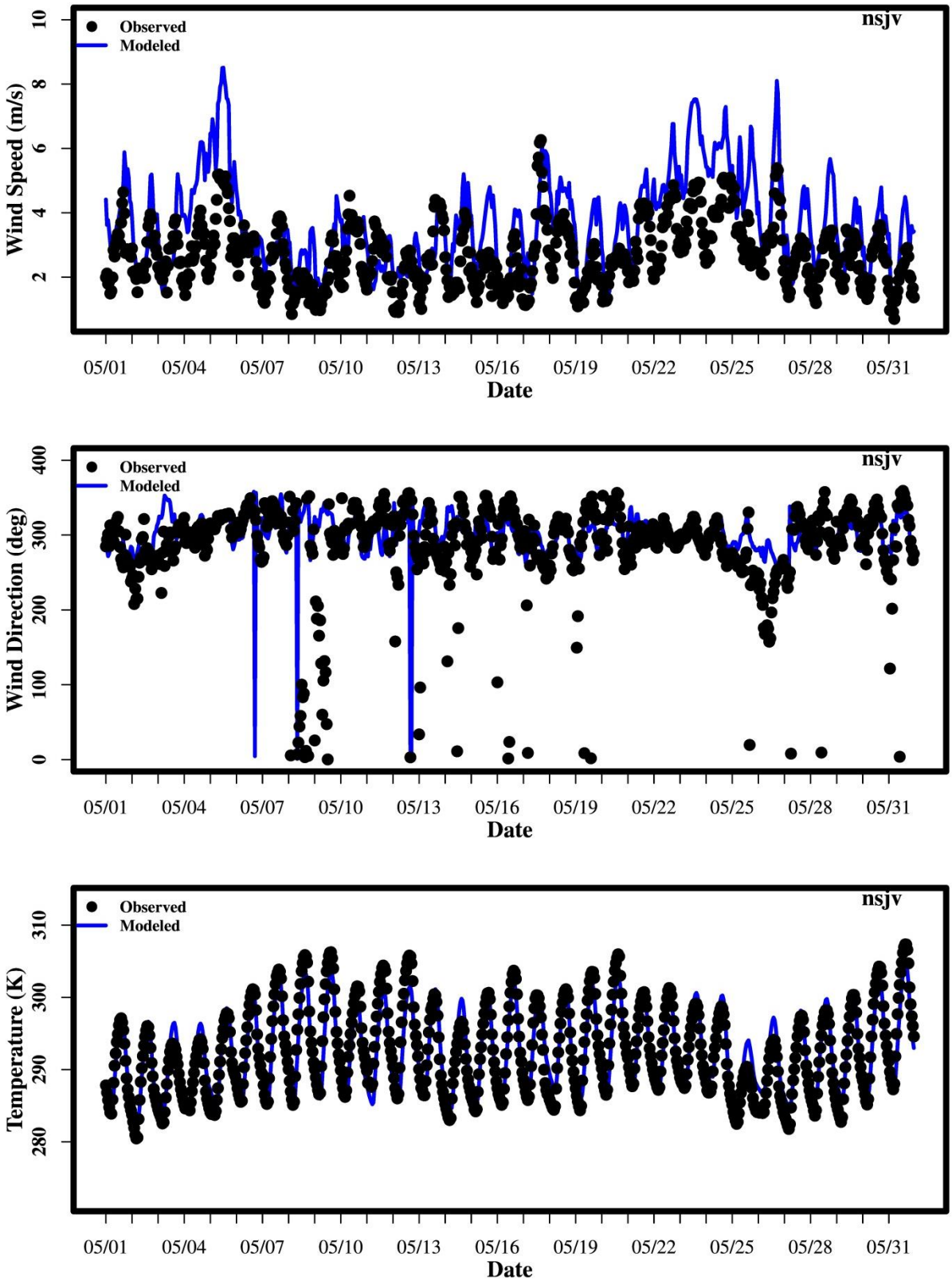

Figure S. 1 Time series of wind speed, direction, and temperature for the Northern San Joaquin Valley in May 2012.

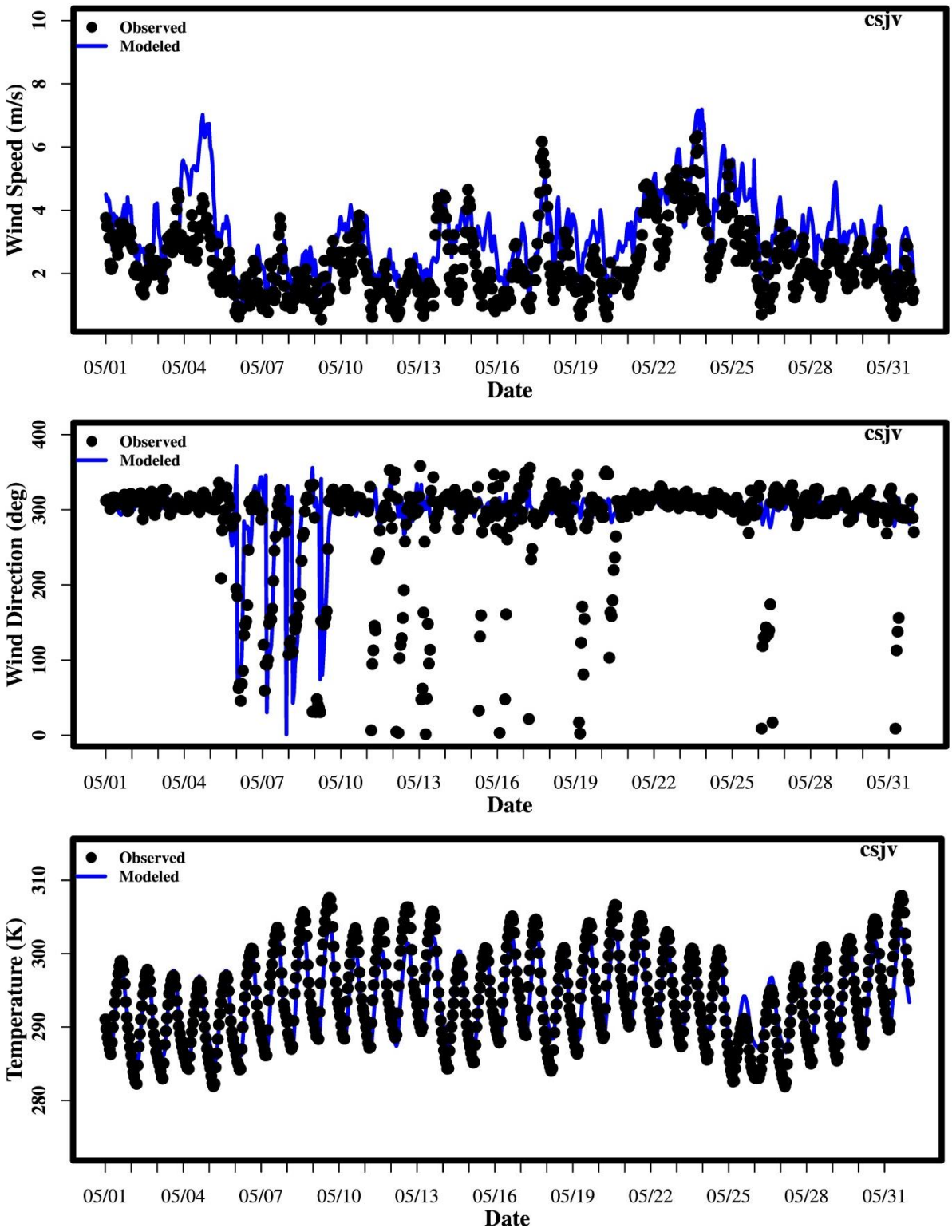

Figure S. 2 Time series of wind speed, direction, and temperature for the Central San Joaquin Valley in May 2012.

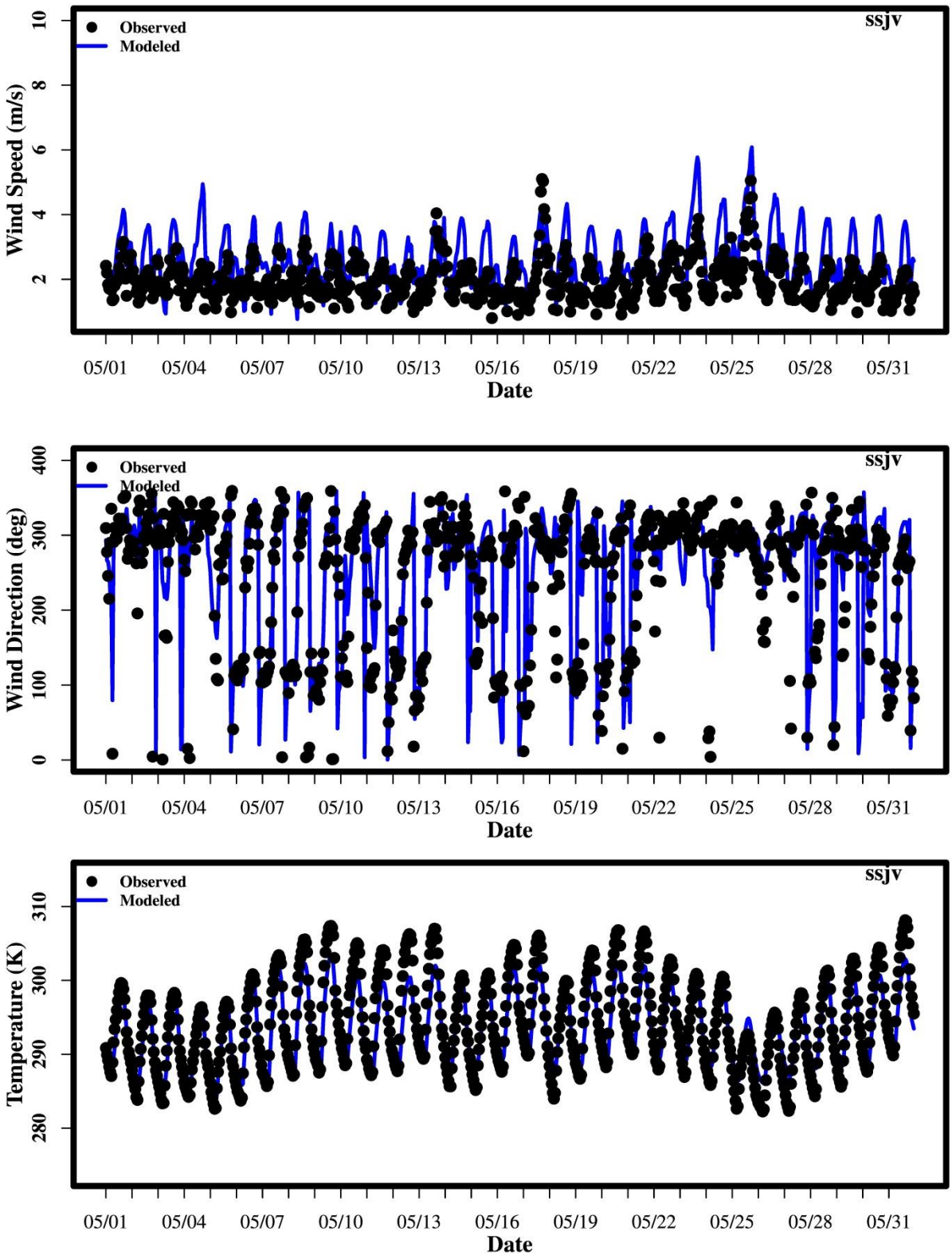

Figure S. 3 Time series of wind speed, direction, and temperature for the Southern San Joaquin Valley in May 2012.

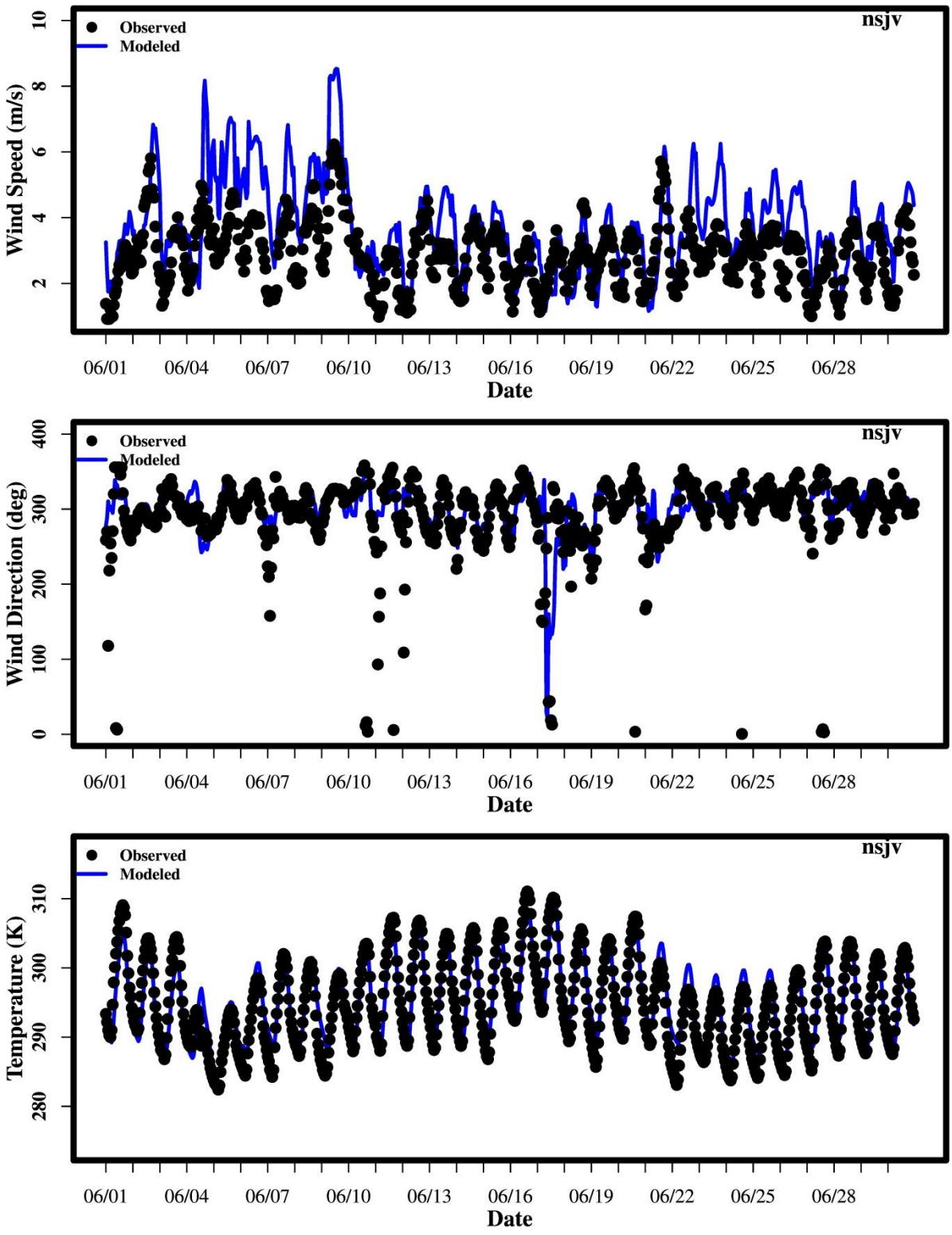

Figure S. 4 Time series of wind speed, direction, and temperature for the Northern San Joaquin Valley in June 2012.

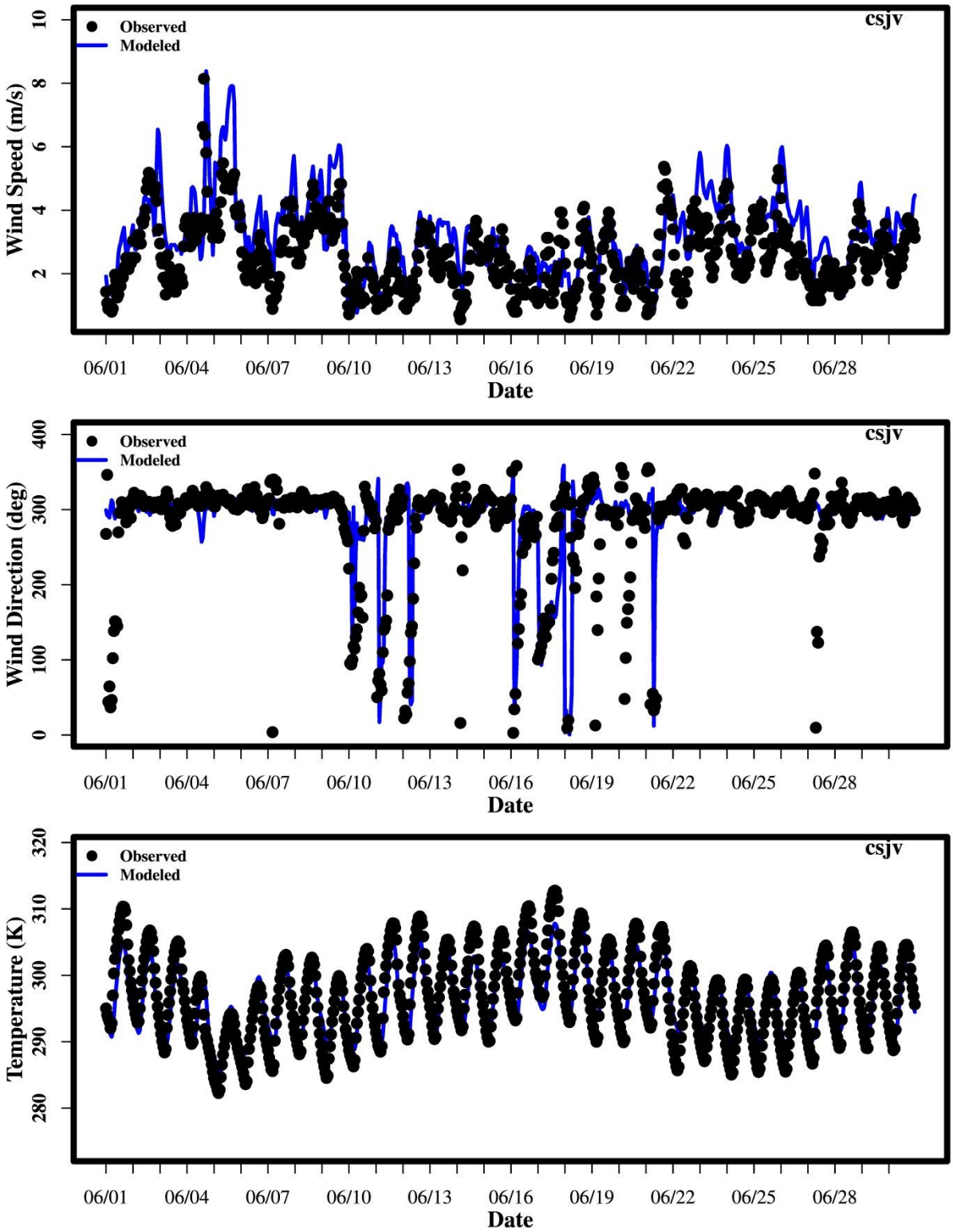

Figure S. 5 Time series of wind speed, direction, and temperature for the Central San Joaquin Valley in June 2012.

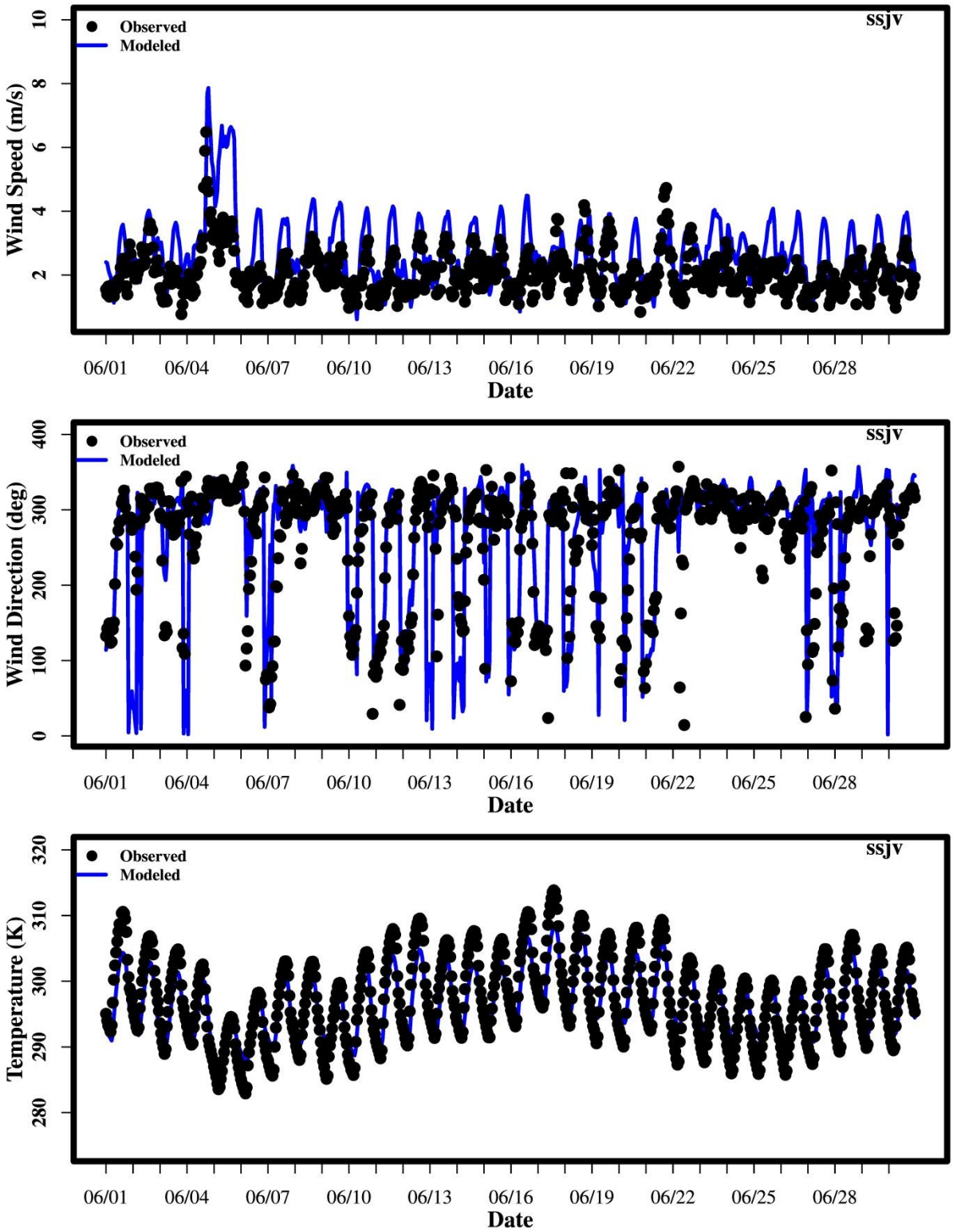

Figure S. 6 Time series of wind speed, direction, and temperature for the Southern San Joaquin Valley in June 2012.

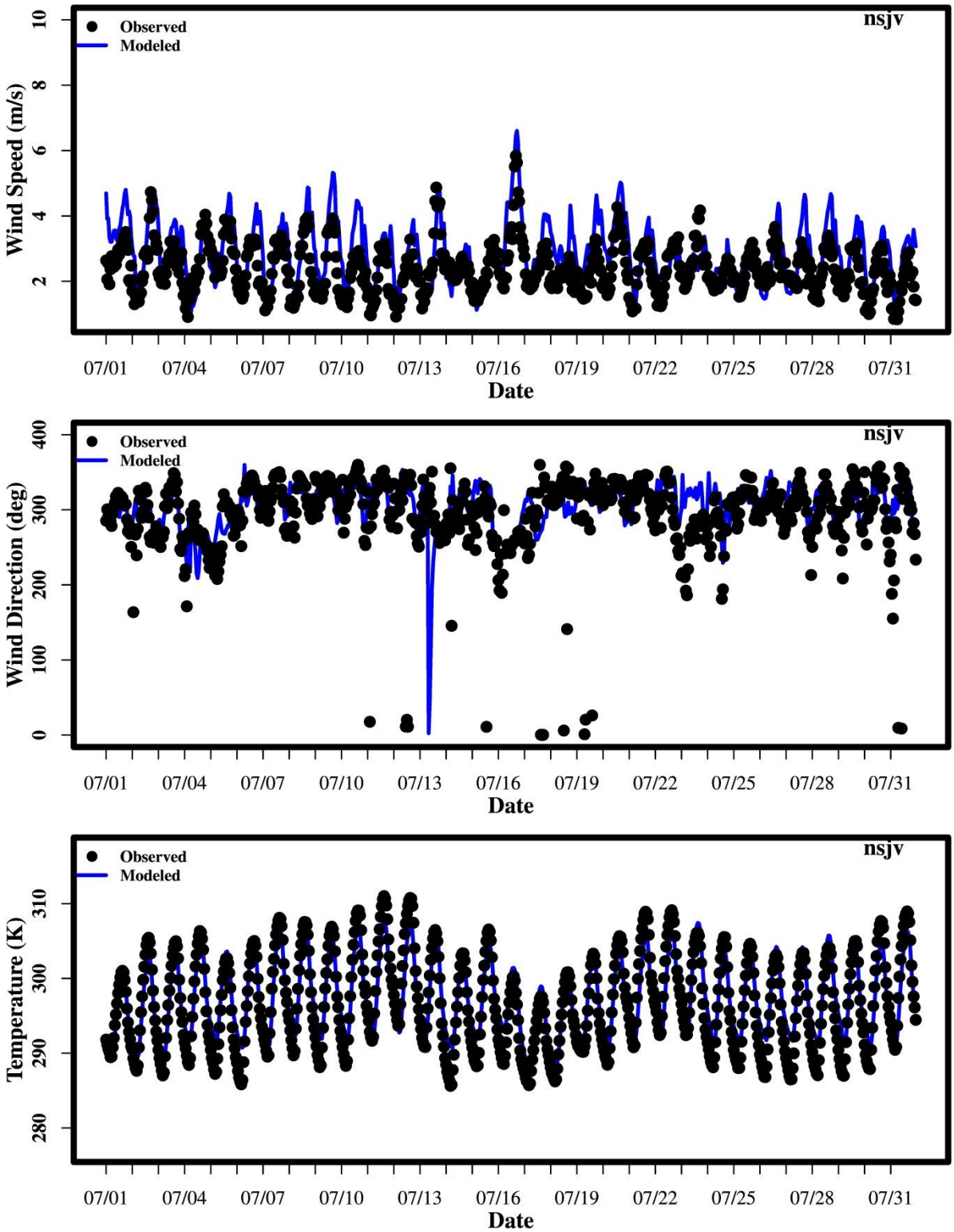

Figure S. 7 Time series of wind speed, direction, and temperature for the Northern San Joaquin Valley in July 2012.

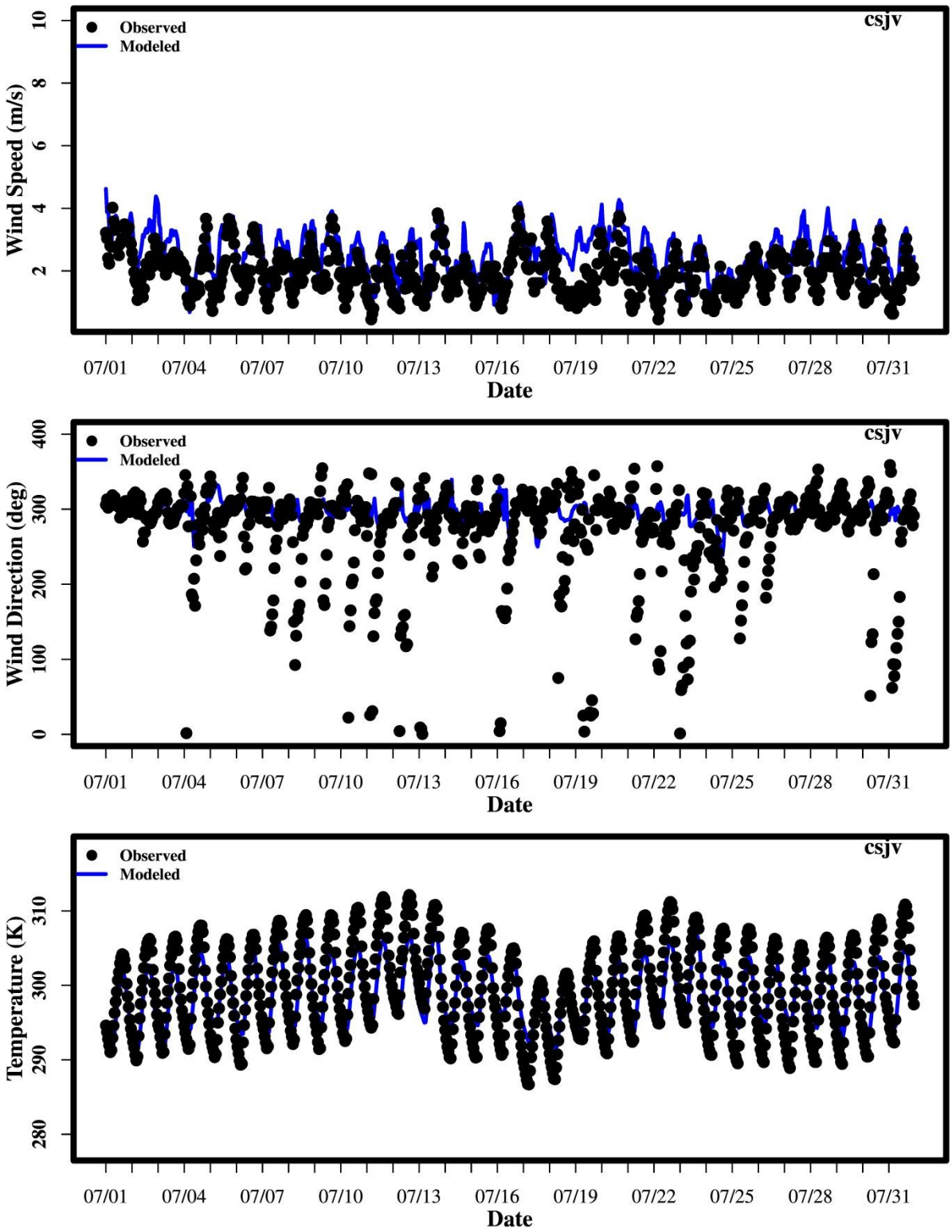

Figure S. 8 Time series of wind speed, direction, and temperature for the Central San Joaquin Valley in July 2012.

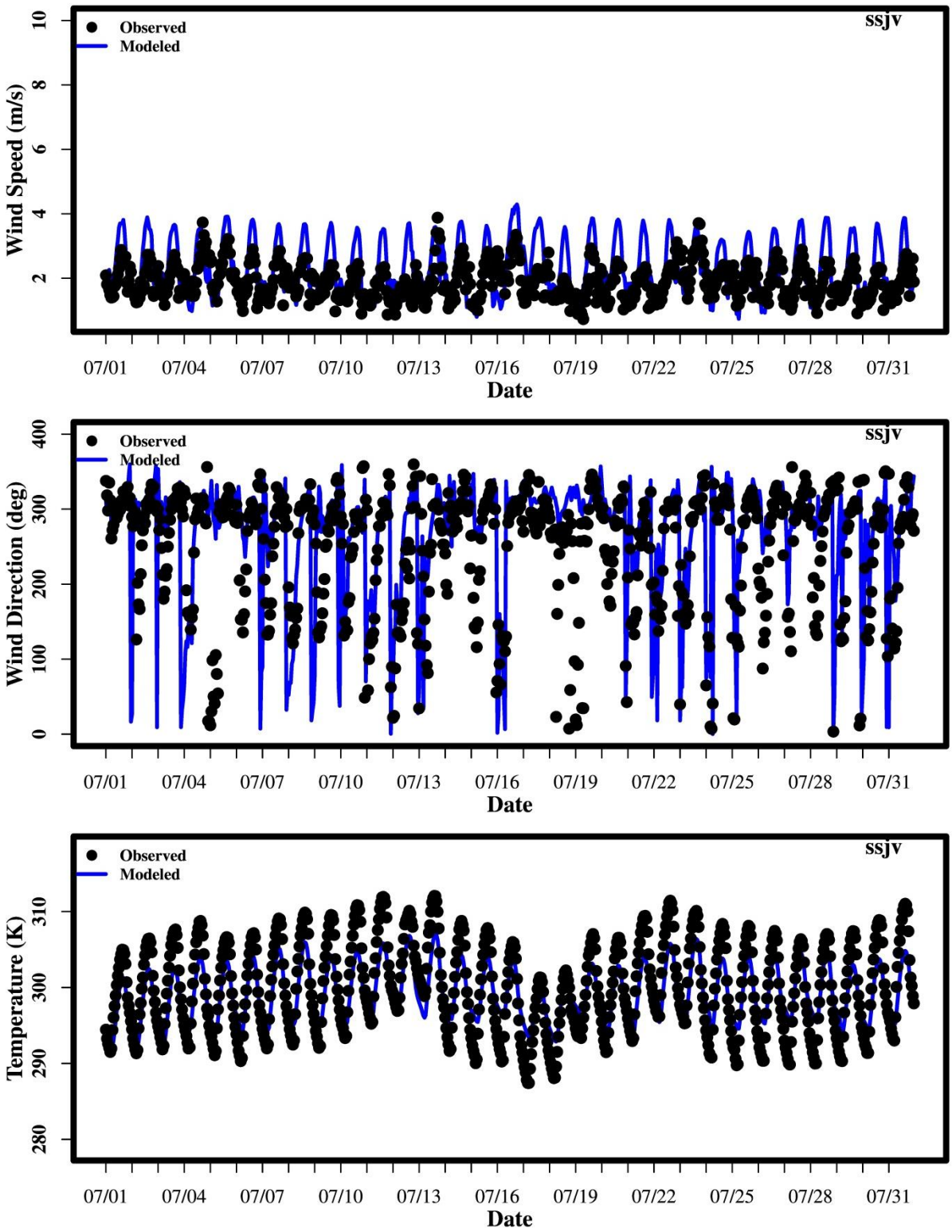

Figure S. 9 Time series of wind speed, direction, and temperature for the Southern San Joaquin Valley in July 2012.

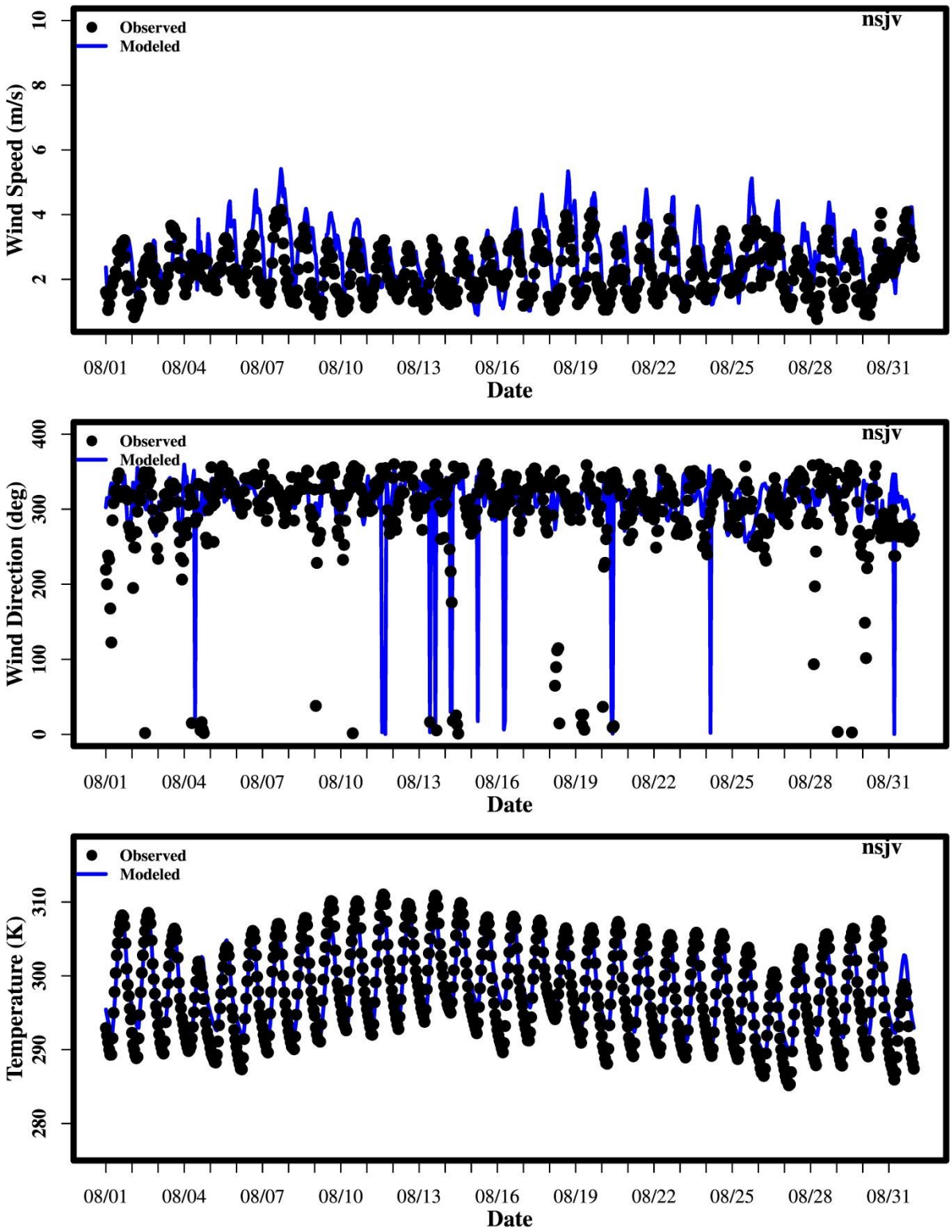

Figure S. 10 Time series of wind speed, direction, and temperature for the Northern San Joaquin Valley in August 2012.

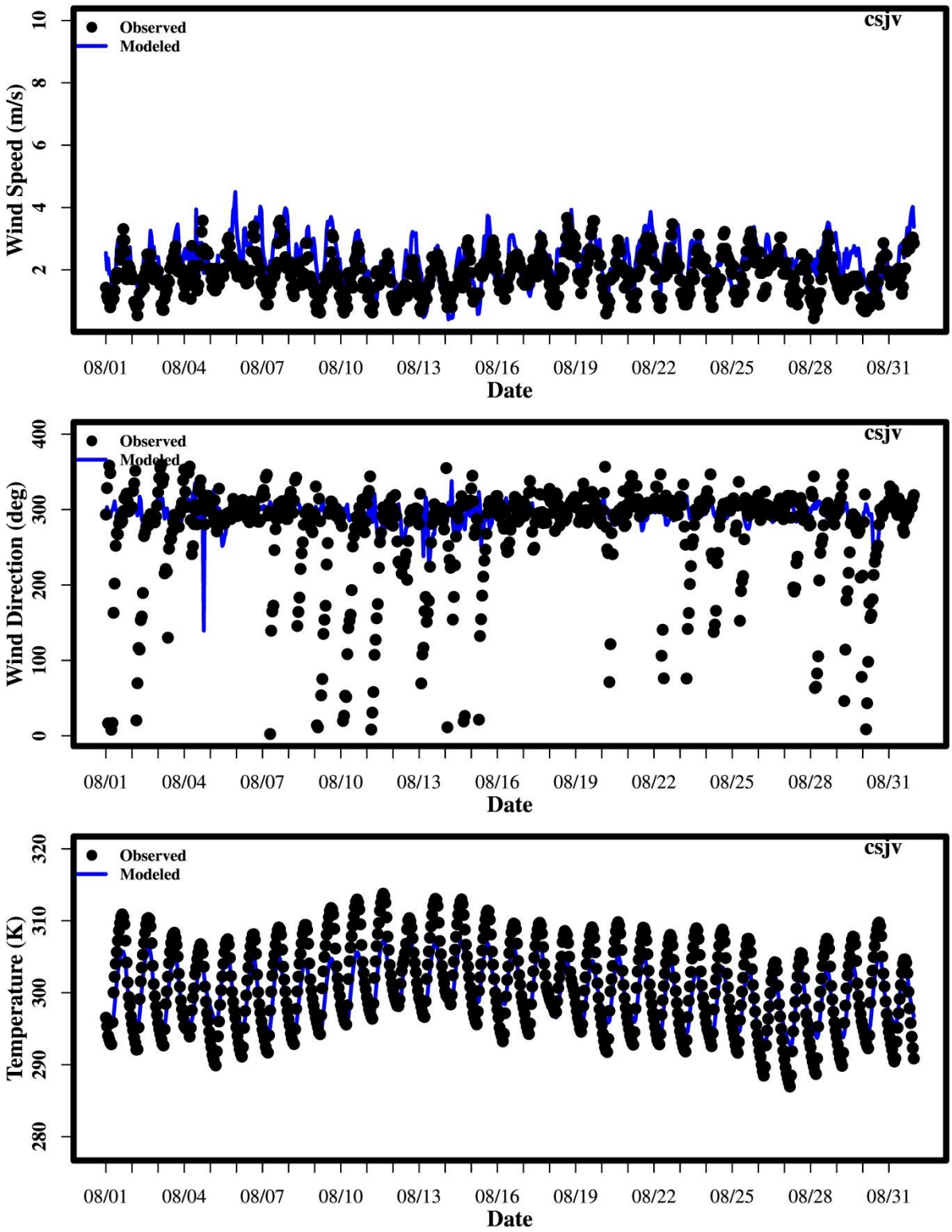

Figure S. 11 Time series of wind speed, direction, and temperature for the Central San Joaquin Valley in August 2012.

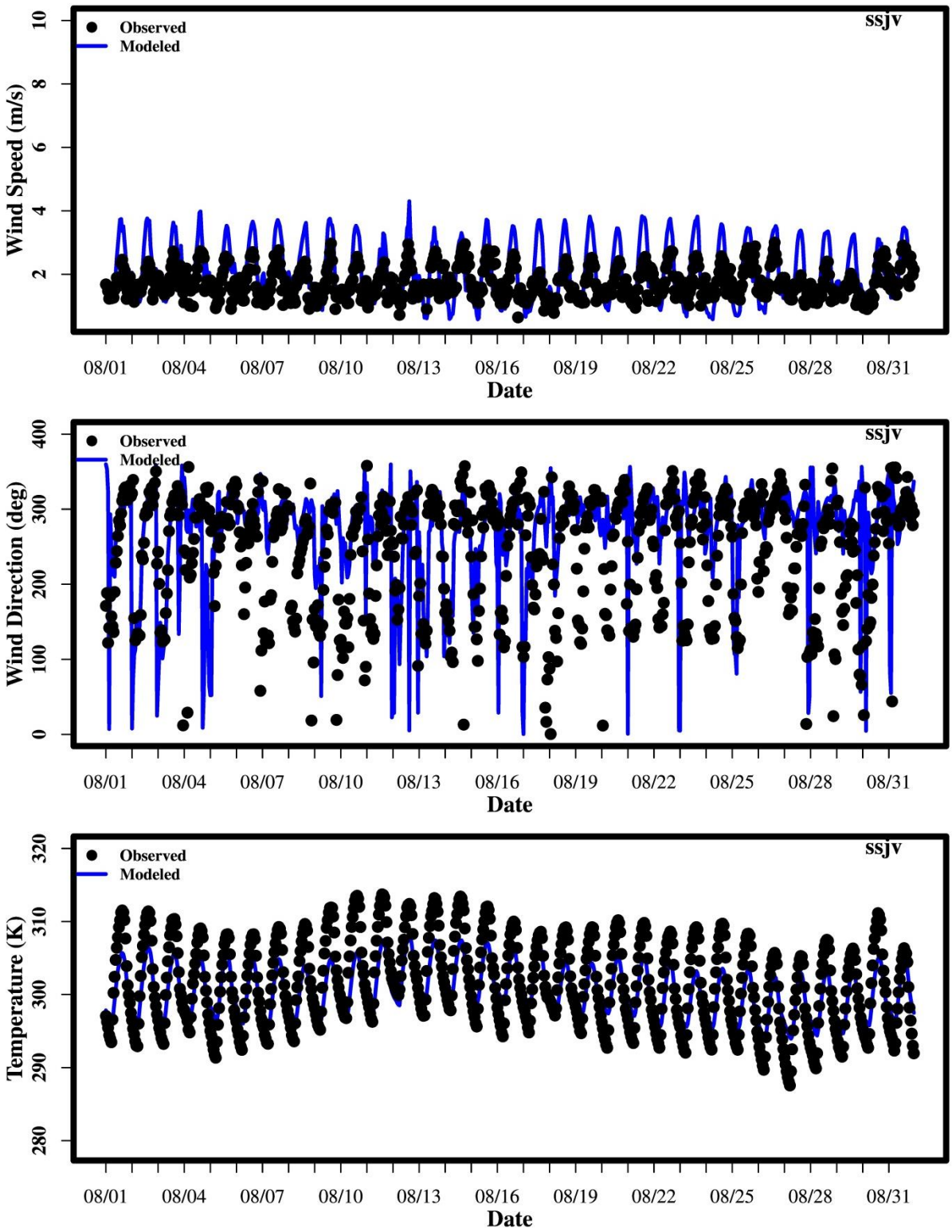

Figure S. 12 Time series of wind speed, direction, and temperature for the Southern San Joaquin Valley in August 2012.

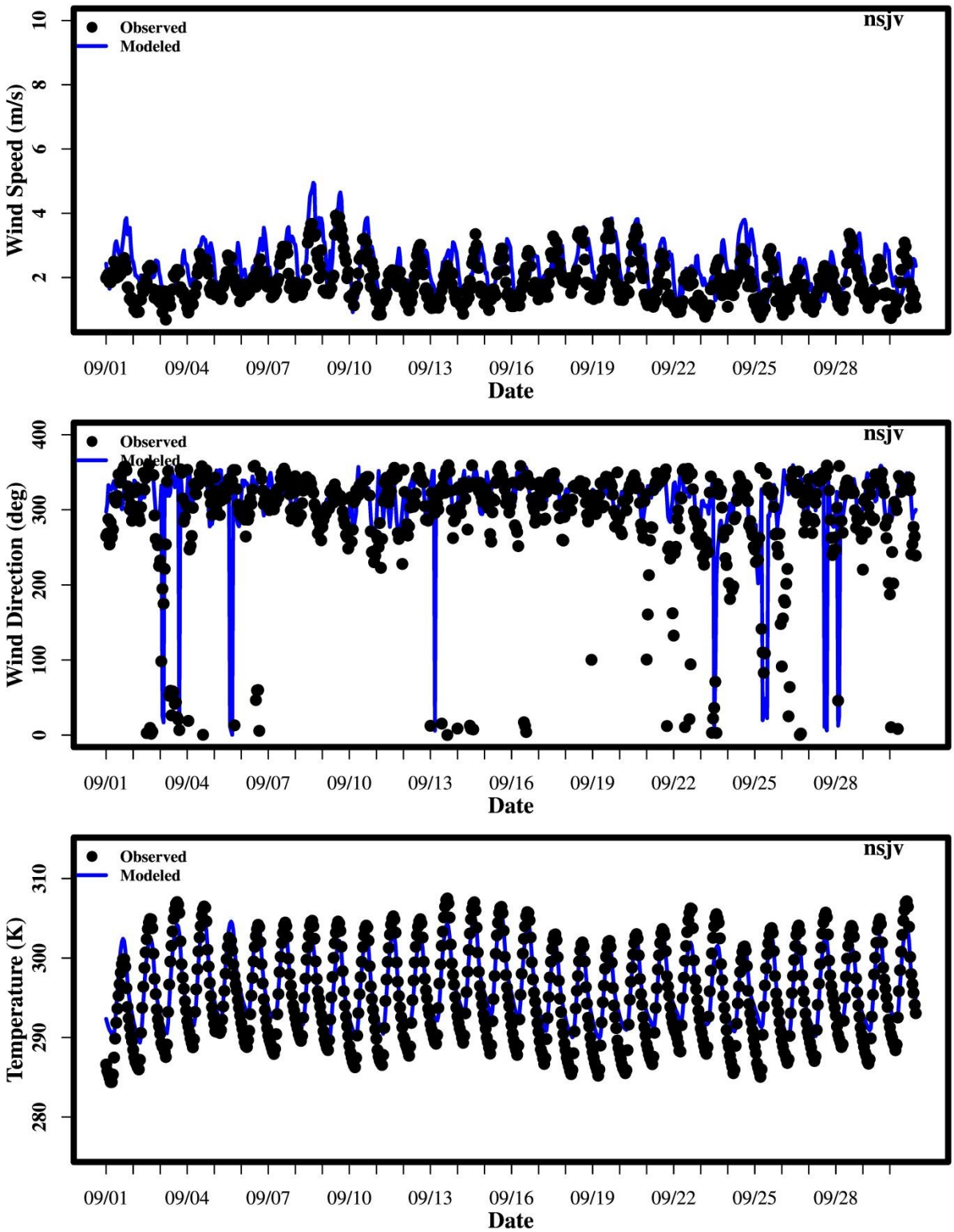

Figure S. 13 Time series of wind speed, direction, and temperature for the Northern San Joaquin Valley in September 2012.

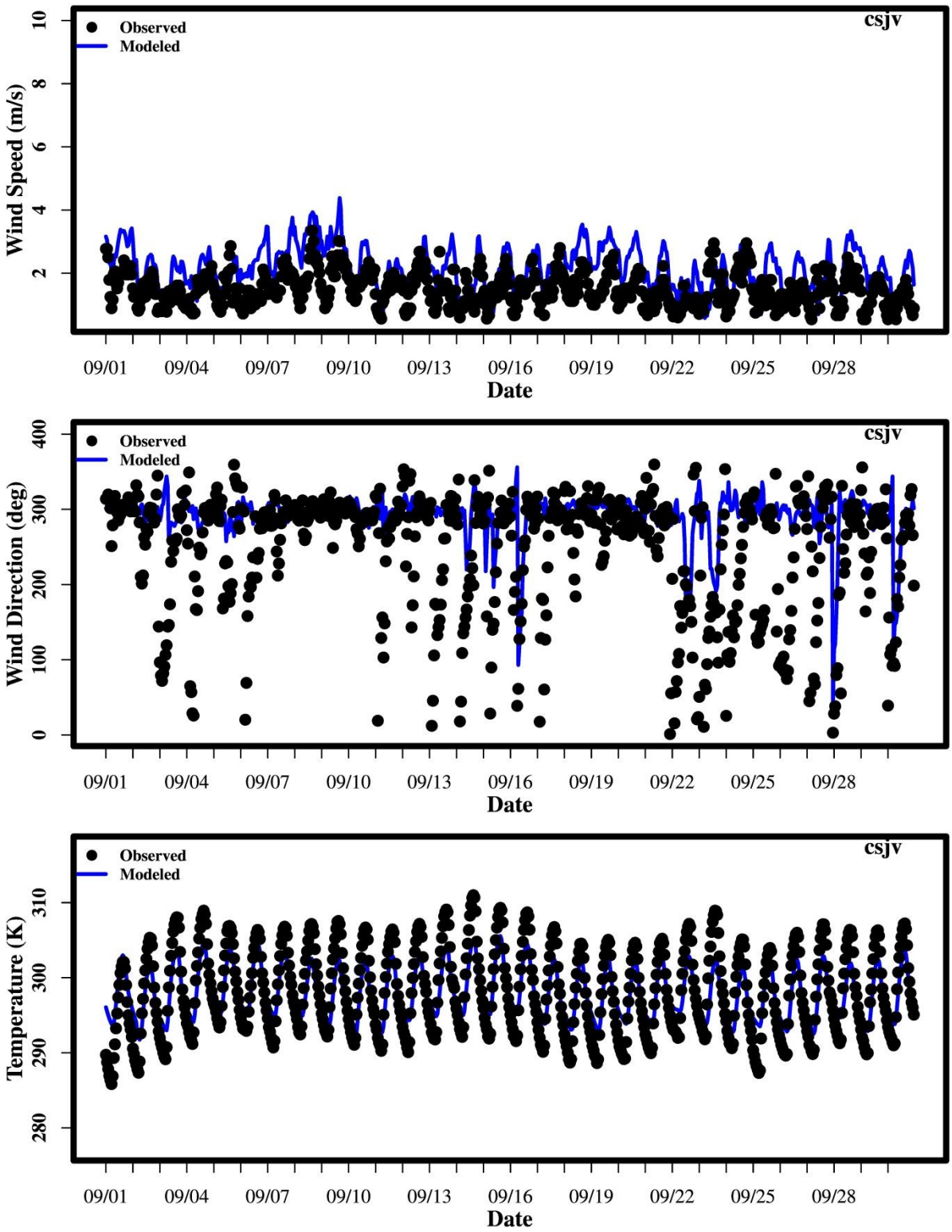

Figure S. 14 Time series of wind speed, direction, and temperature for the Central San Joaquin Valley in September 2012.

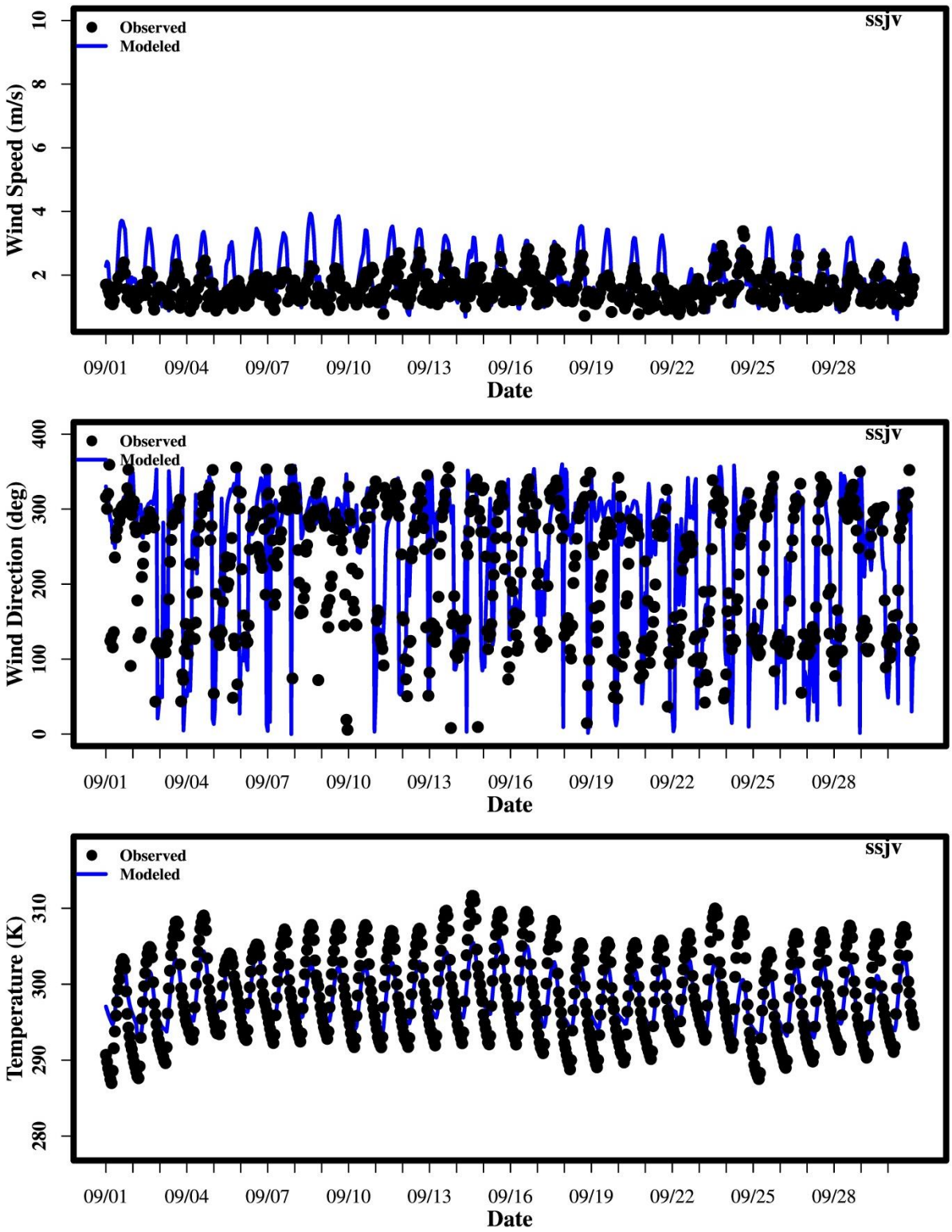

Figure S. 15 Time series of wind speed, direction, and temperature for the Southern San Joaquin Valley in September 2012.

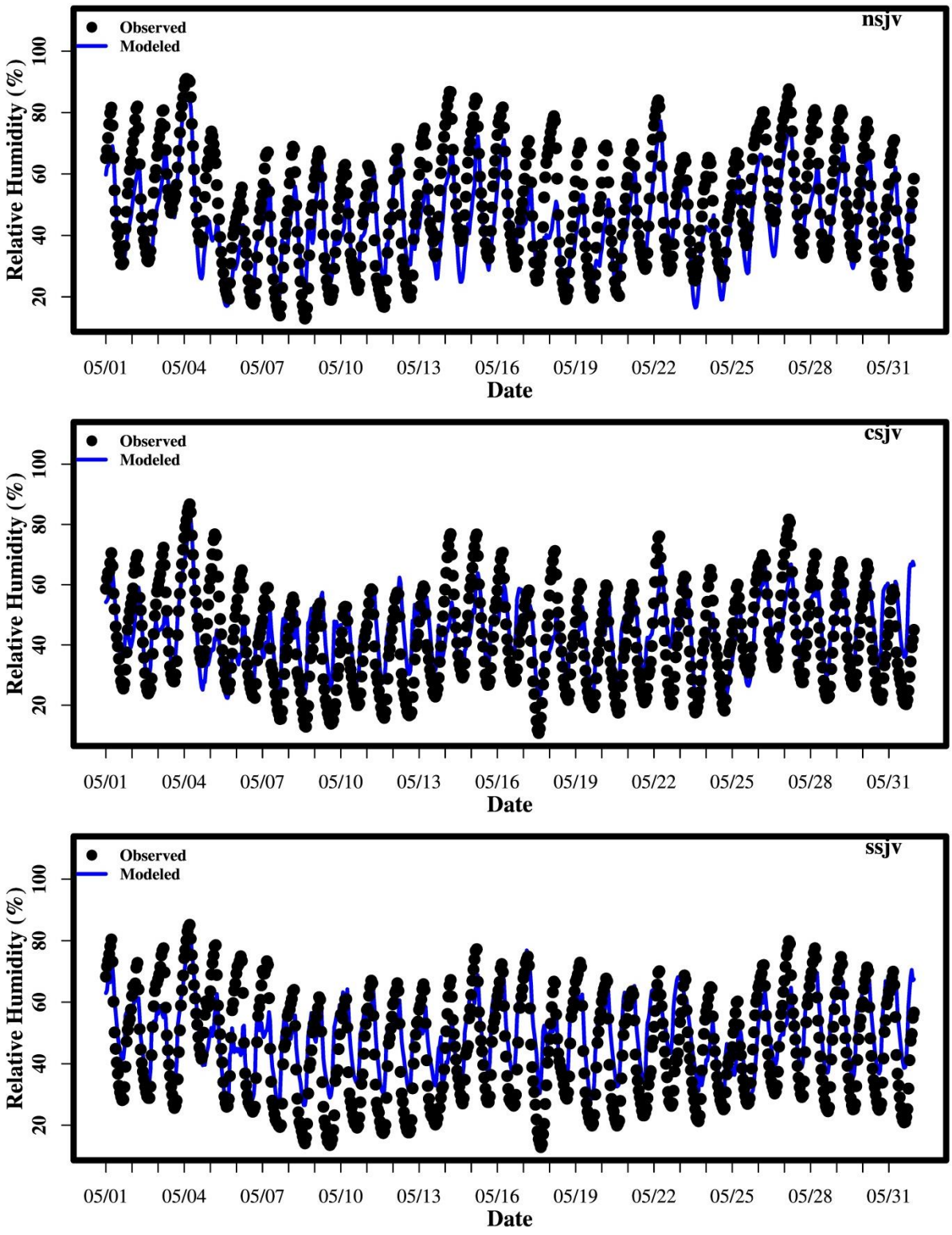

Figure S. 16 Time series of relative humidity for the (top) Northern SJV, (middle) Central SJV, and (bottom) Southern SJV in May 2012.

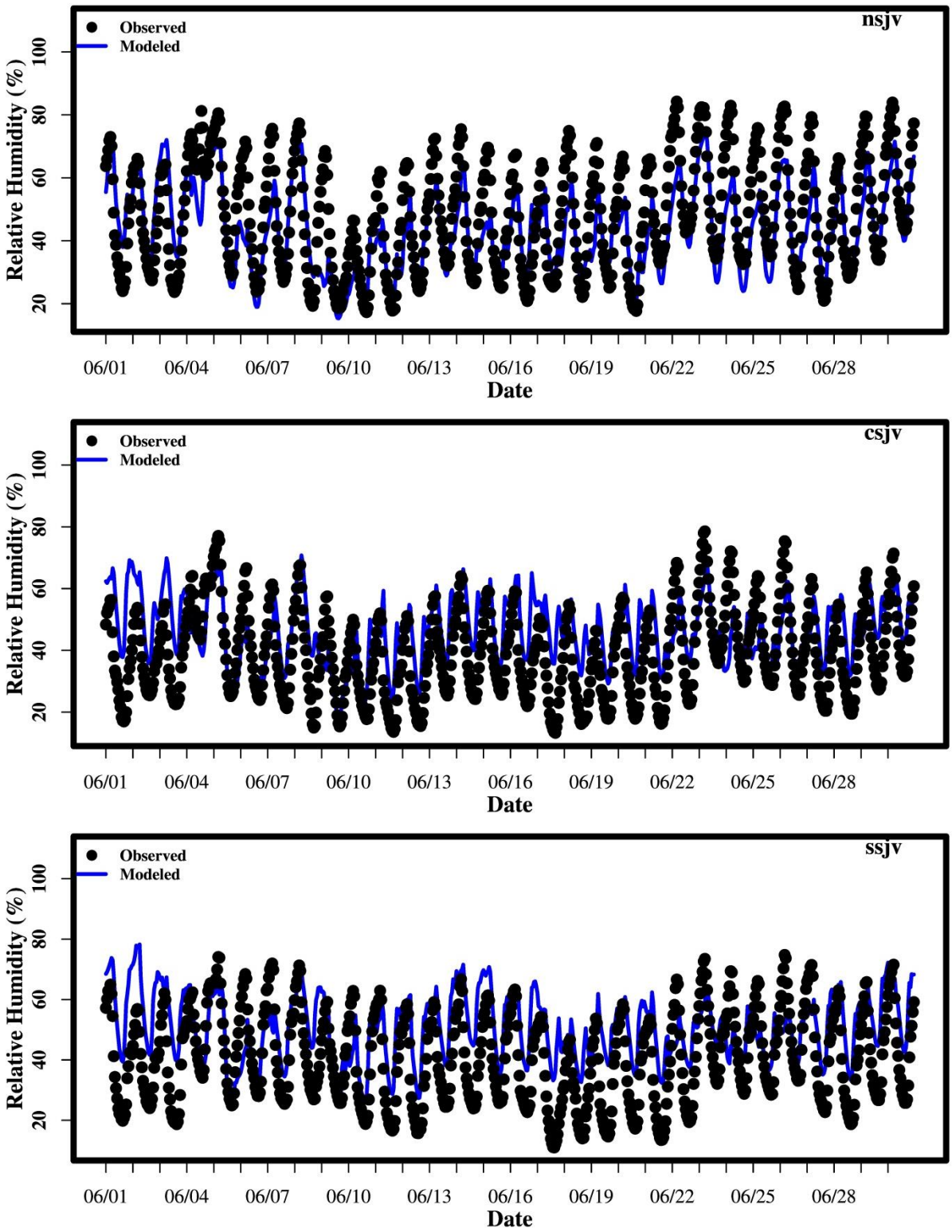

Figure S. 17 Time series of relative humidity for the (top) Northern SJV, (middle) Central SJV, and (bottom) Southern SJV in June 2012.

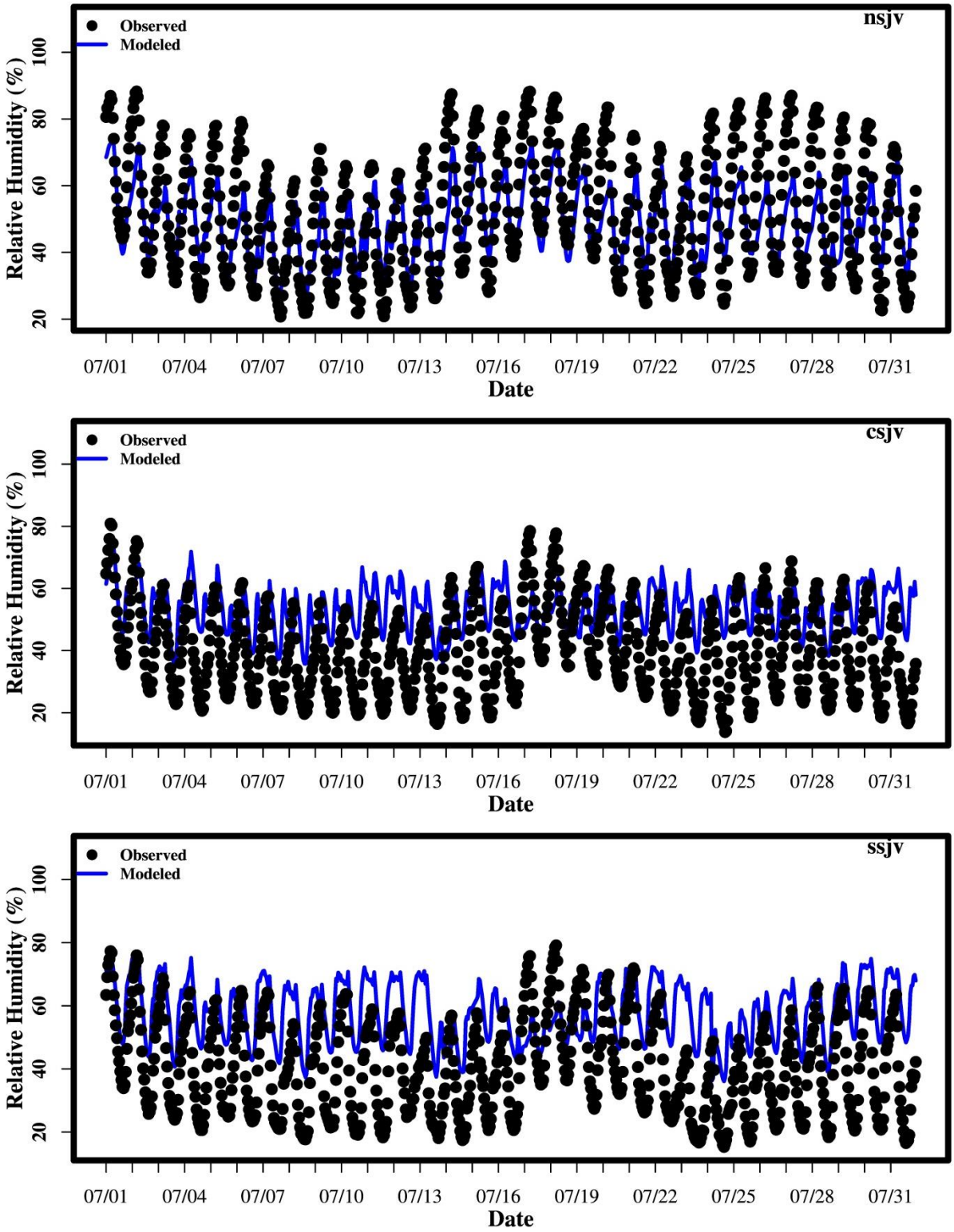

Figure S. 18 Time series of relative humidity for the (top) Northern SJV, (middle) Central SJV, and (bottom) Southern SJV in July 2012.

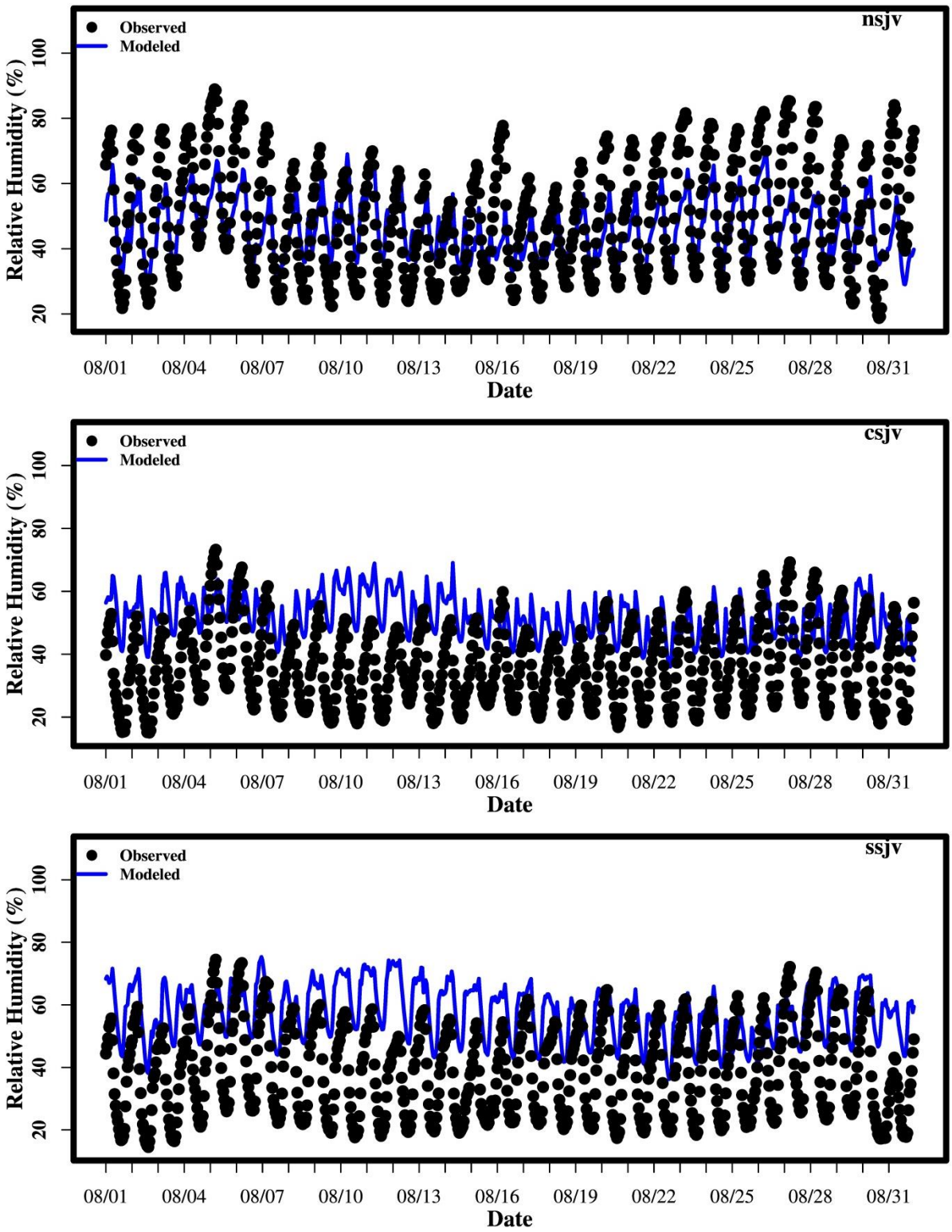

Figure S. 19 Time series of relative humidity for the (top) Northern SJV, (middle) Central SJV, and (bottom) Southern SJV in August 2012.

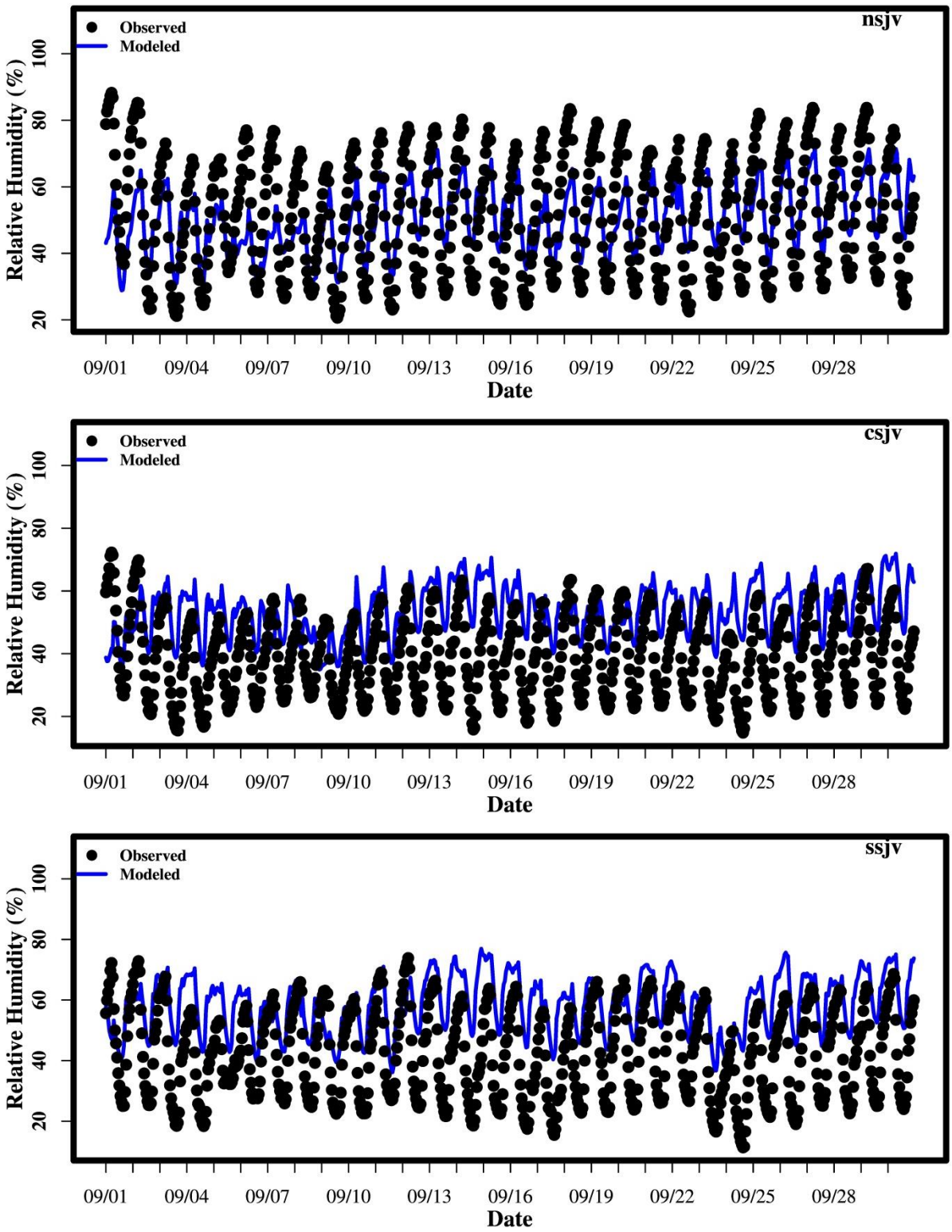

Figure S. 20 Time series of relative humidity for the (top) Northern SJV, (middle) Central SJV, and (bottom) Southern SJV in September 2012.

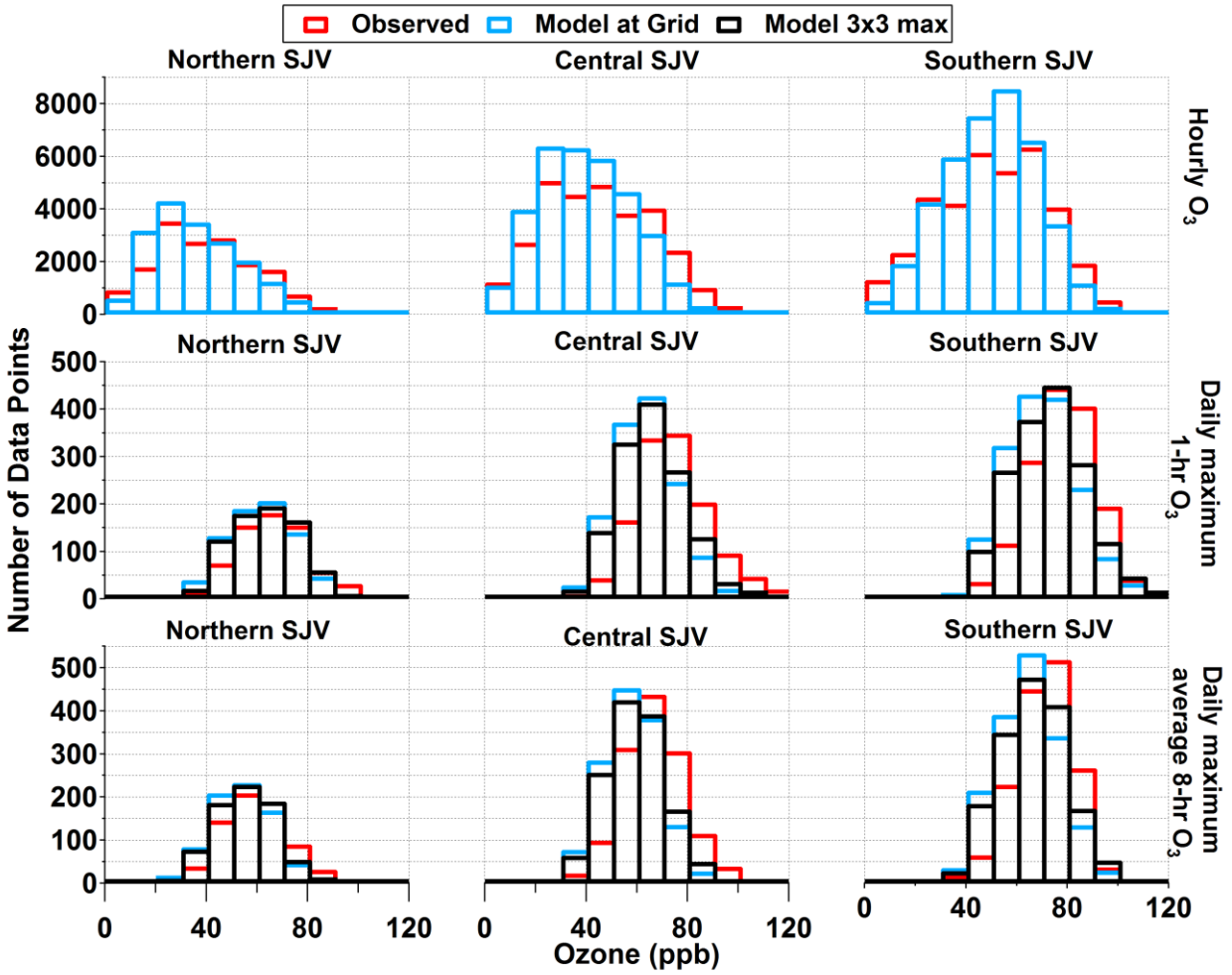

Figure S. 21 Observed and modeled ozone frequency distribution for the ozone season (May – September 2012)

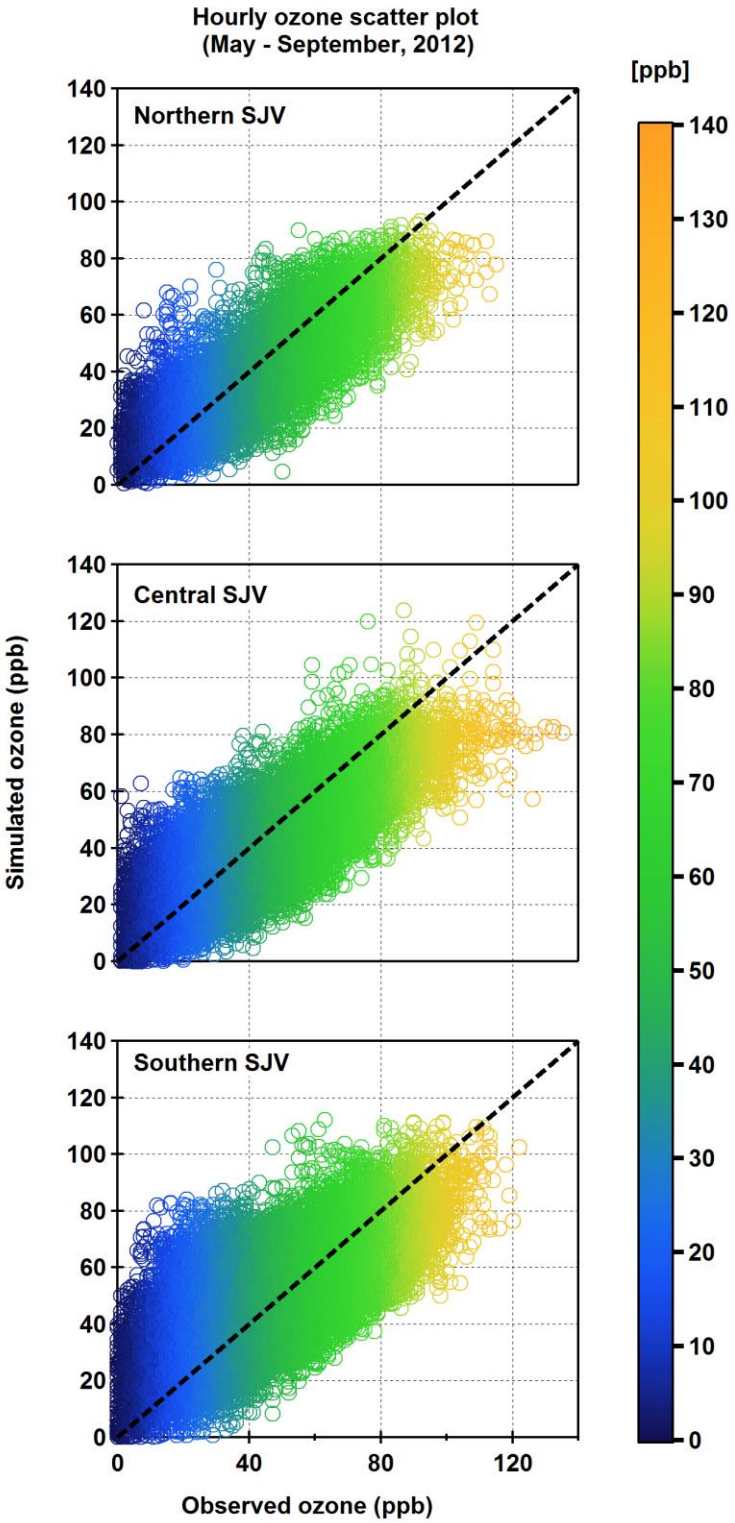

Figure S. 22 Scatter plot of hourly ozone for the ozone season (May – September 2012)

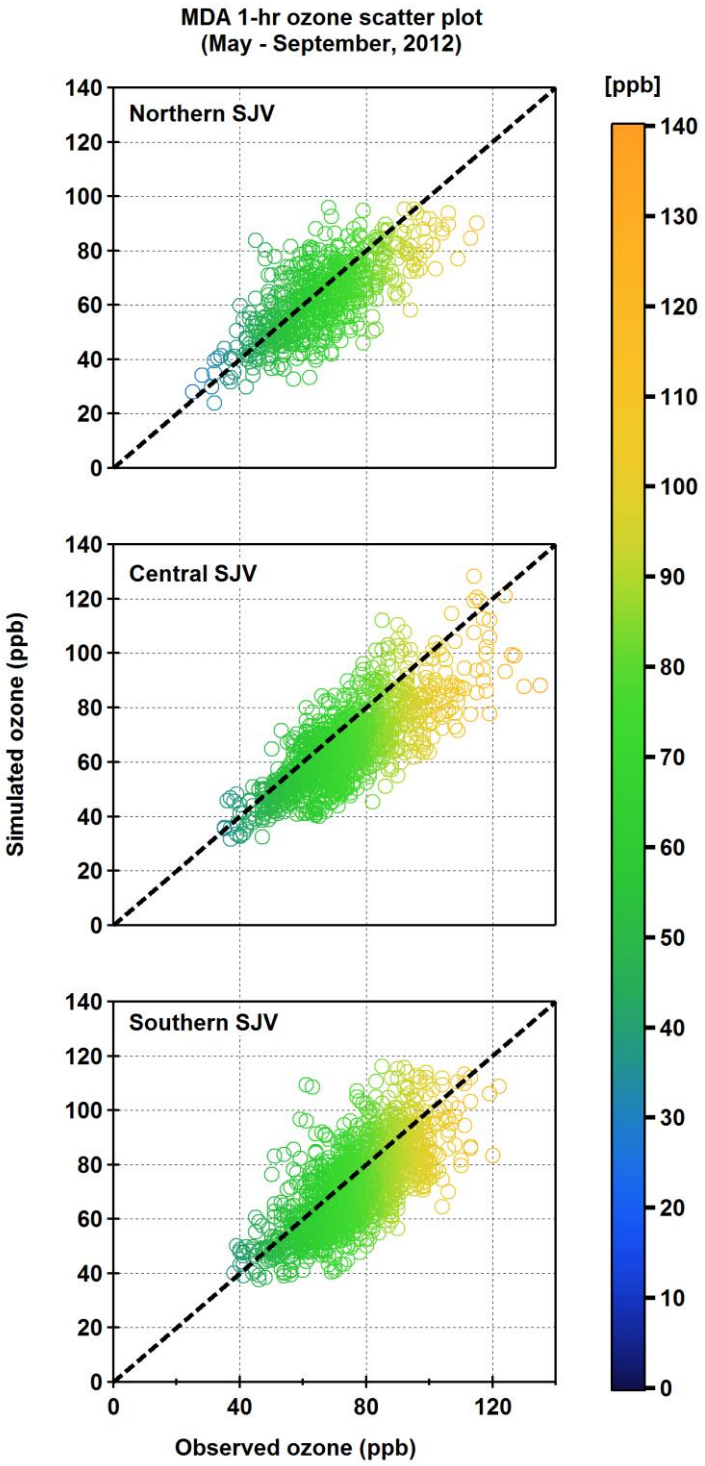

Figure S. 23 Scatter plot of daily maximum 1-hour ozone for the ozone season (May – September 2012)

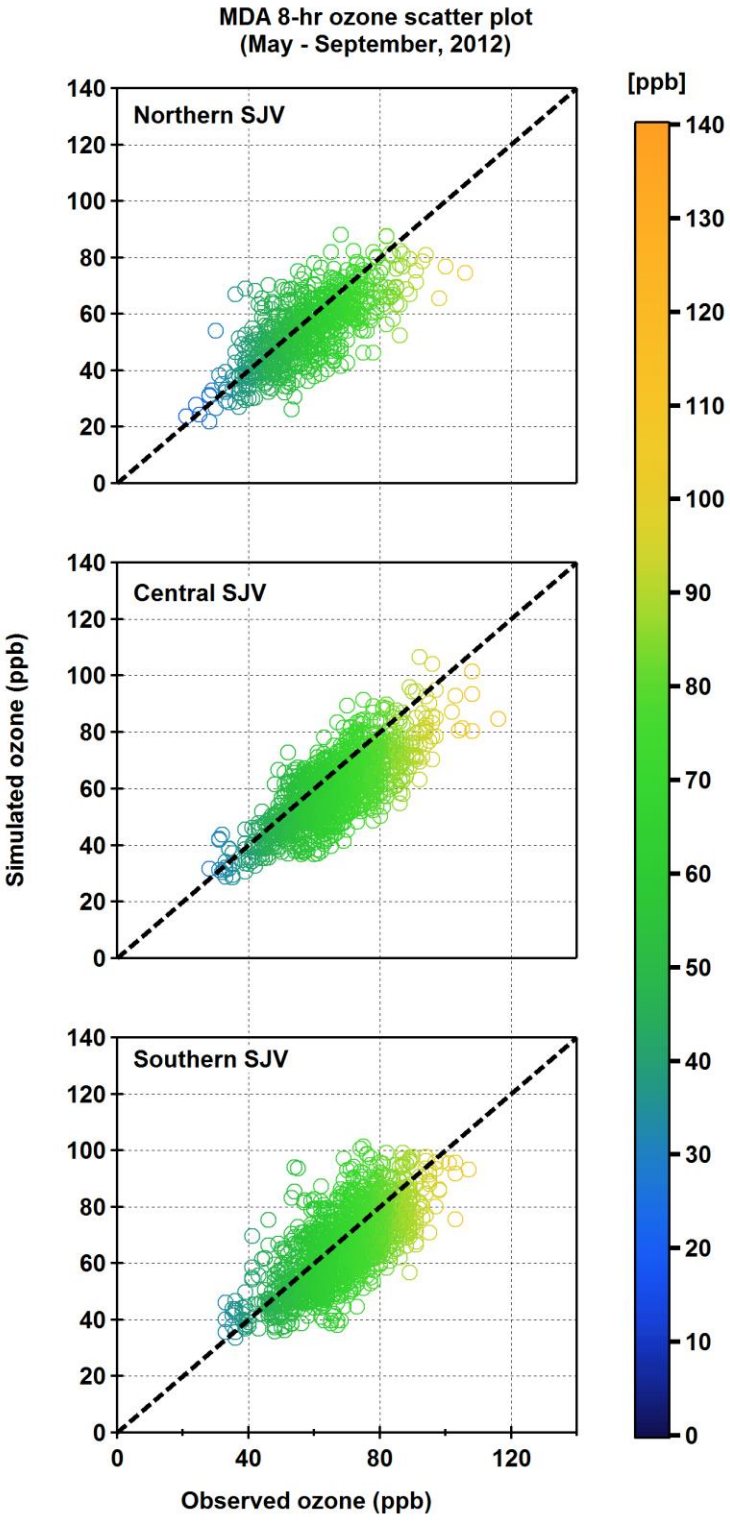

Figure S. 24 Scatter plot of daily maximum 8-hour ozone for the ozone season (May – September 2012)

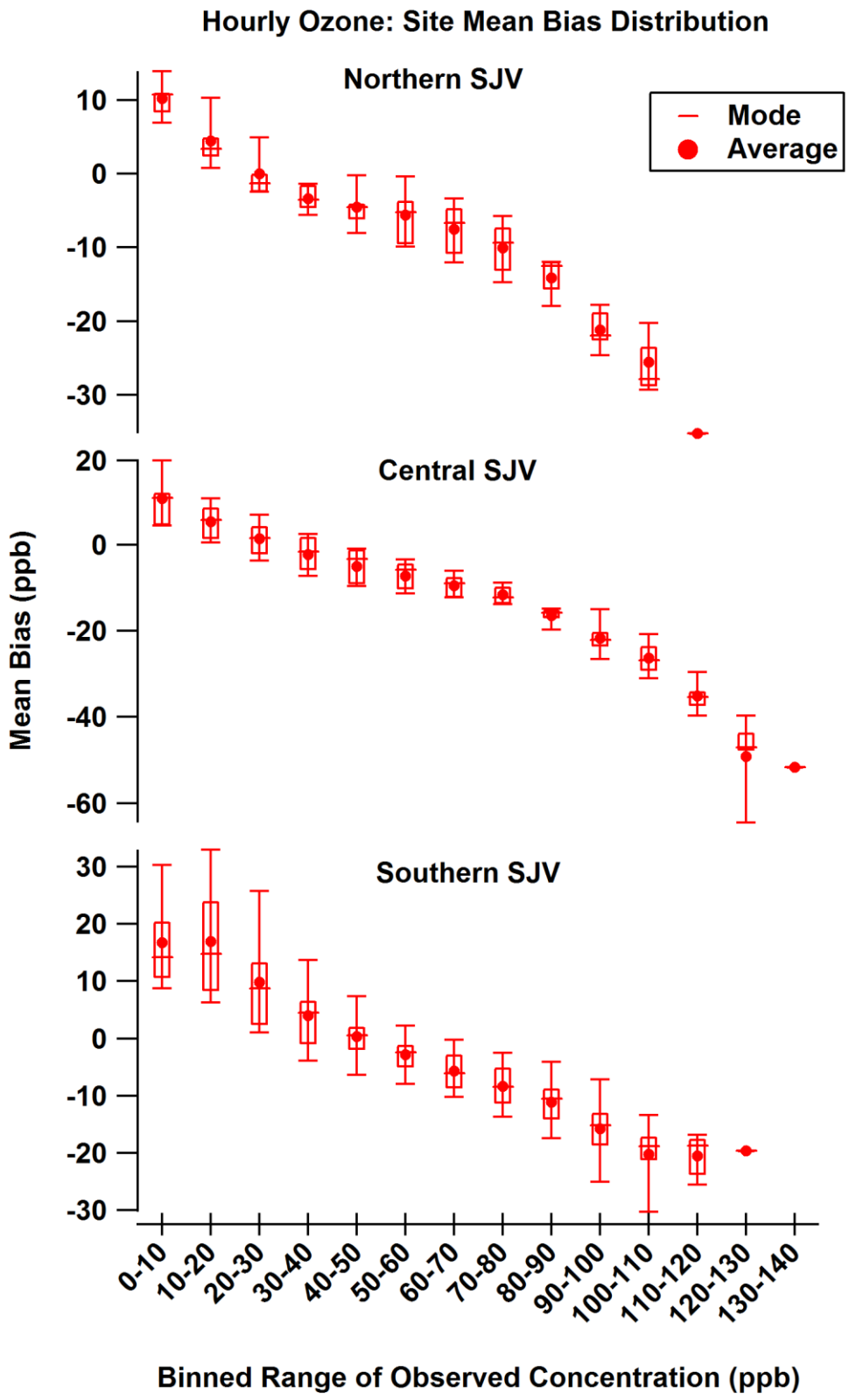

Figure S. 25 Hourly Ozone Site Mean Bias Distribution for the ozone season (May – September 2012)

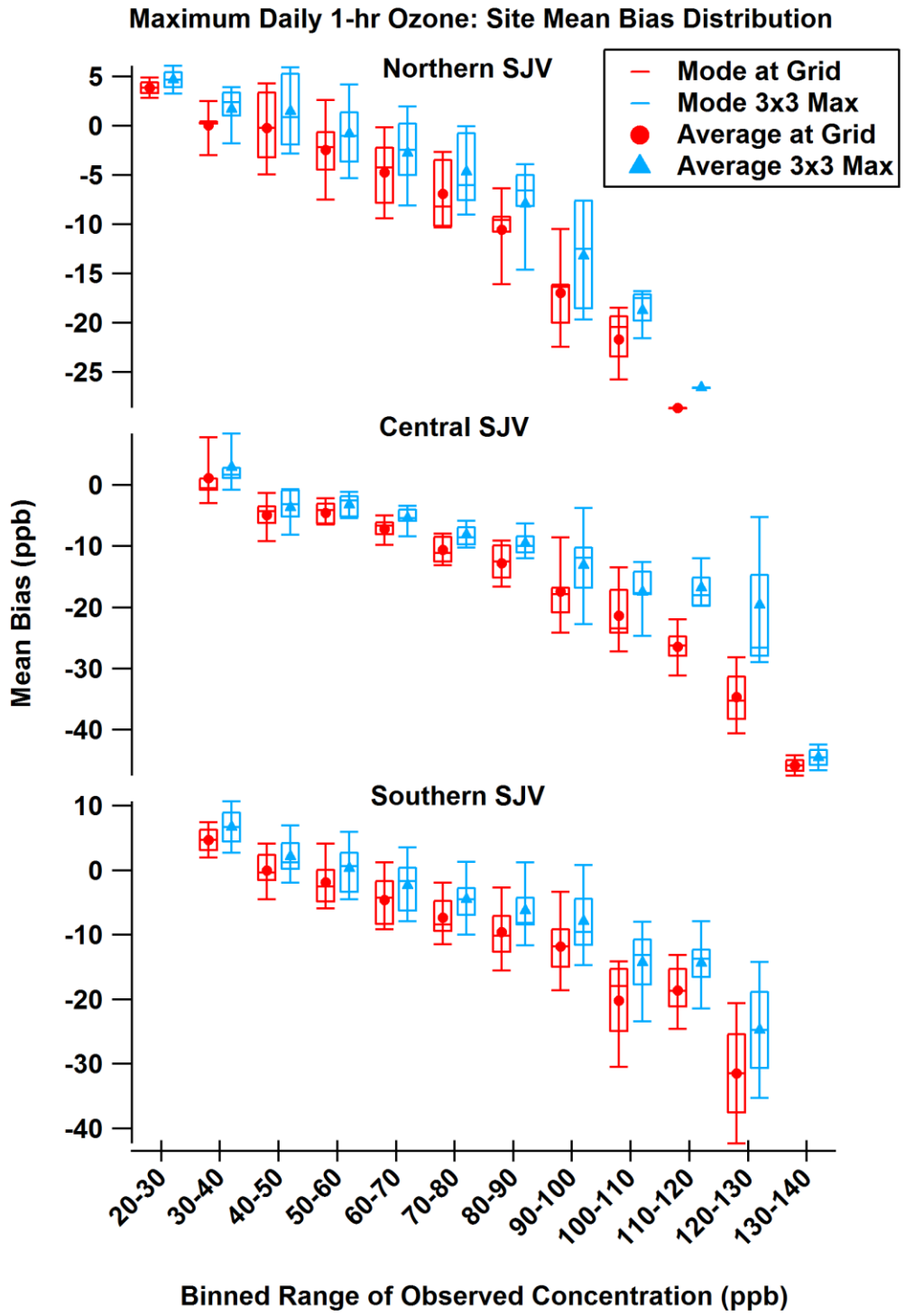

Figure S. 26 Daily Maximum 1-hour Ozone Site Mean Bias Distribution for the ozone season (May – September 2012)

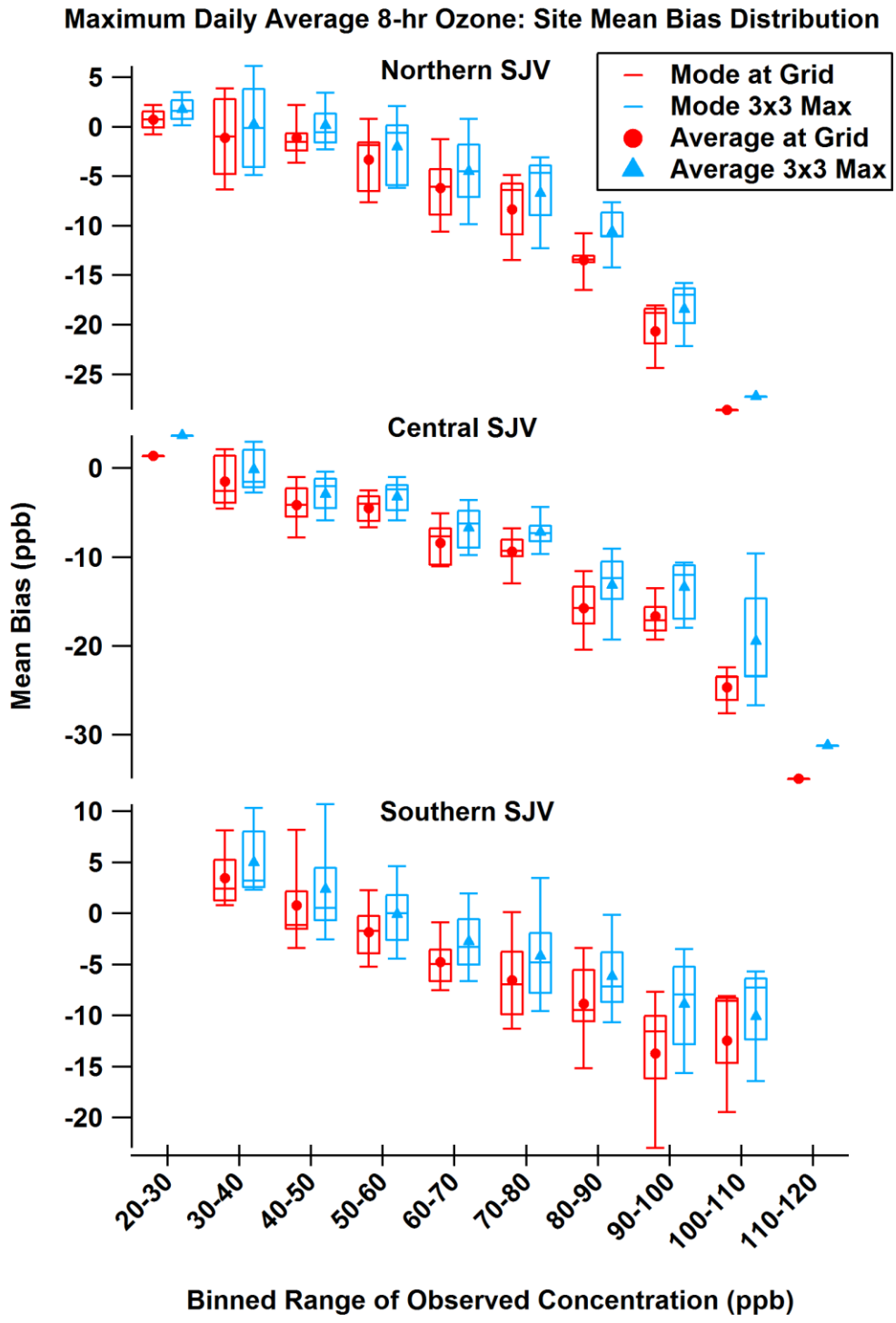

Figure S. 27 Daily Maximum Average 8-hour Ozone Site Mean Bias Distribution for the ozone season (May – September 2012)

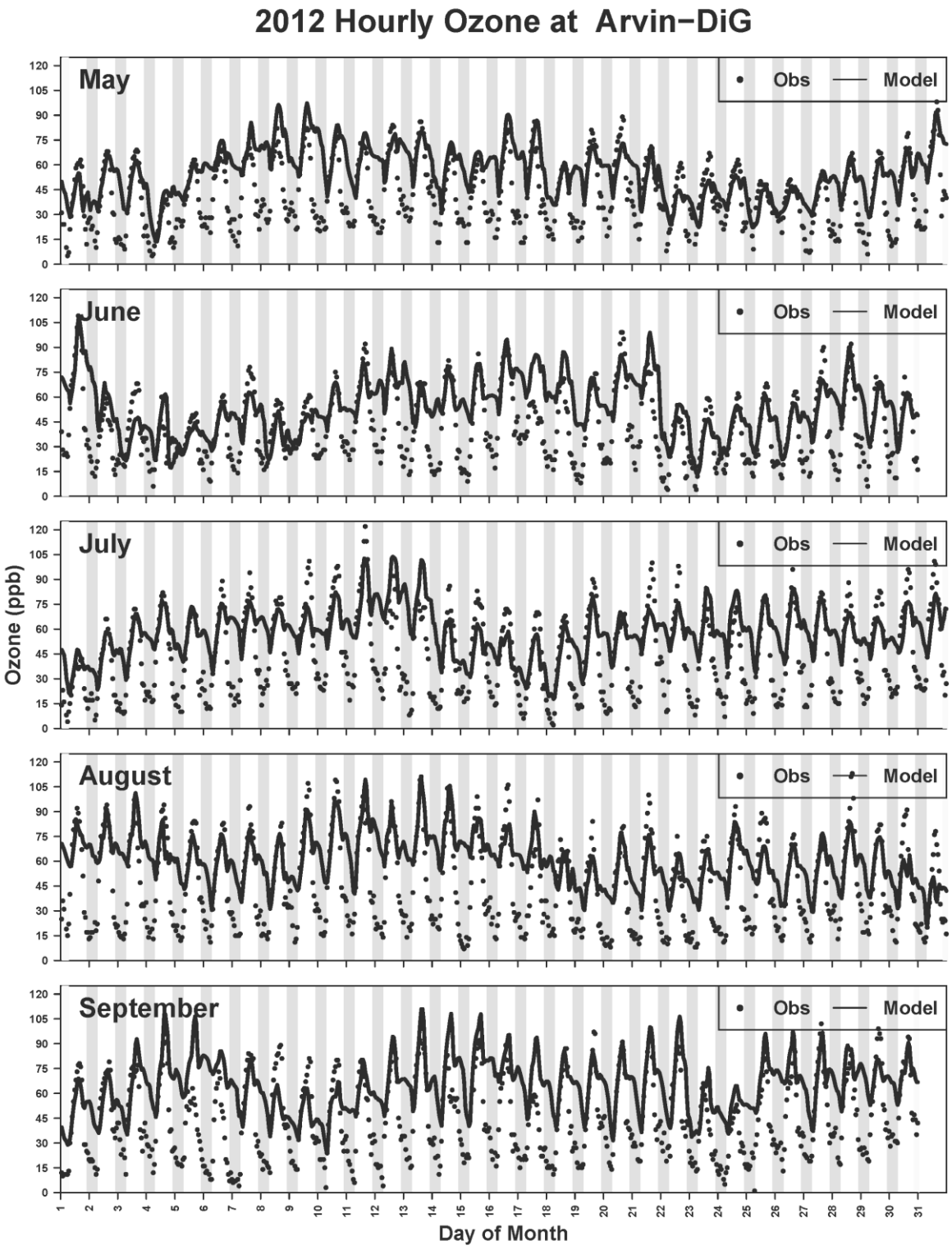

Figure S. 28 Time-series of hourly ozone at Arvin-Di Giorgio.

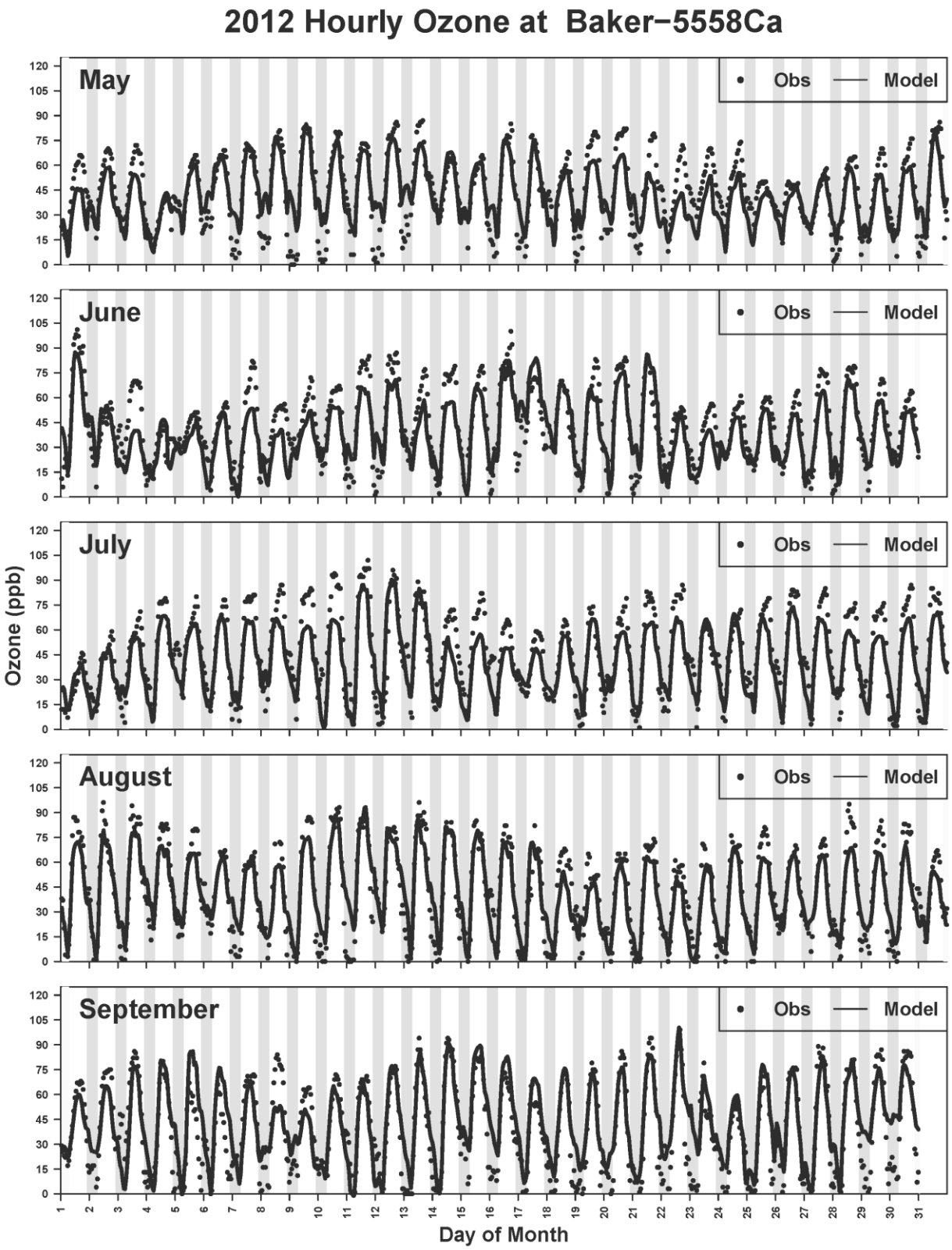

Figure S. 29 Time-series of hourly ozone at Bakersfield-5558 California Avenue.

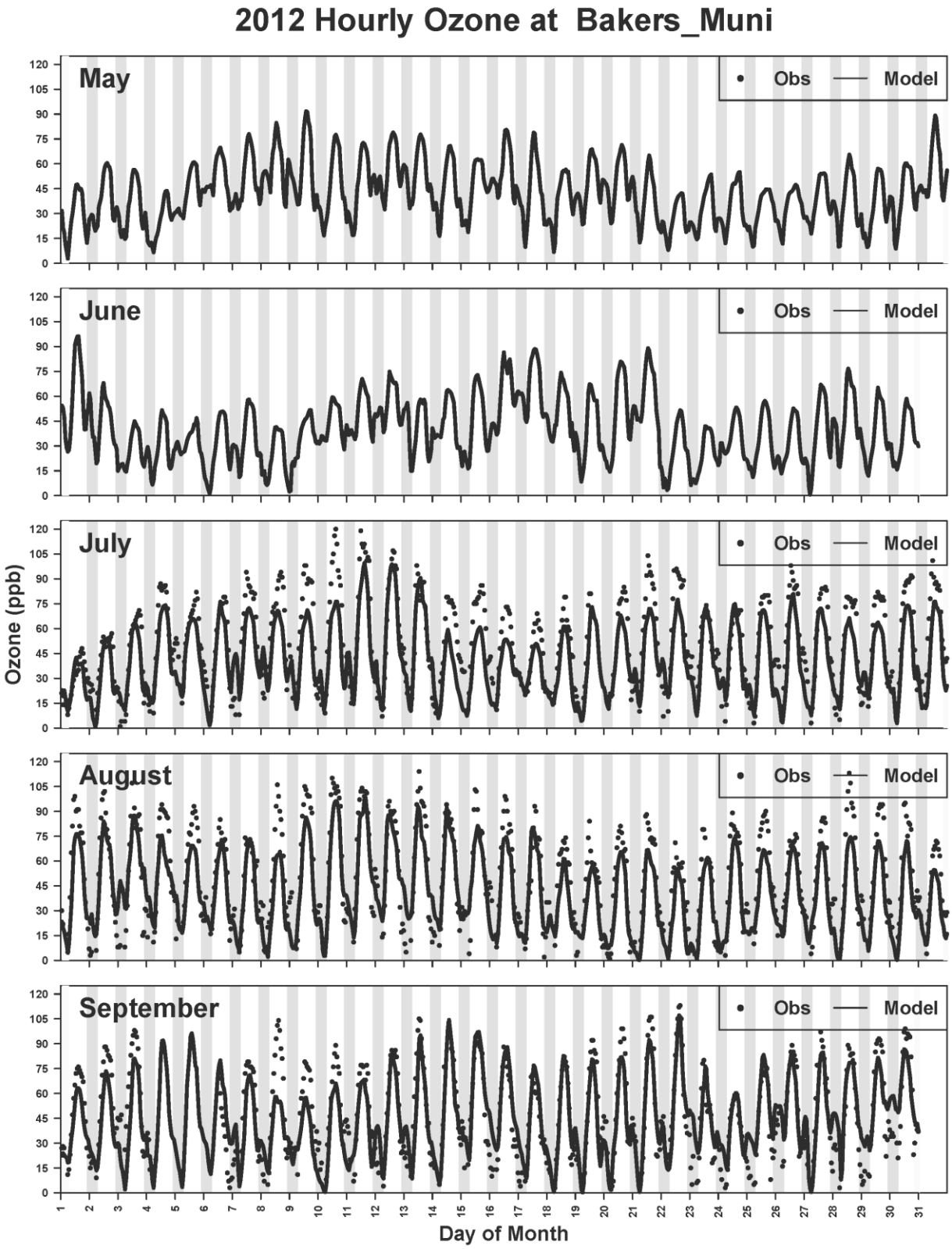

Figure S. 30 Time-series of hourly ozone at Bakersfield Municipal Airport

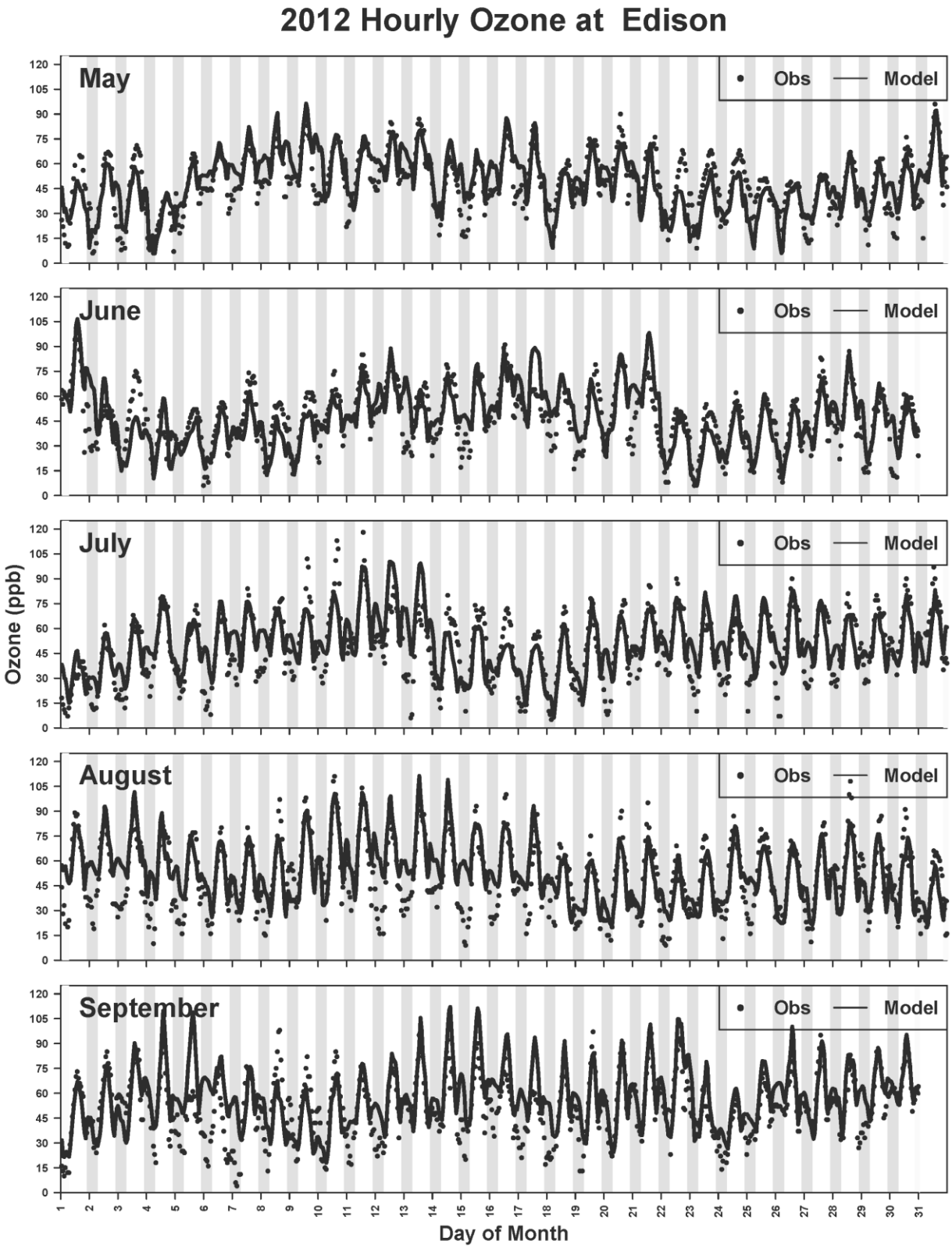

Figure S. 31 Time-series of hourly ozone at Edison

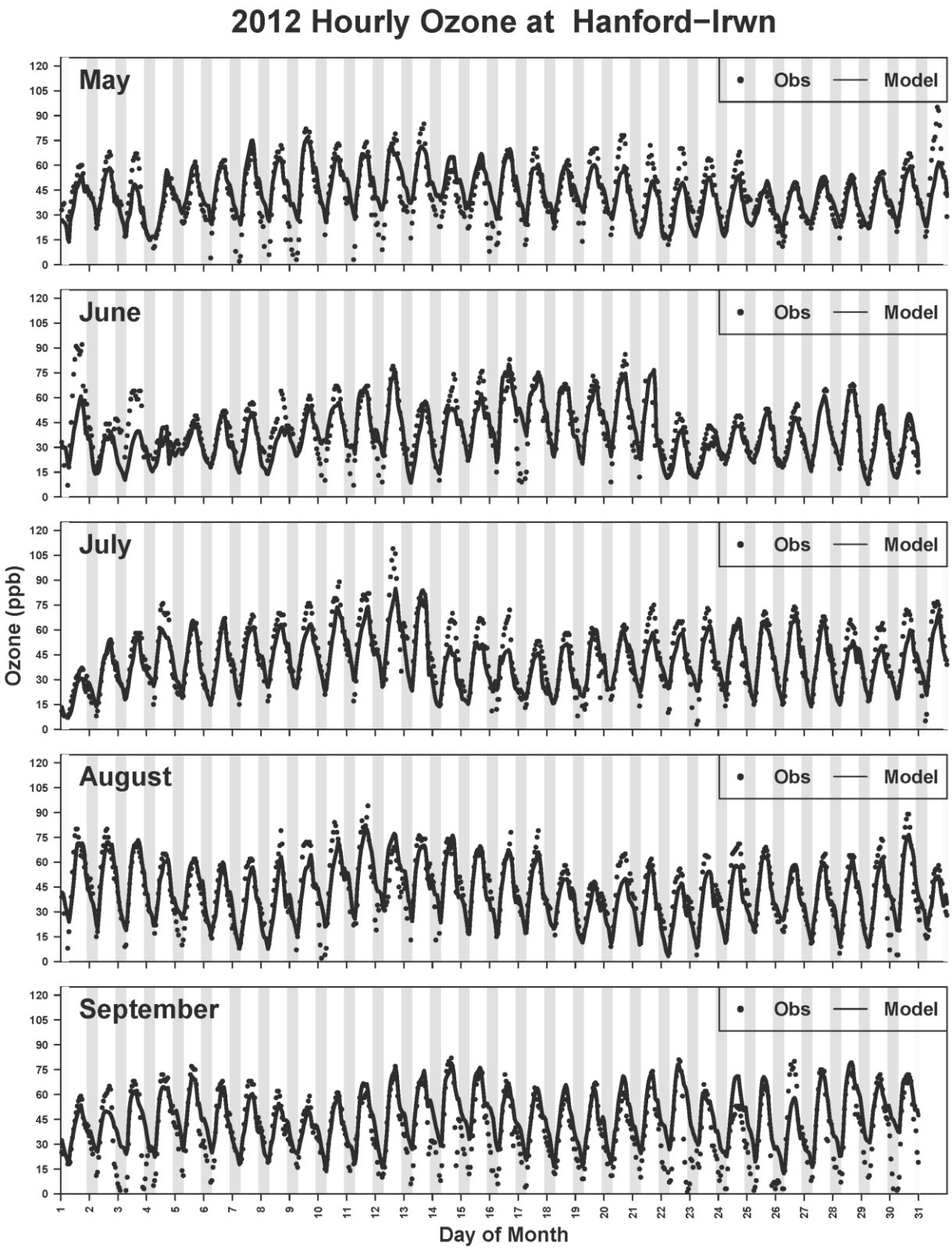

Figure S. 32 Time-series of hourly ozone at Hanford-S Irwin Street

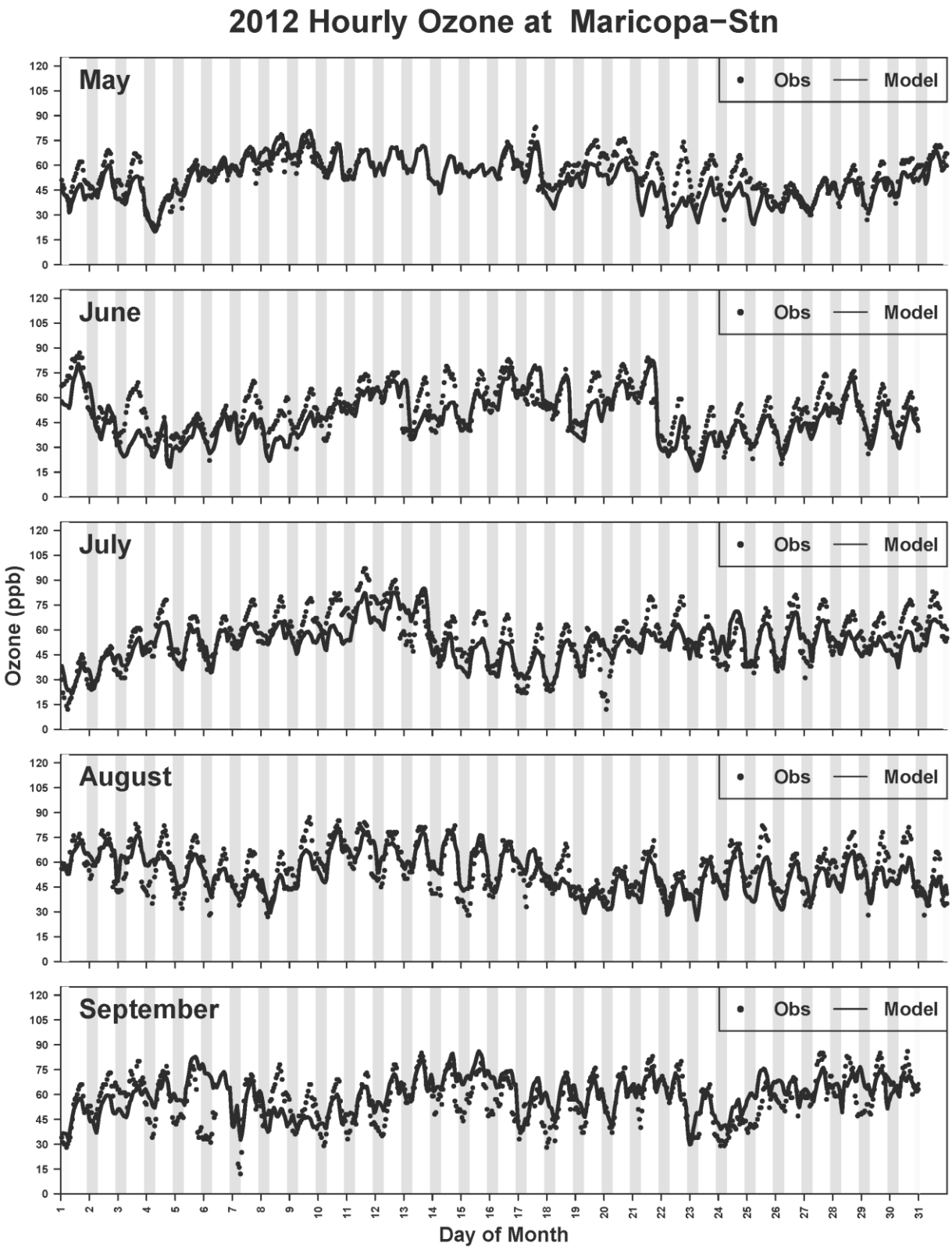

Figure S. 33 Time-series of hourly ozone at Maricopa Stanislaus Street

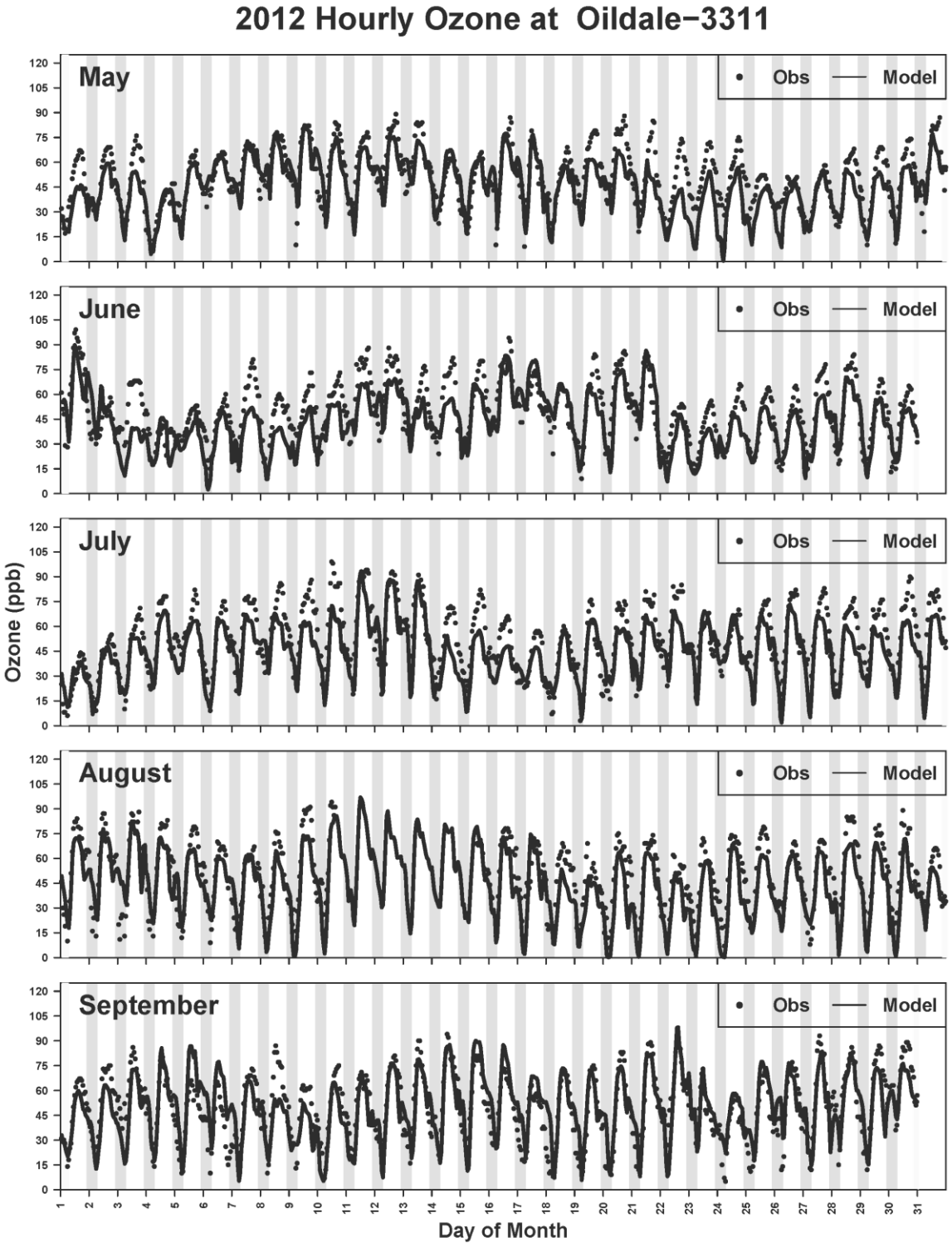

Figure S. 34 Time-series of hourly ozone at Oildale-3311 Manor Street

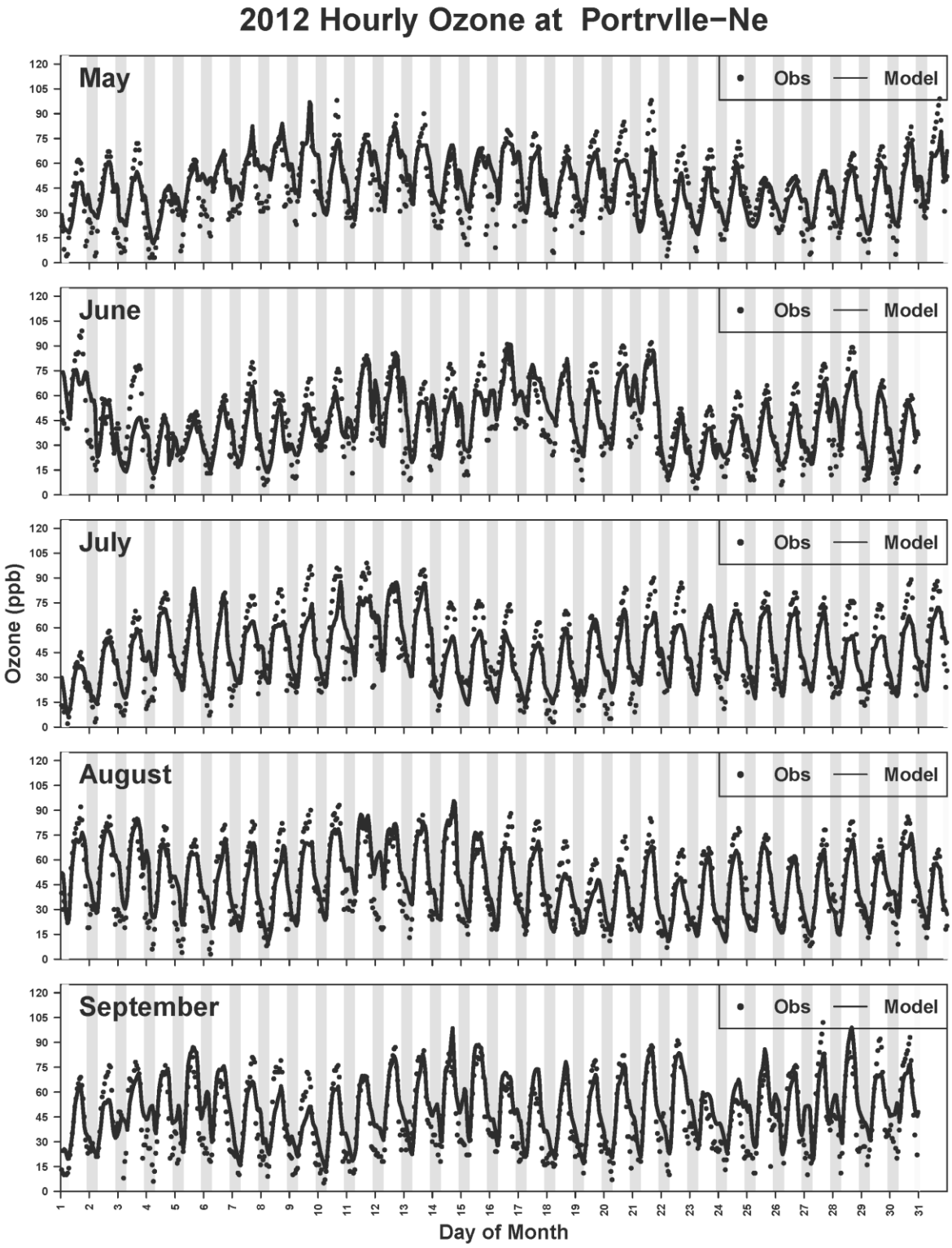

Figure S. 35 Time-series of hourly ozone at Porterville 1839 Newcomb Street

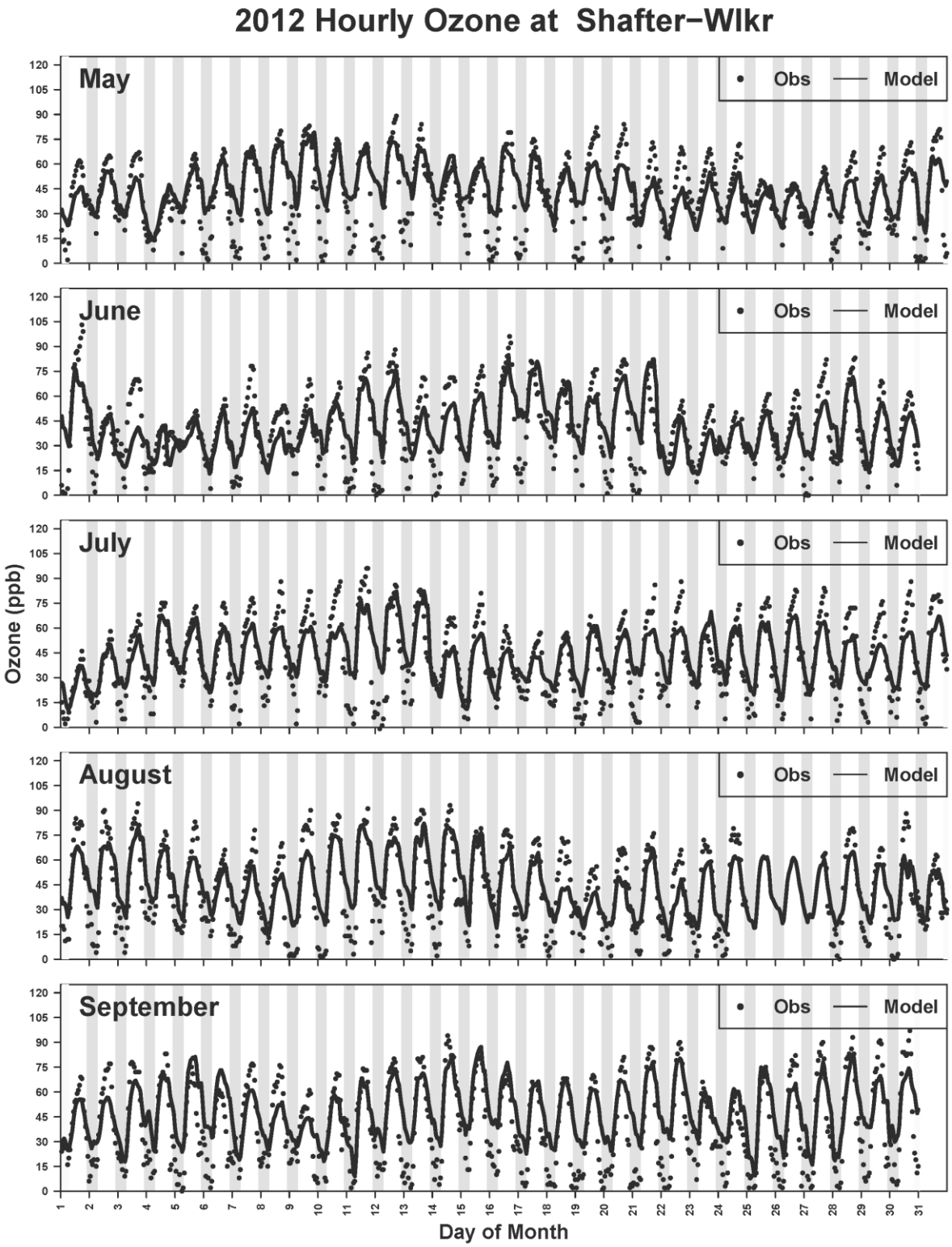

Figure S. 36 Time-series of hourly ozone at Shafter Walker Street

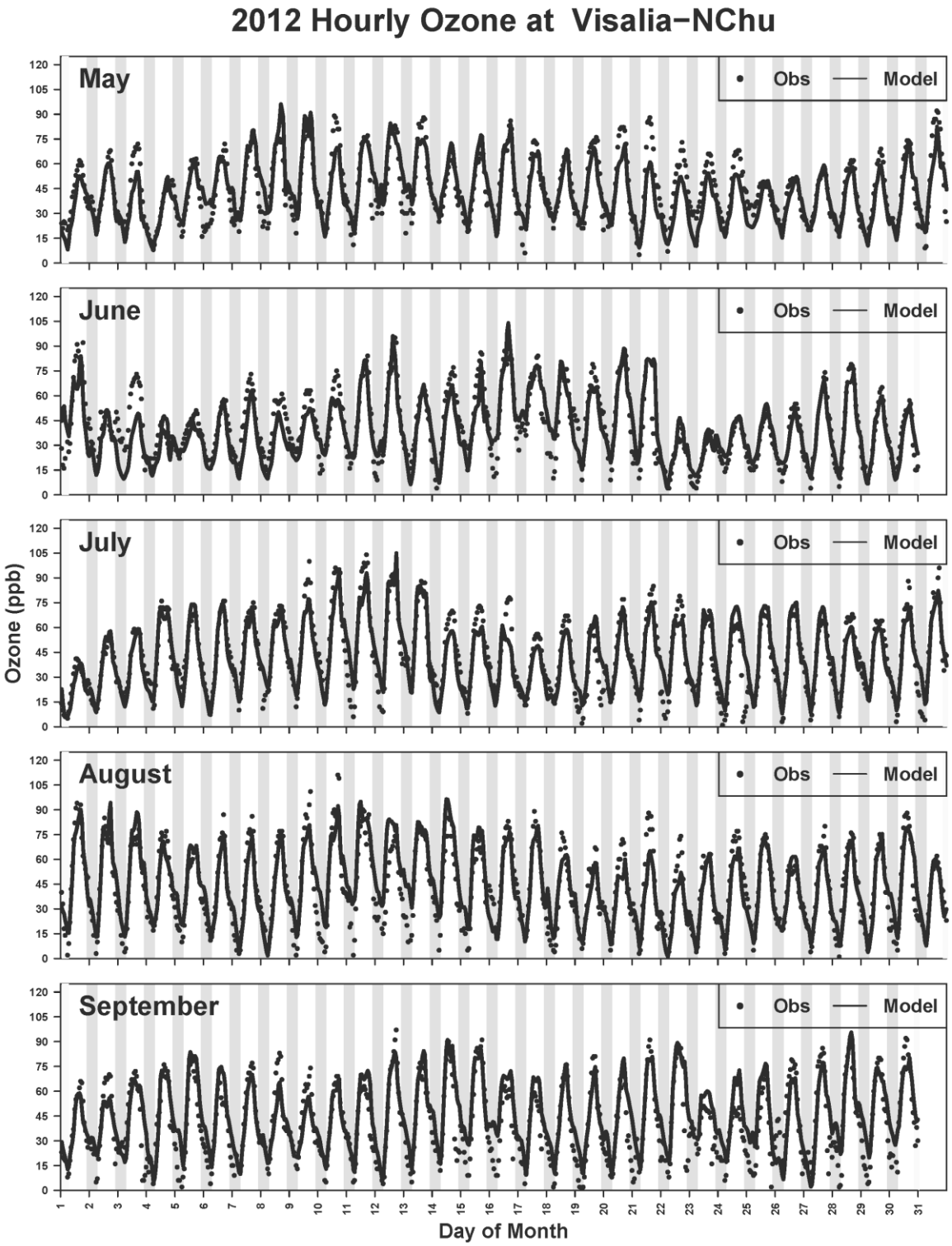

Figure S. 37 Time-series of hourly ozone at Visalia N. Church Street

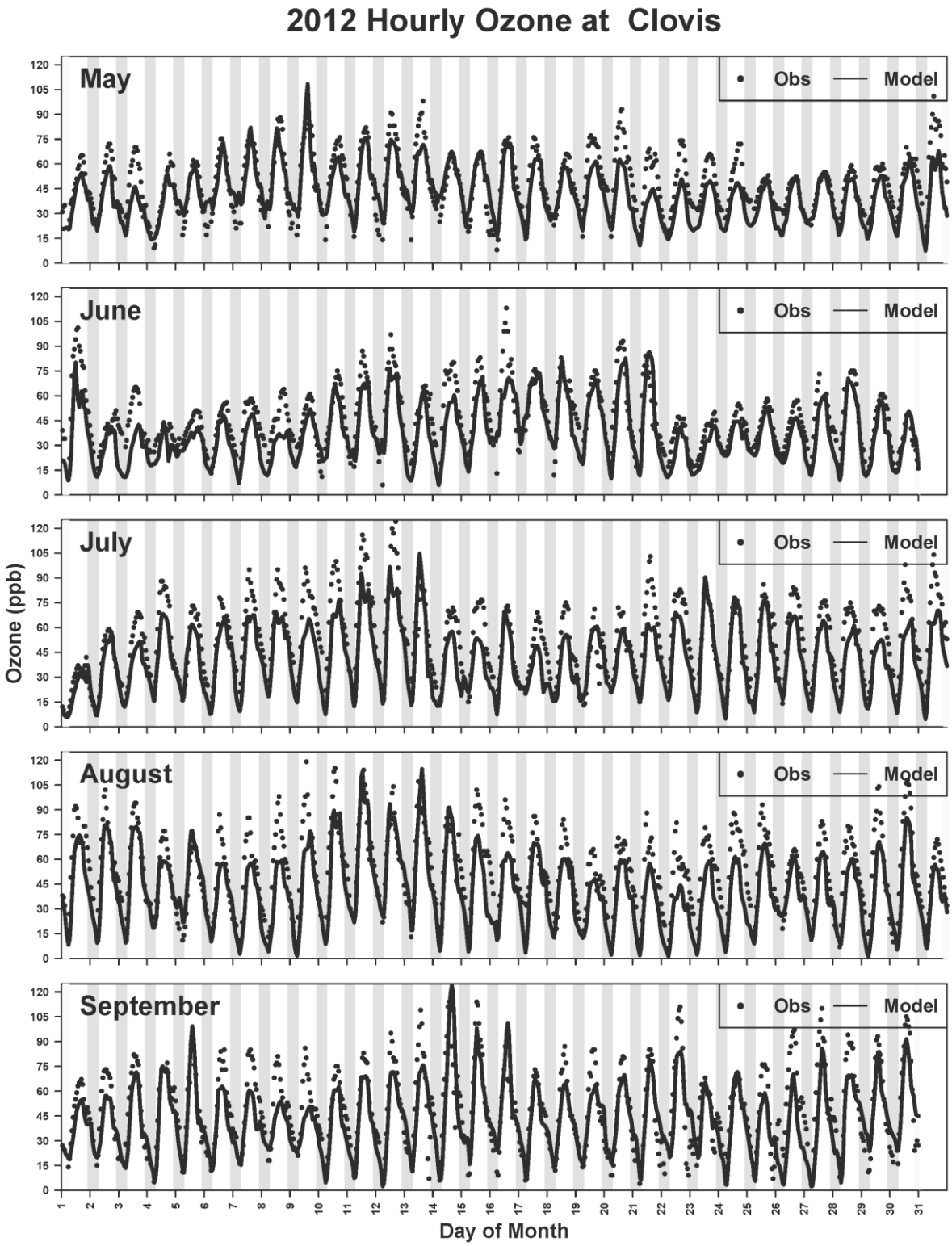

Figure S. 38 Time-series of hourly ozone at Clovis N. Villa Avenue

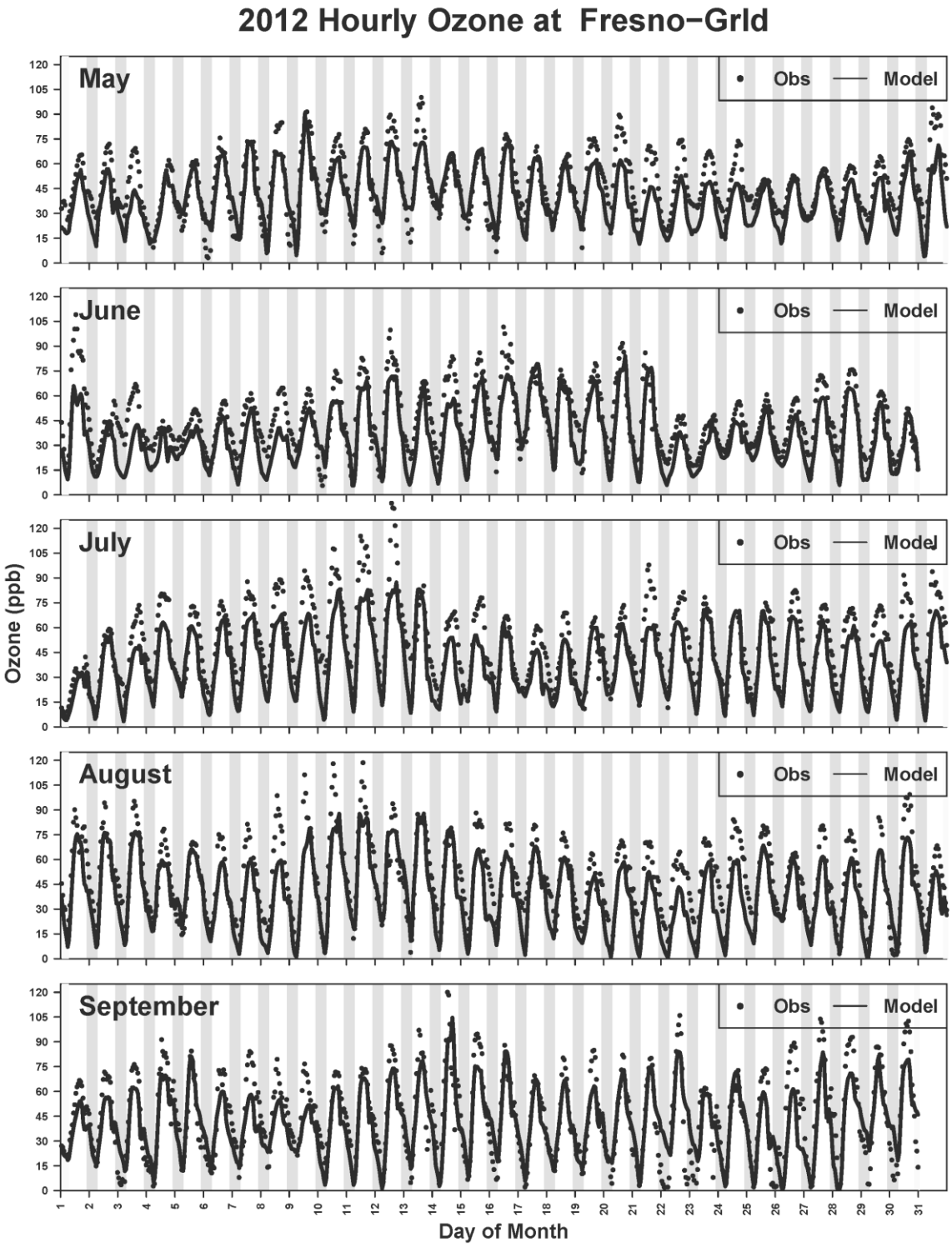

Figure S. 39 Time-series of hourly ozone at Fresno-Garland

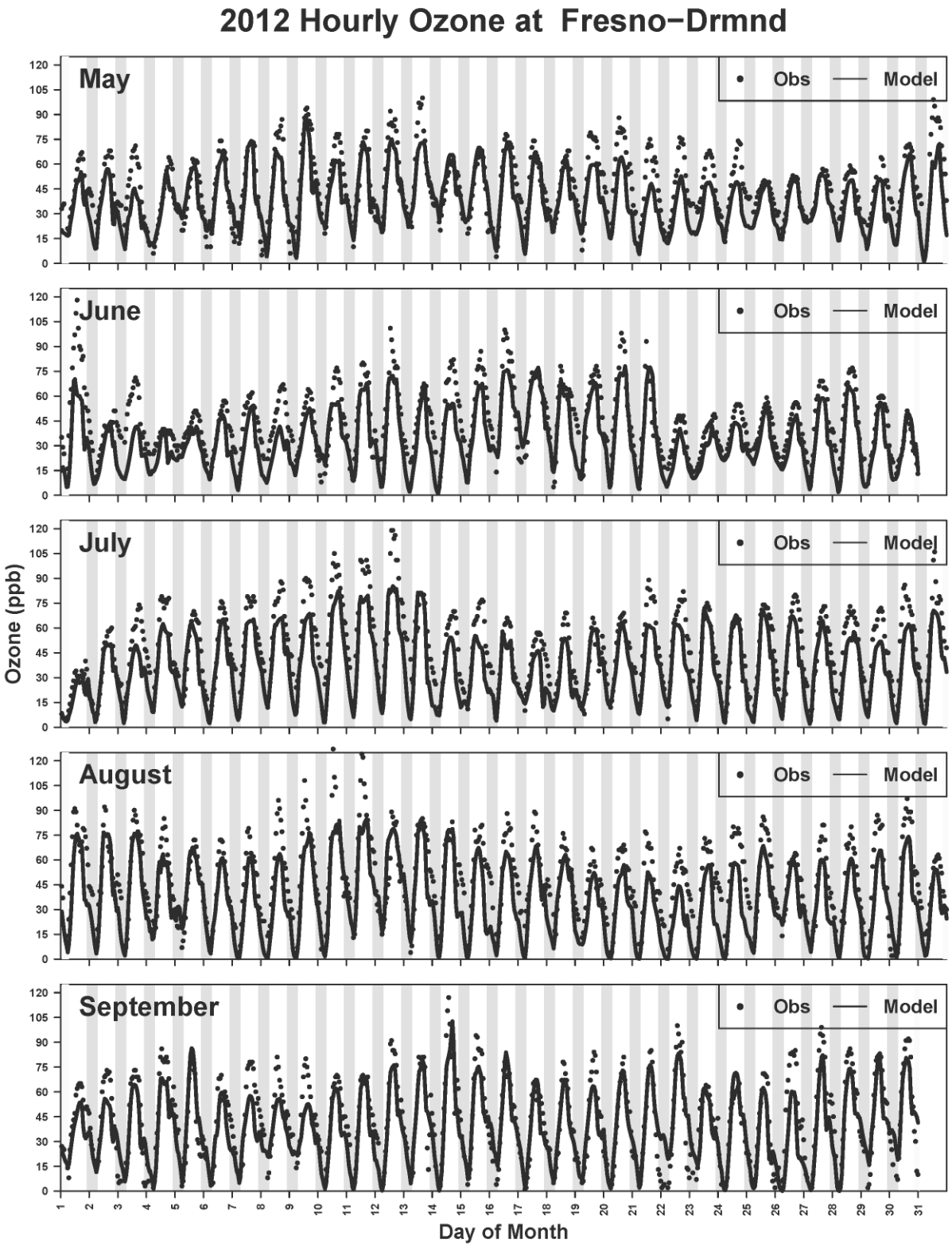

Figure S. 40 Time-series of hourly ozone at Fresno Drummond

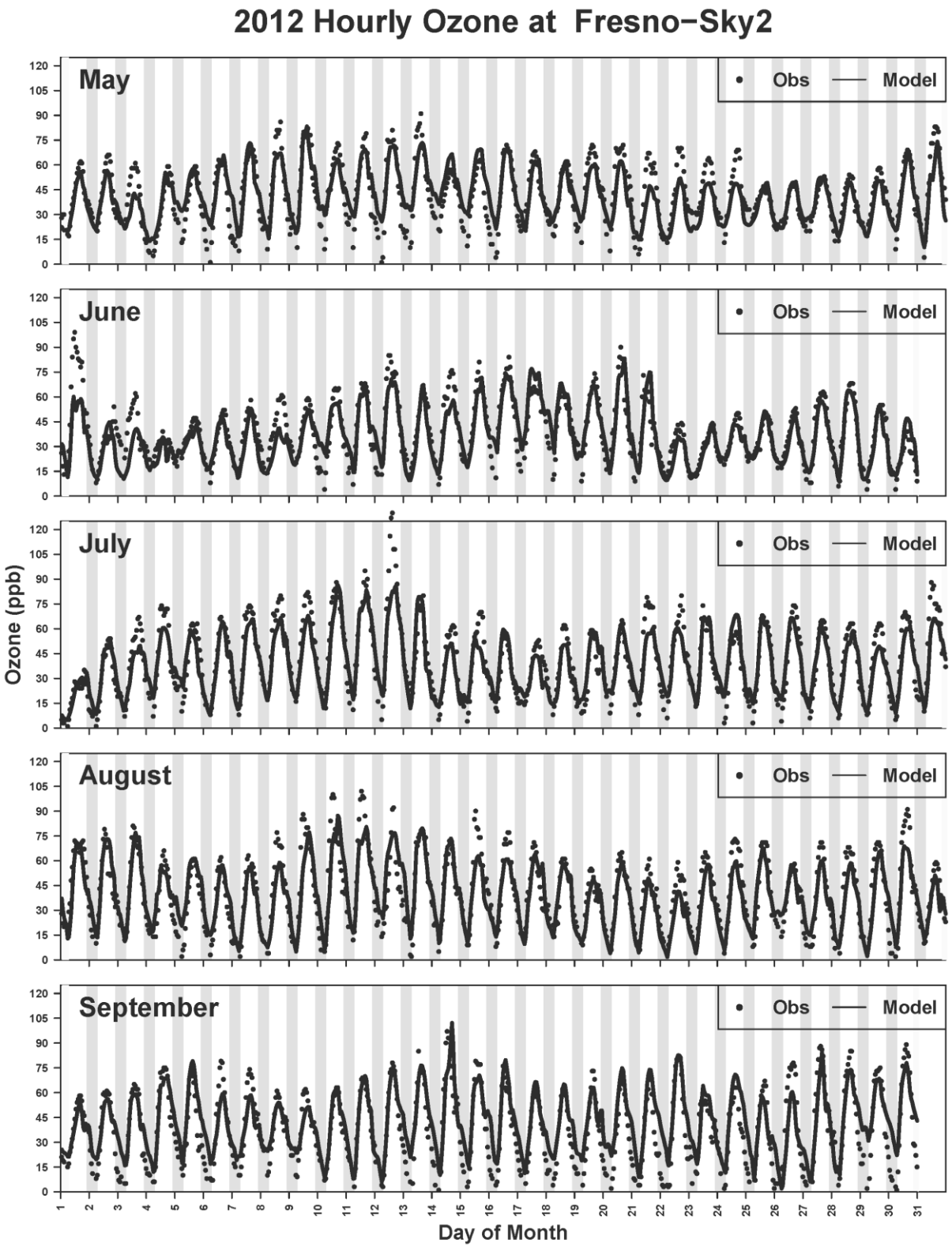

Figure S. 41 Time-series of hourly ozone at Fresno-Sierra Skypark#2

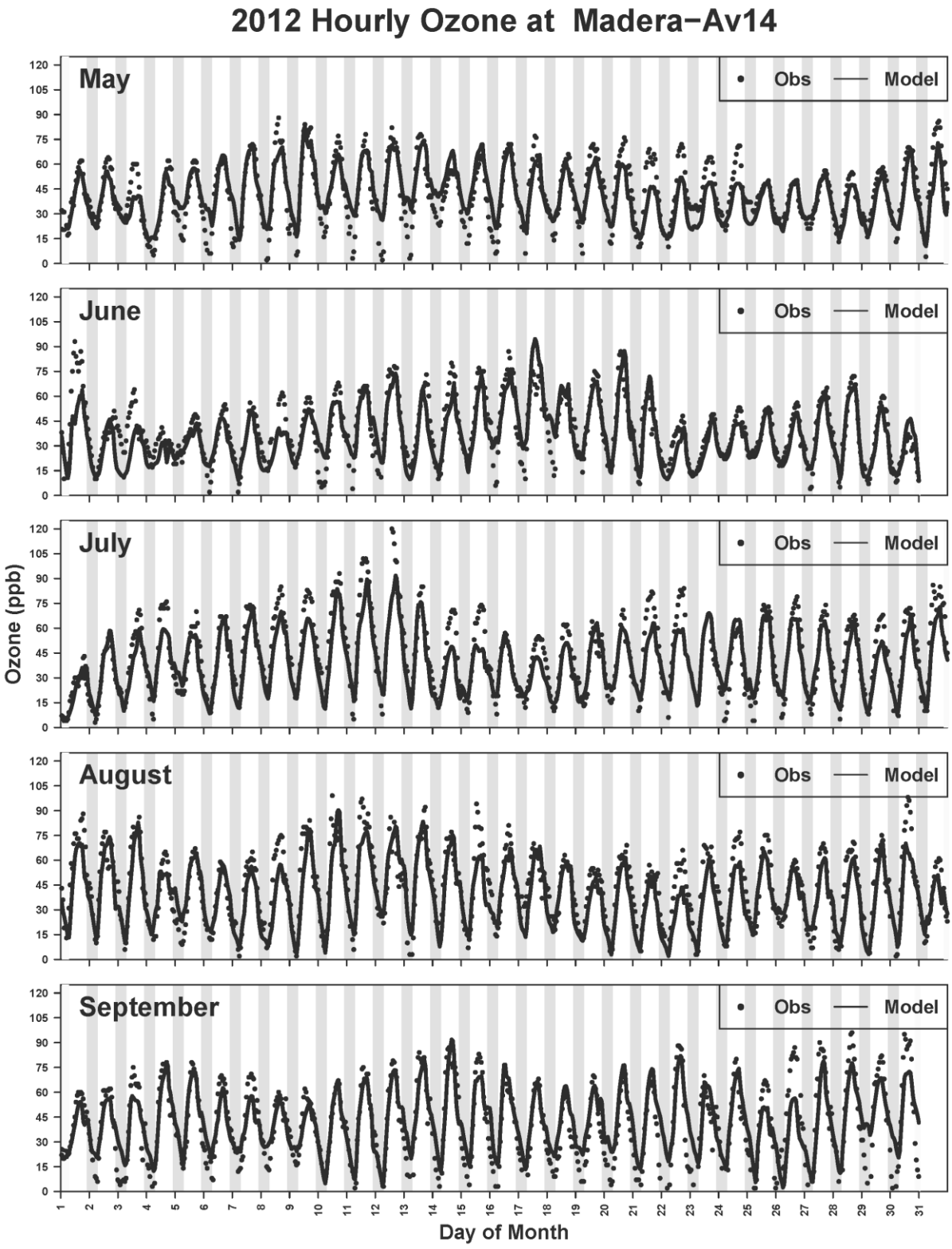

Figure S. 42 Time-series of hourly ozone at Madera-28621 Avenue 14

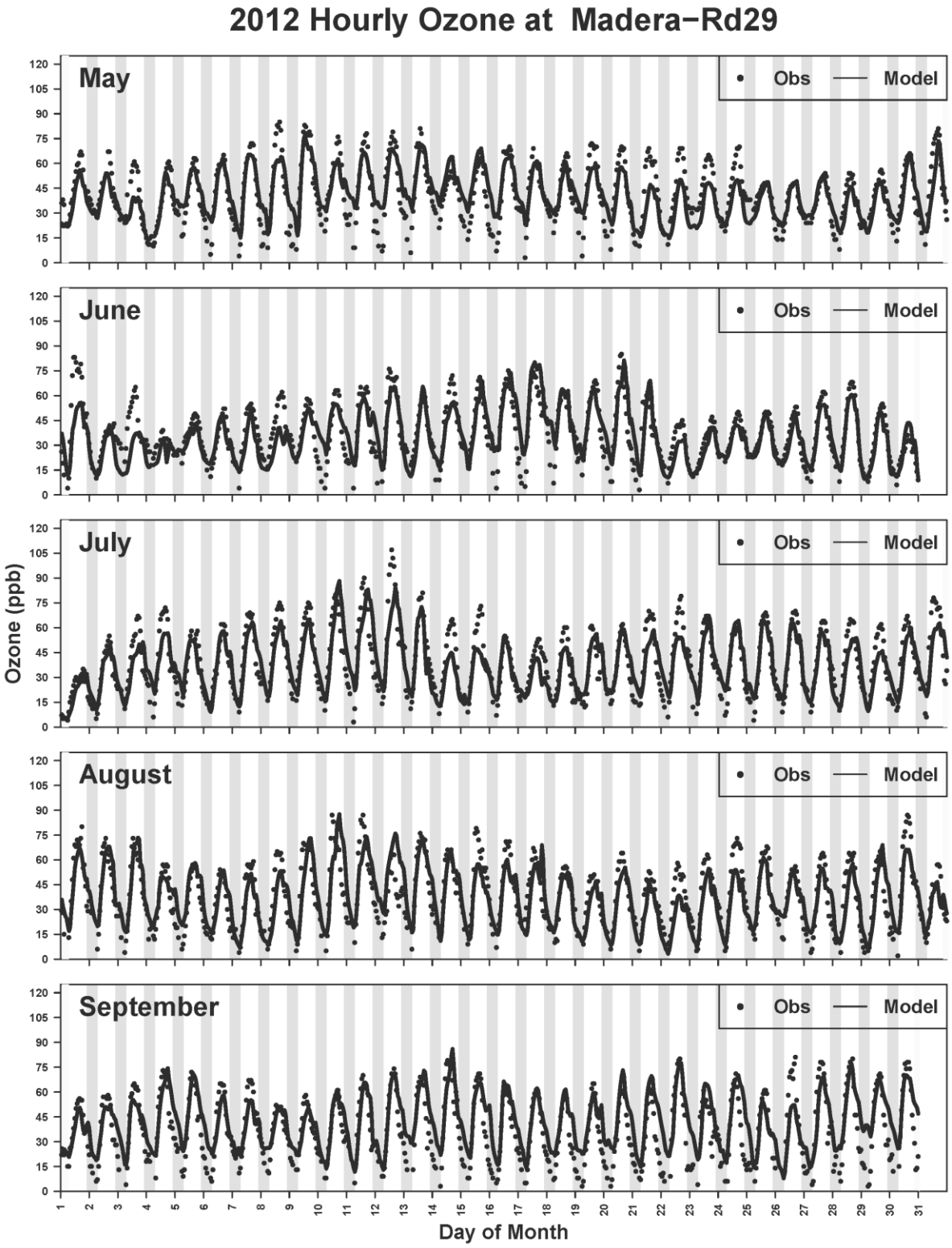

Figure S. 43 Time-series of hourly ozone at Madera-Pump Yard

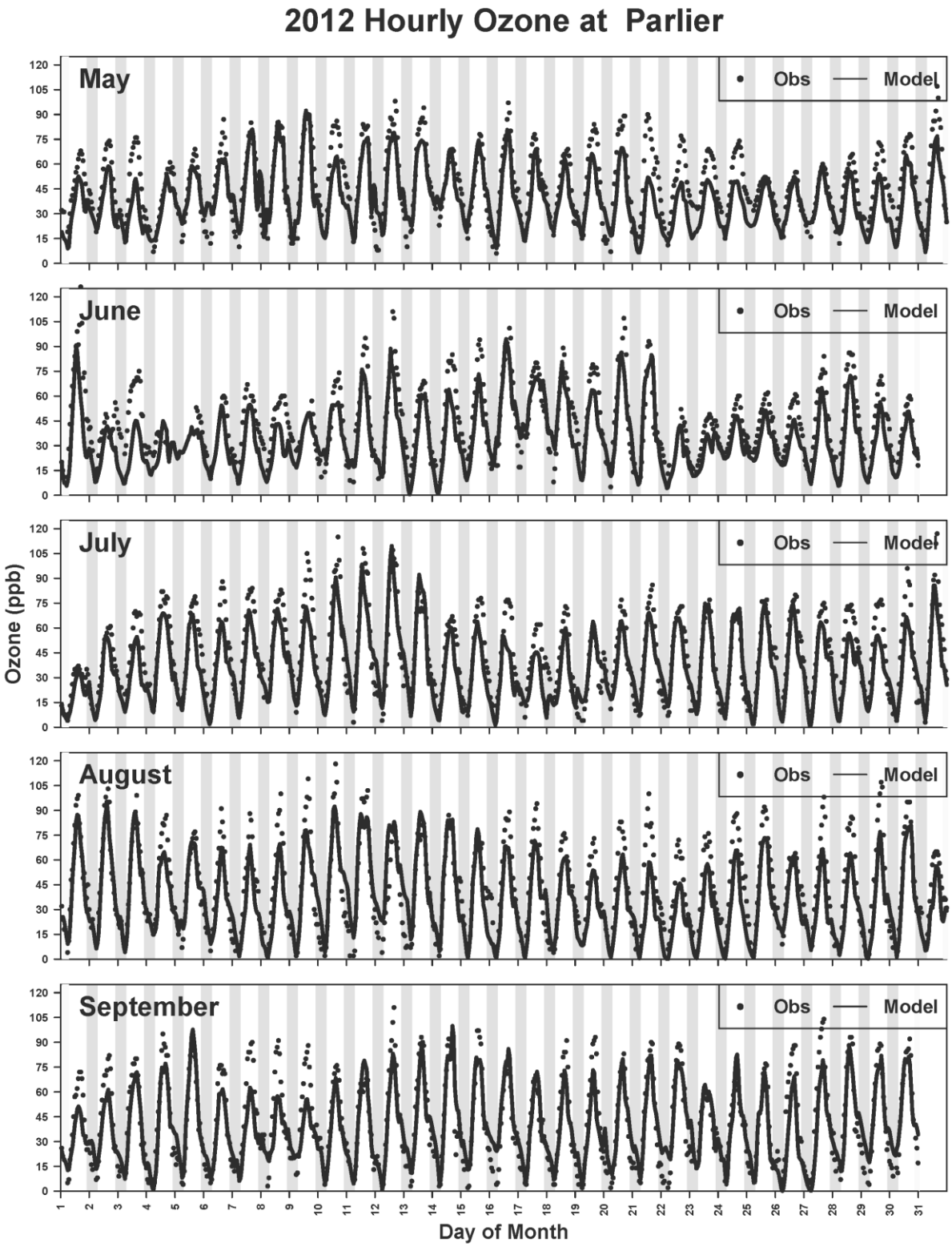

Figure S. 44 Time-series of hourly ozone at Parlier

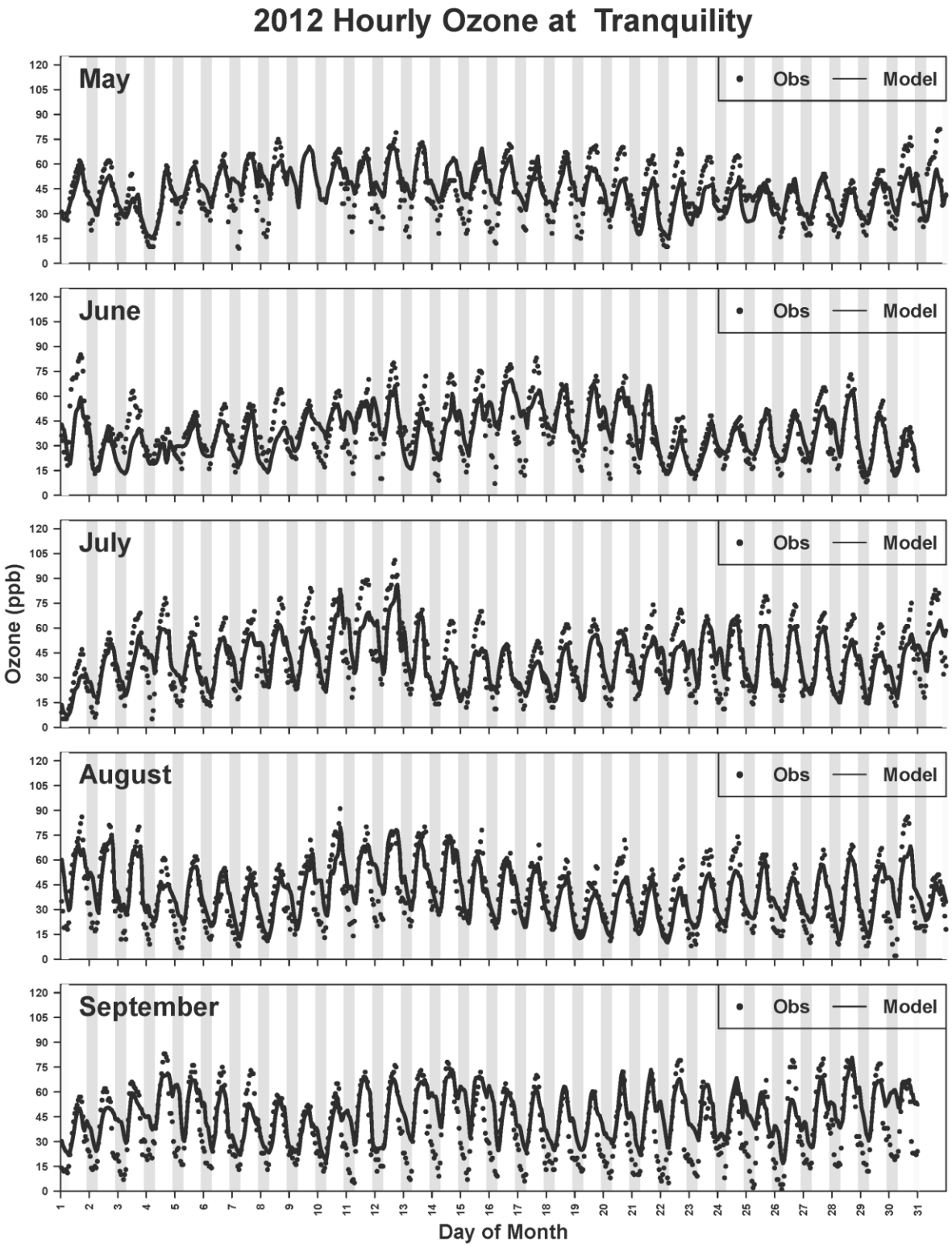

Figure S. 45 Time-series of hourly ozone at Tranquility-32650 West Adams Avenue

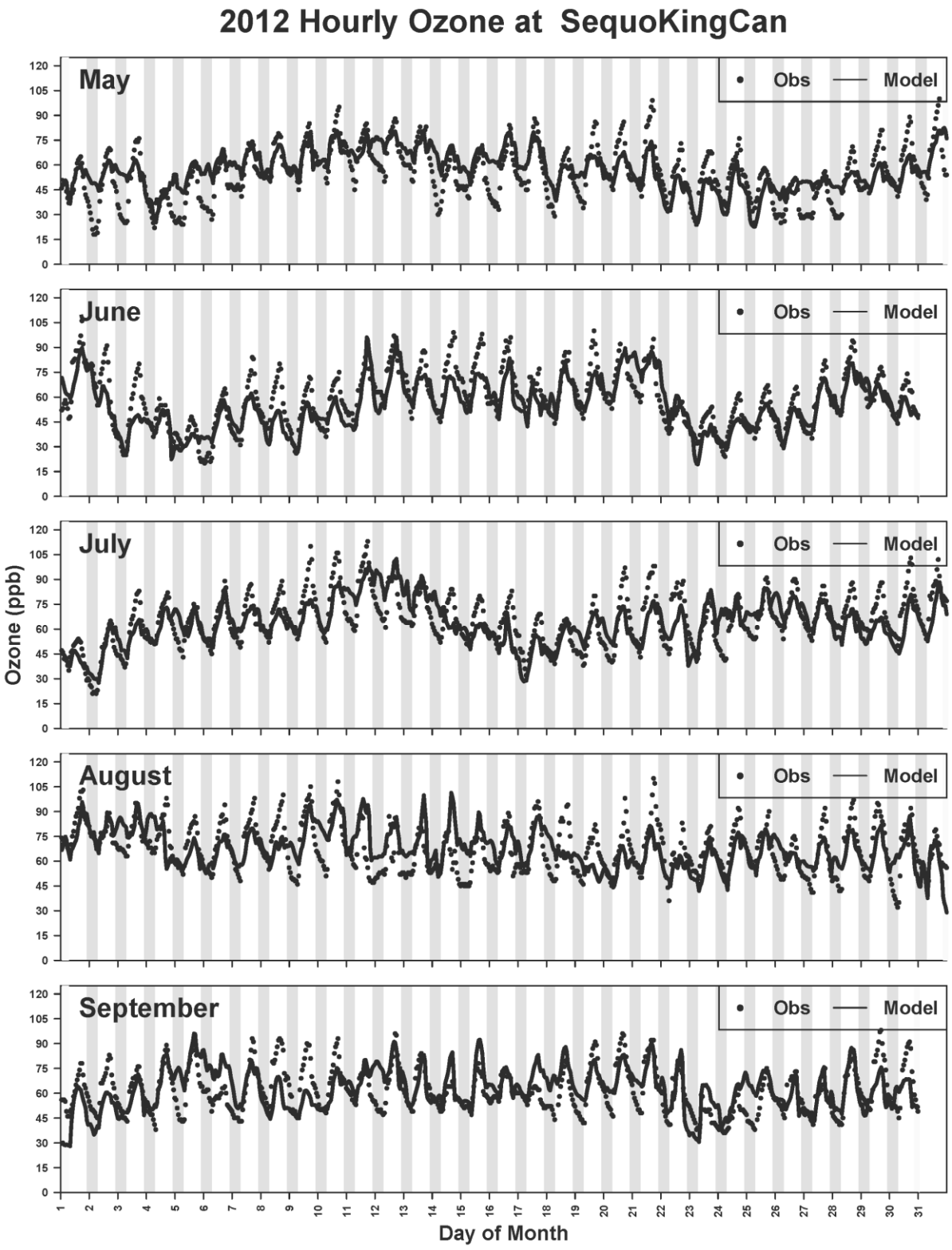

Figure S. 46 Time-series of hourly ozone at Sequoia and Kings Canyon Natl Park

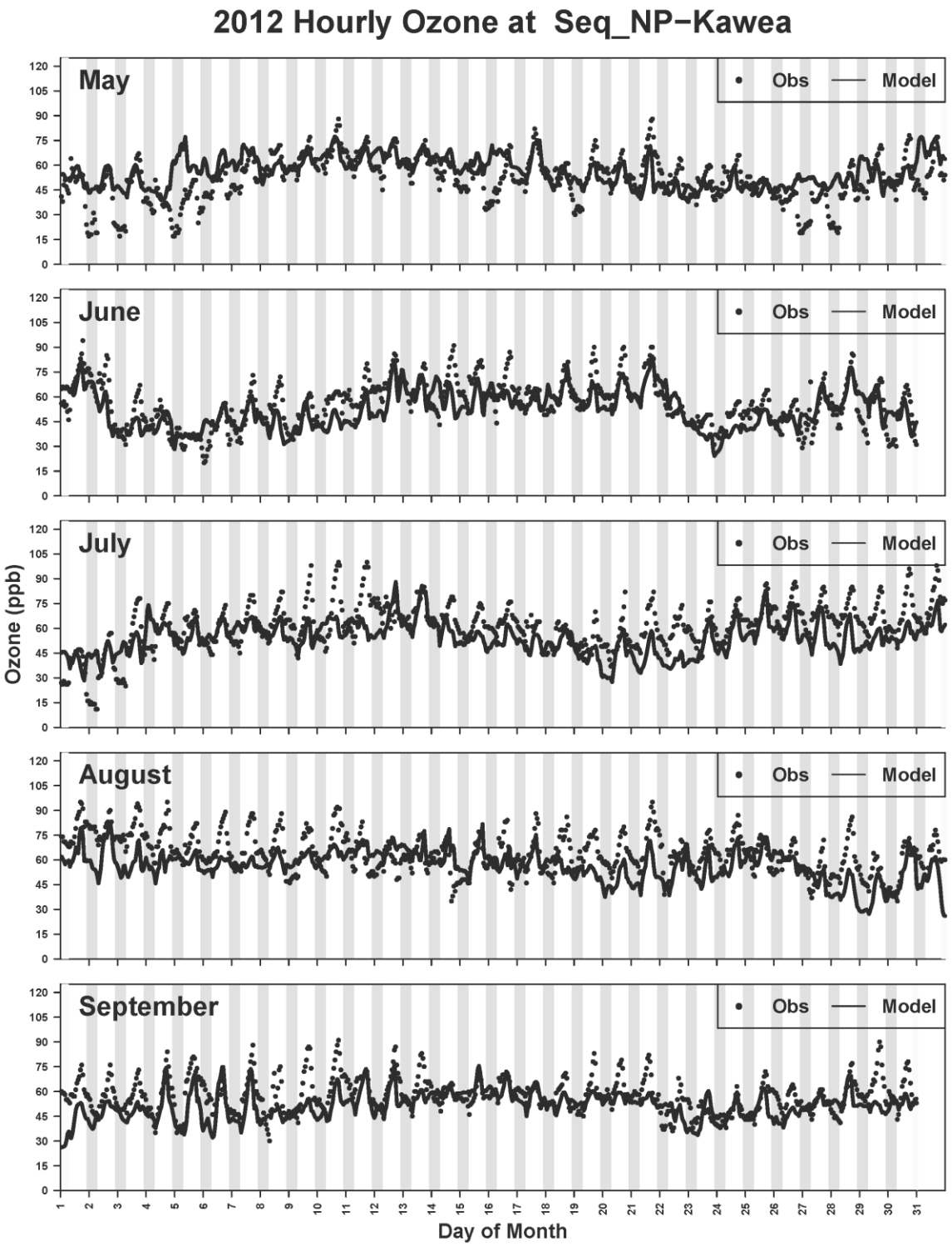

Figure S. 47 Time-series of hourly ozone at Sequoia Natl Park-Lower Kaweah

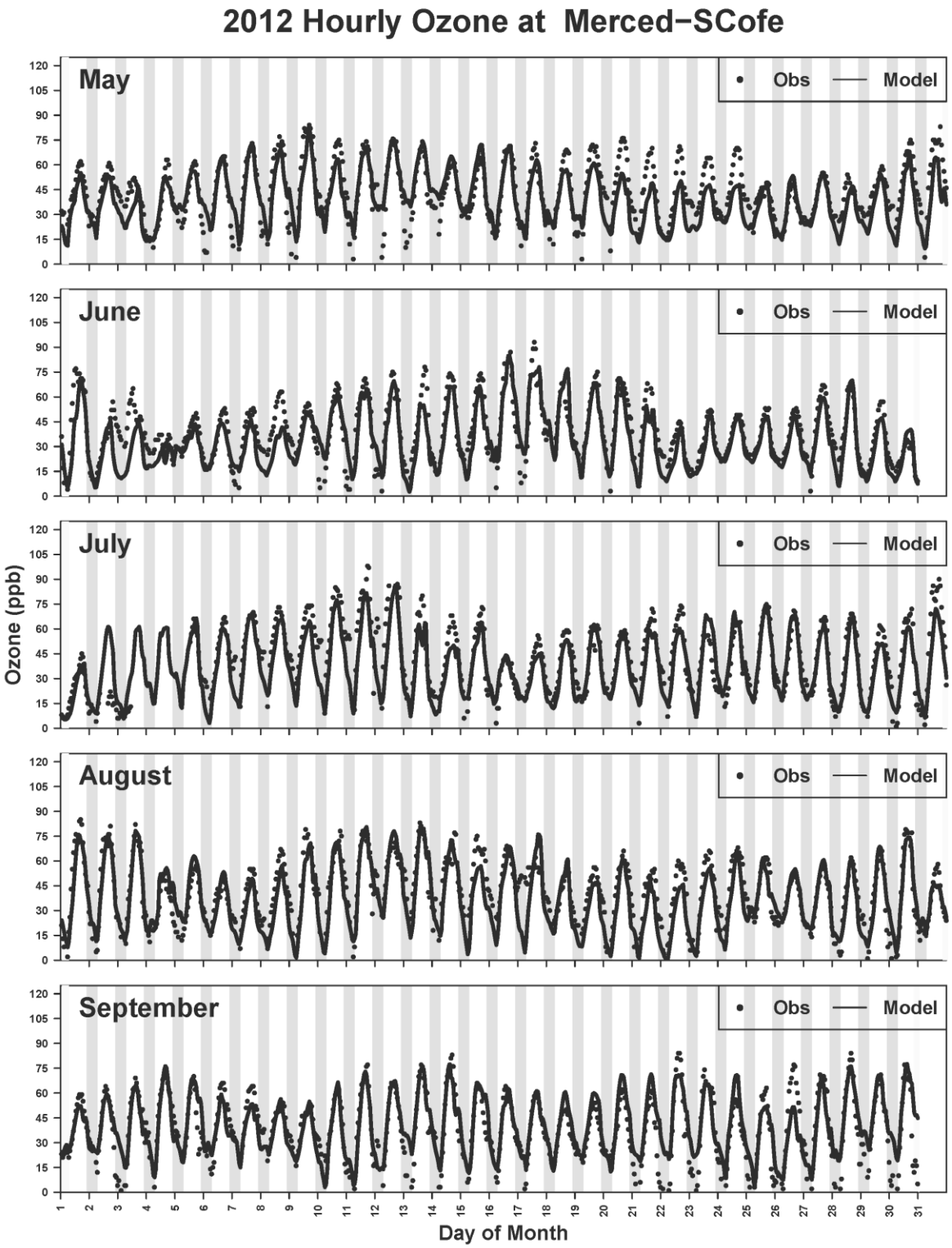

Figure S. 48 Time-series of hourly ozone at Merced-S Coffee Avenue

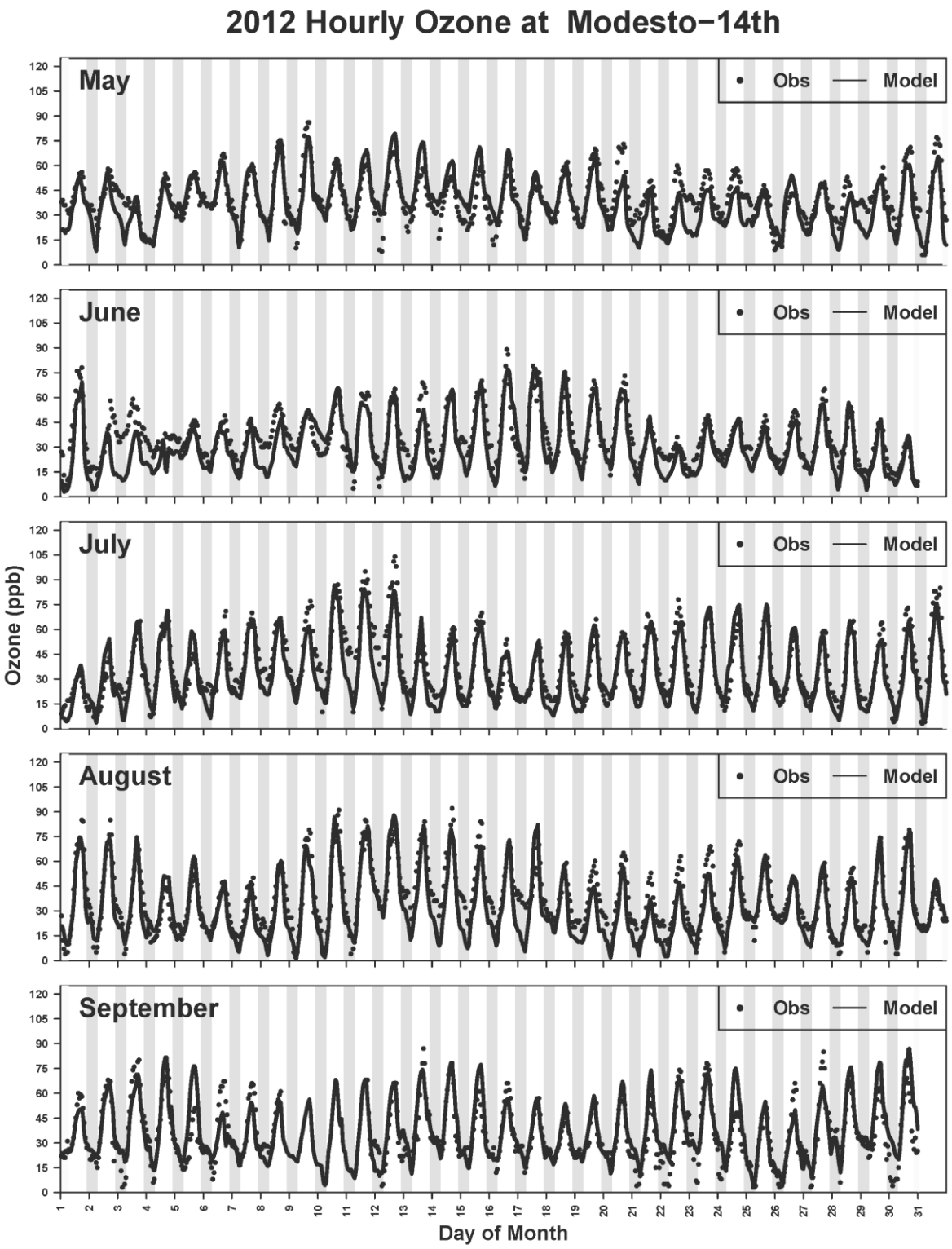

Figure S. 49 Time-series of hourly ozone at Modesto-14th Street

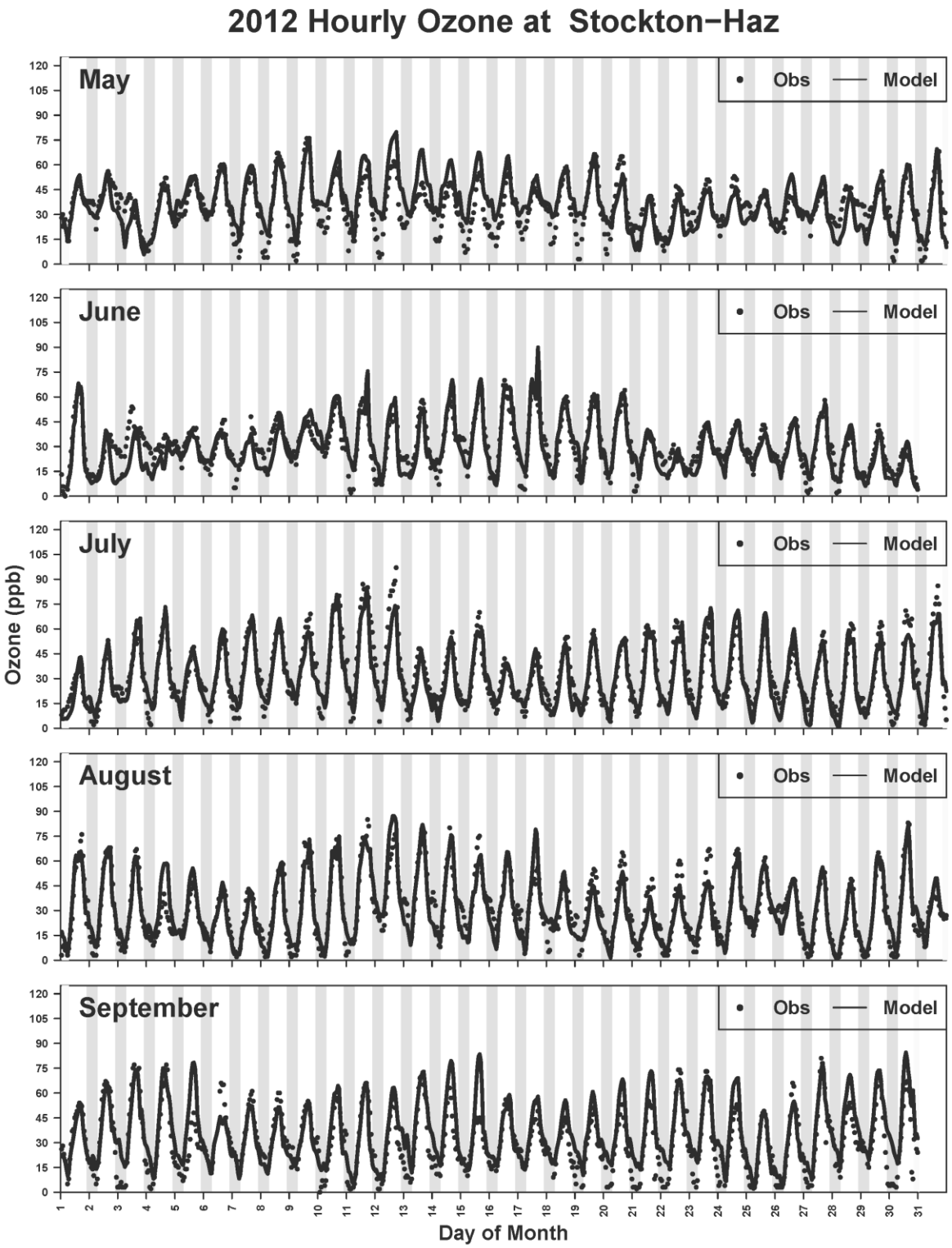

Figure S. 50 Time-series of hourly ozone at Stockton-Hazelton Street

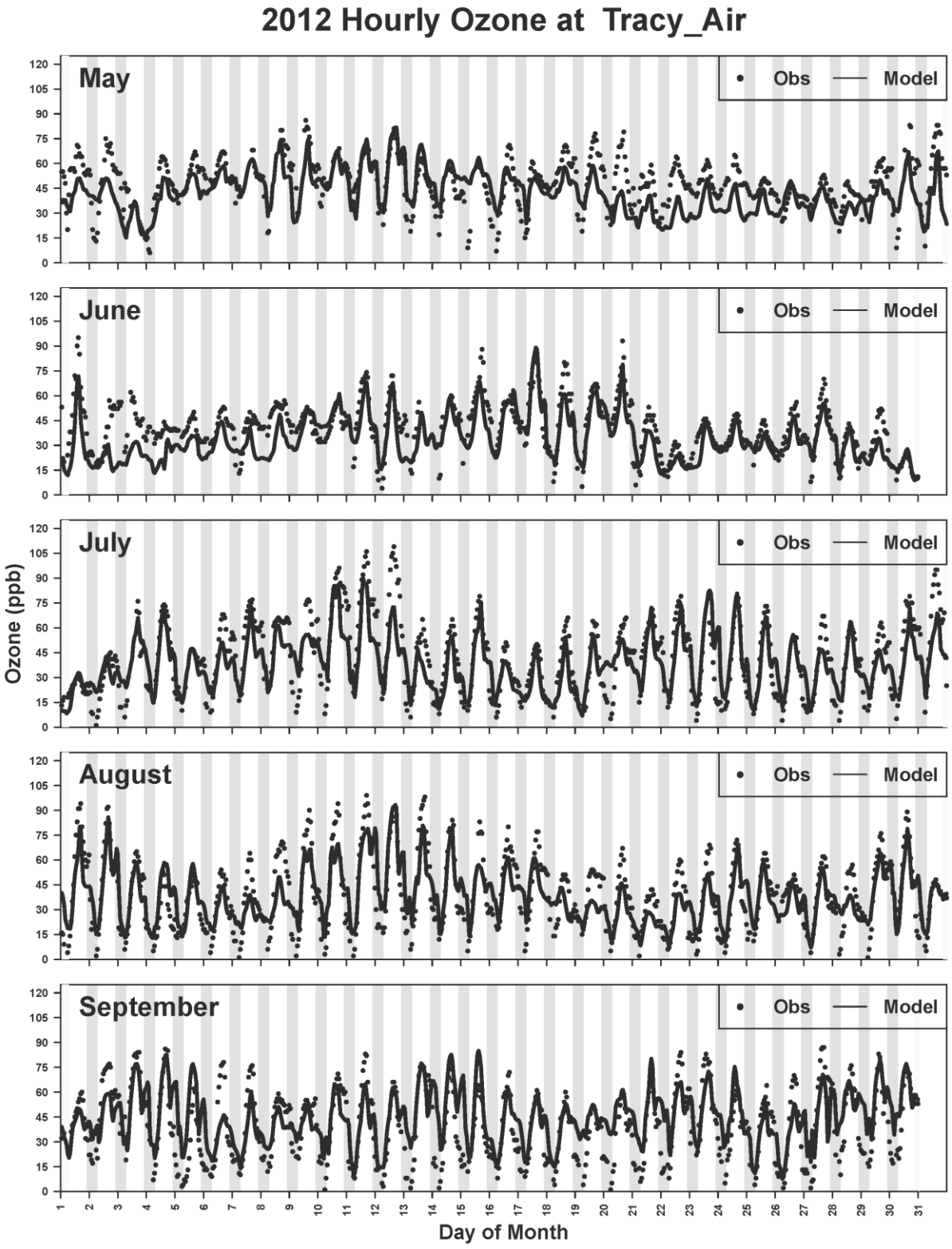

Figure S. 51 Time-series of hourly ozone at Tracy-Airport

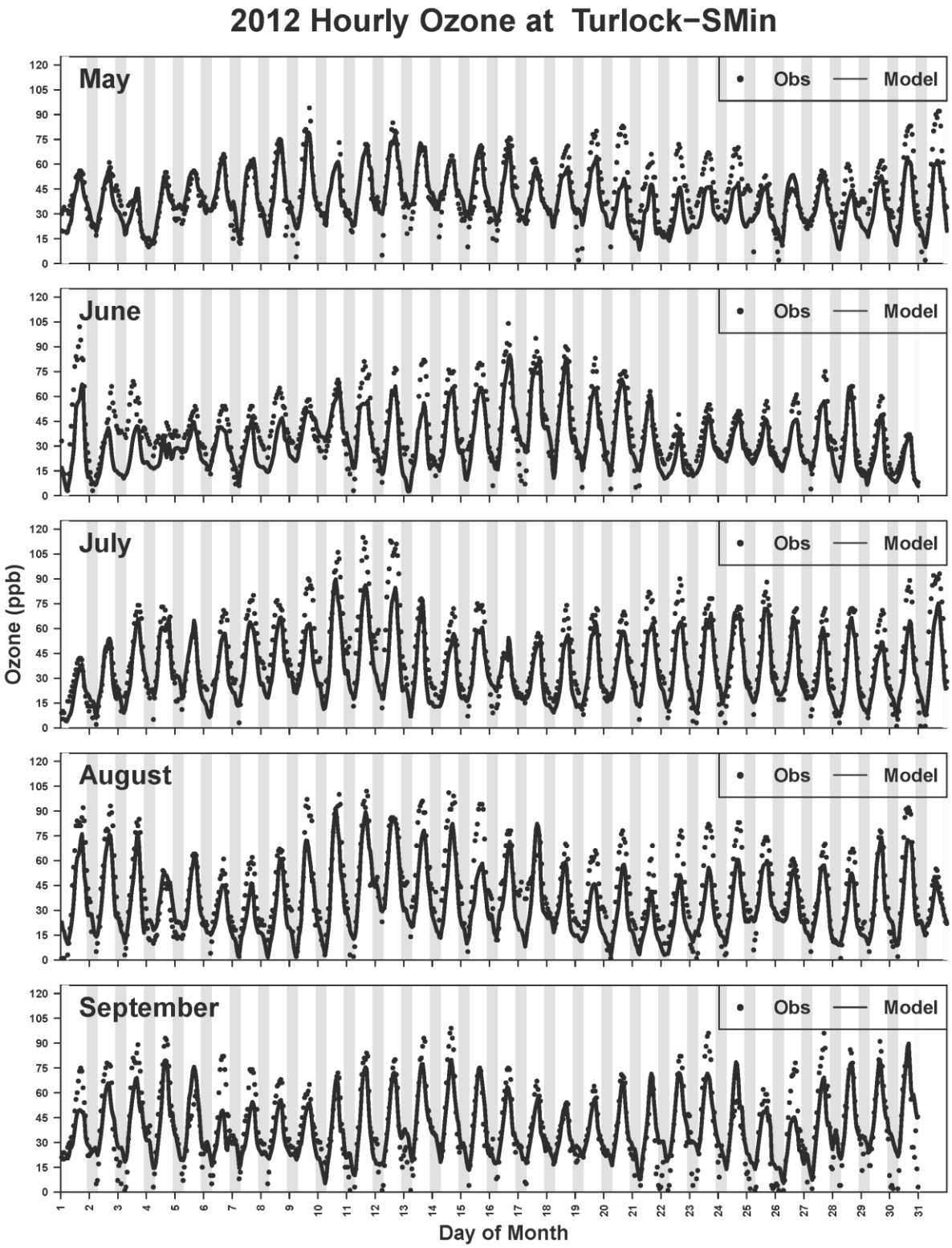

Figure S. 52 Time-series of hourly ozone at Turlock-S Minaret Street

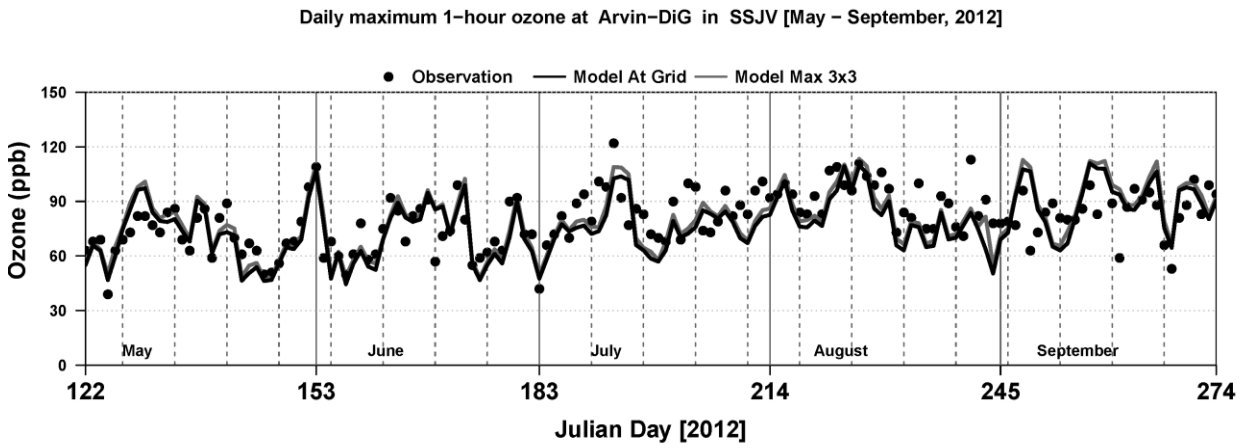

Figure S. 53 Time-series of daily maximum 1-hr ozone at Arvin-Di Giorgio

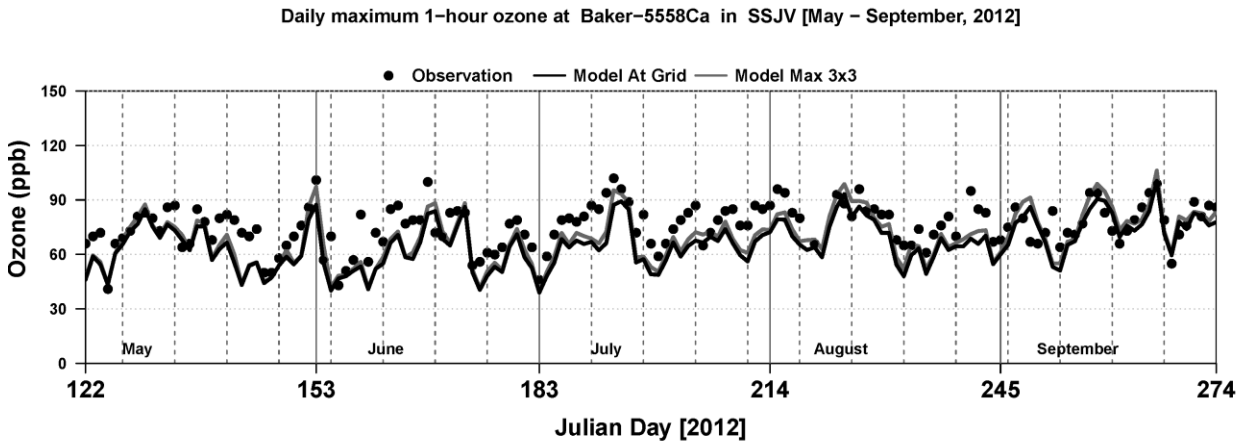

Figure S. 54 Time-series of daily maximum 1-hr ozone at Bakersfield-5558 California Avenue

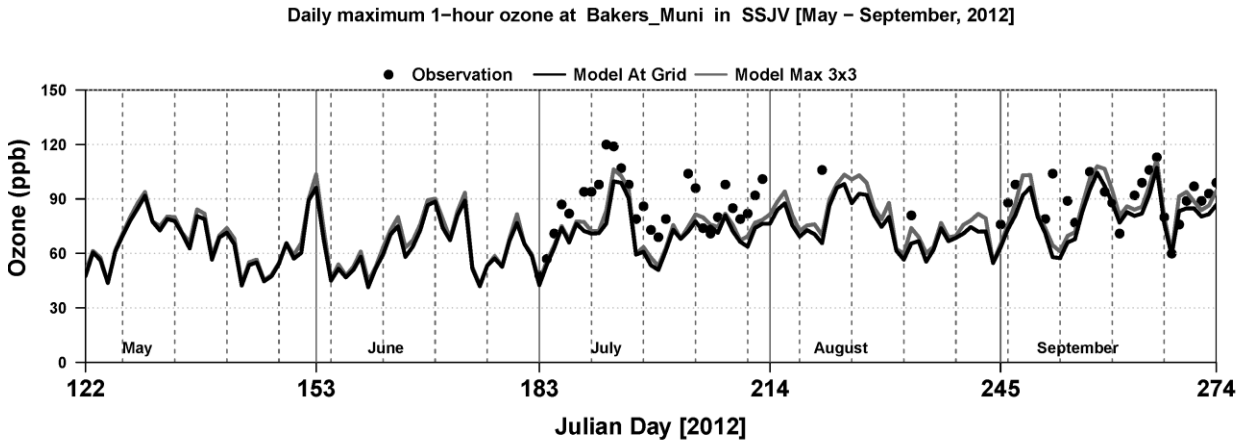

Figure S. 55 Time-series of daily maximum 1-hr ozone at Bakersfield-Municipal Airport

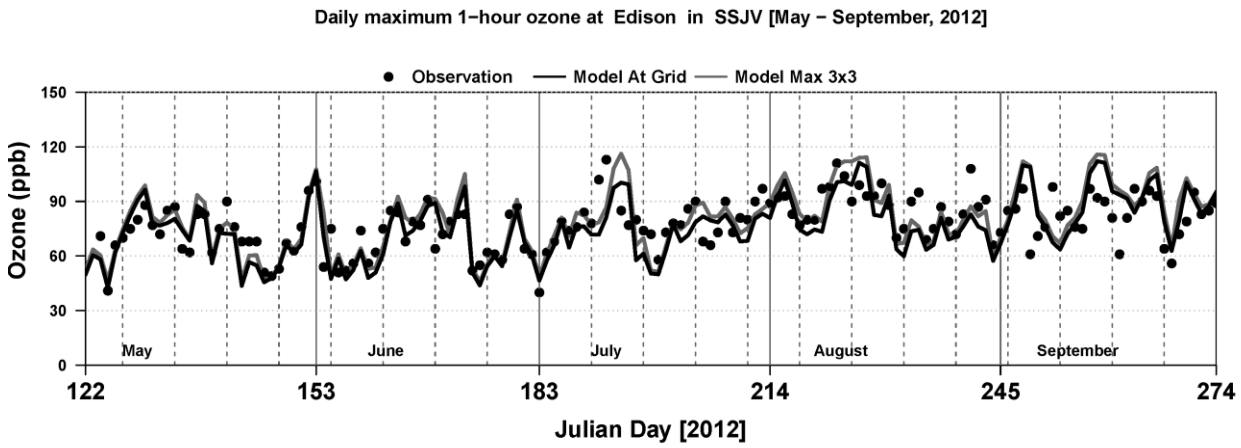

Figure S. 56 Time-series of daily maximum 1-hr ozone at Edison

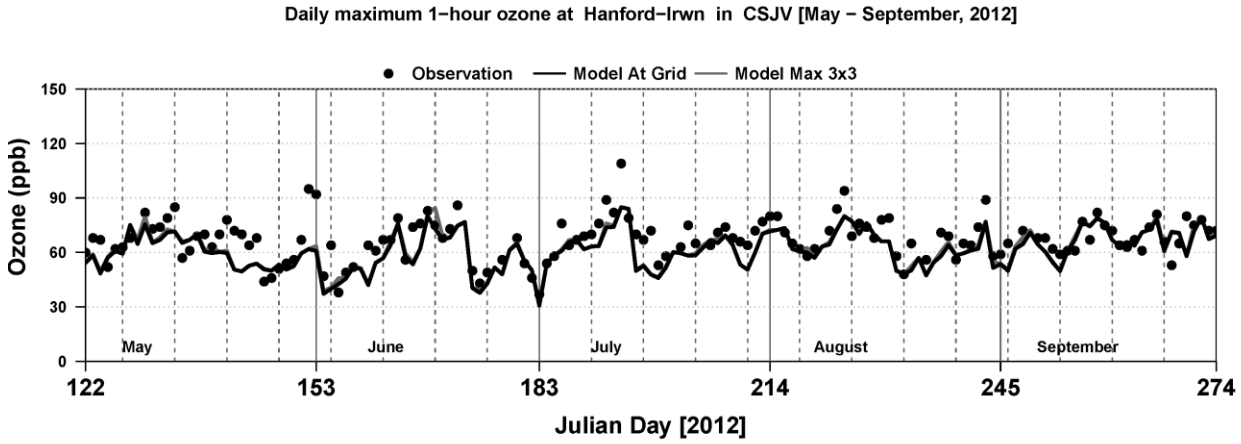

Figure S. 57 Time-series of daily maximum 1-hr ozone at Hanford-S Irwin Street

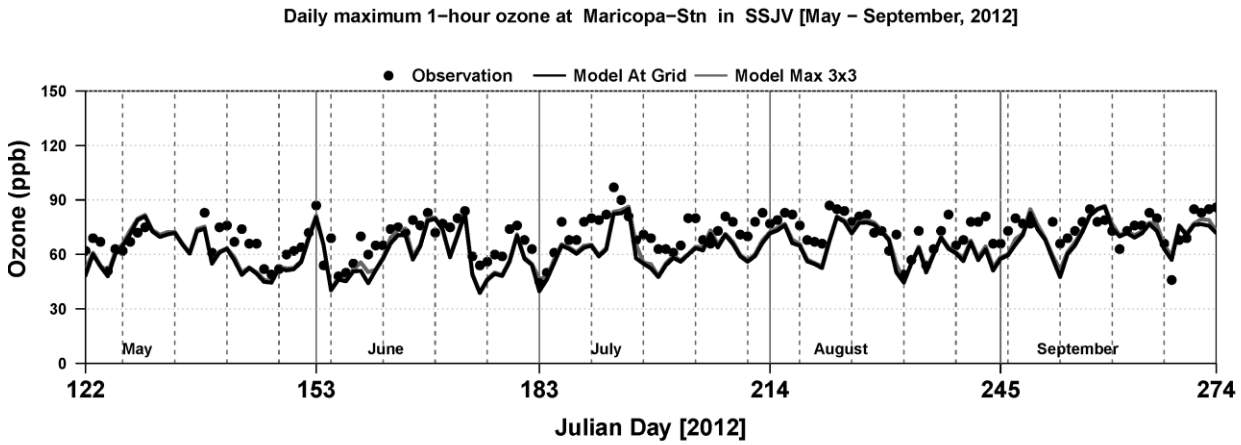

Figure S. 58 Time-series of daily maximum 1-hr ozone at Maricopa-Stanislaus Street

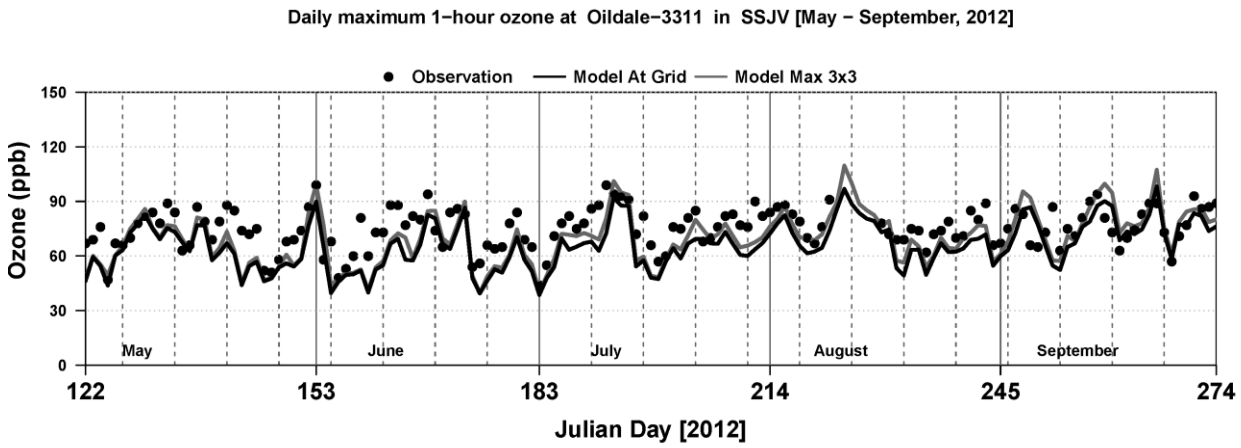

Figure S. 59 Time-series of daily maximum 1-hr ozone at Oildale-3311 Manor Street

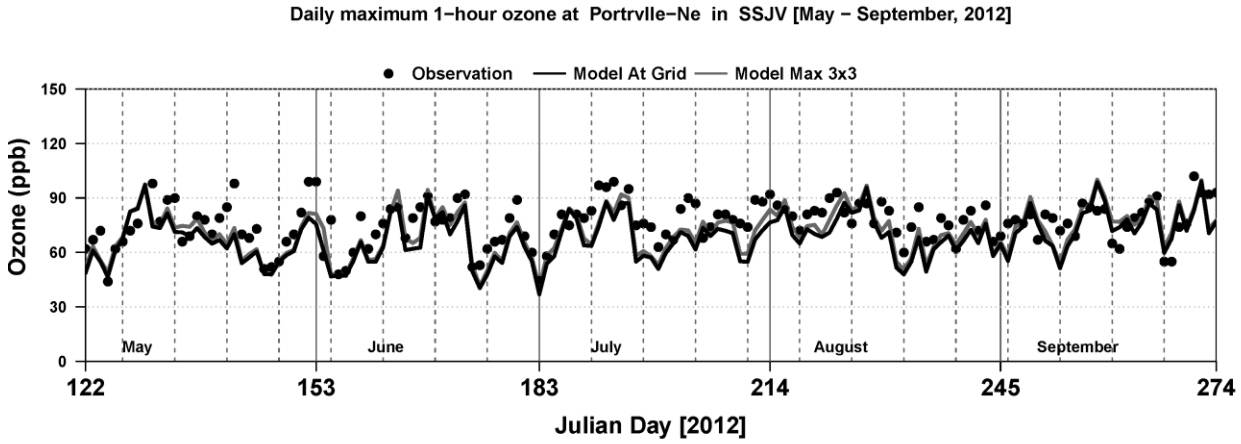

Figure S. 60 Time-series of daily maximum 1-hr ozone at Porterville-1839 Newcomb Street

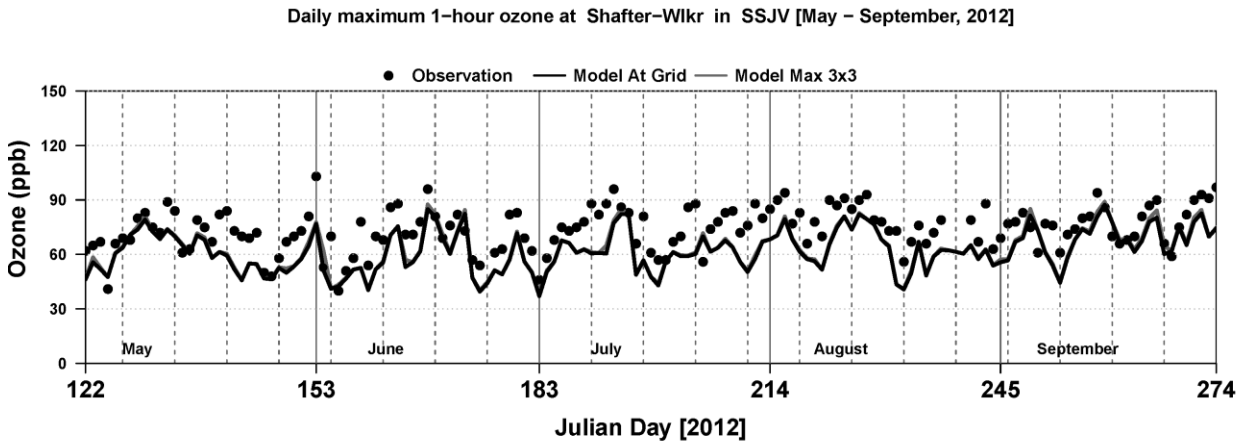

Figure S. 61 Time-series of daily maximum 1-hr ozone at Shafter-Walker Street

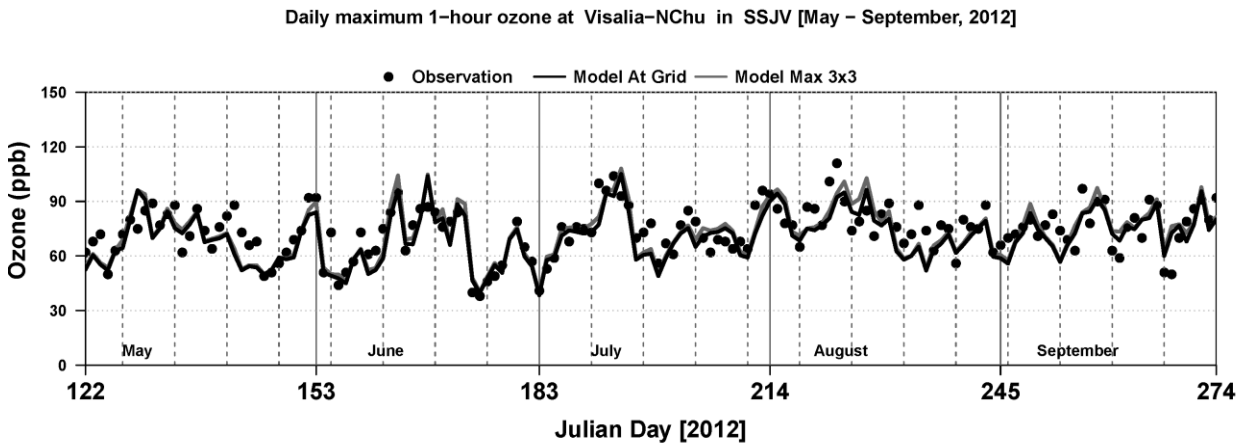

Figure S. 62 Time-series of daily maximum 1-hr ozone at Visalia-N Church Street

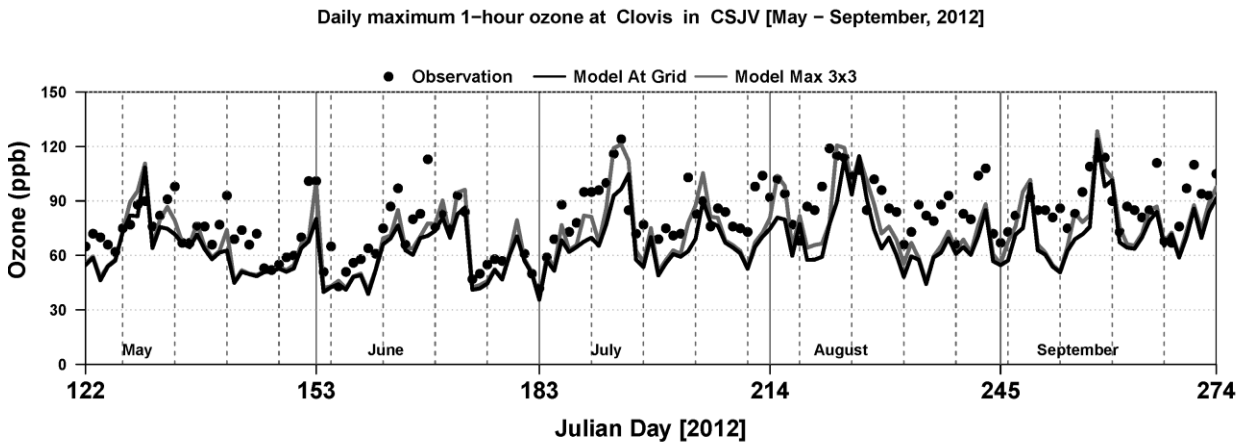

Figure S. 63 Time-series of daily maximum 1-hr ozone at Clovis-N Villa Avenue

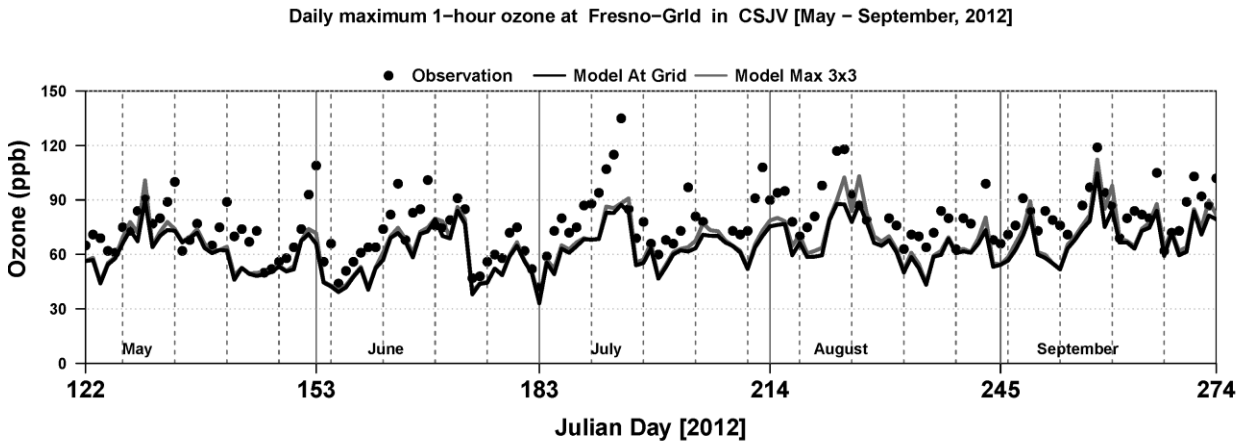

Figure S. 64 Time-series of daily maximum 1-hr ozone at Fresno-Garland

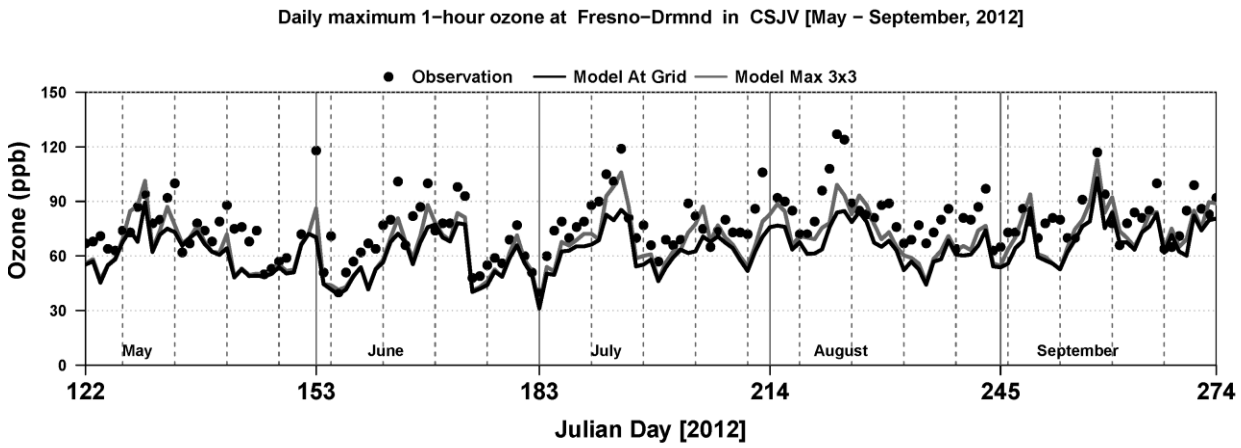

Figure S. 65 Time-series of daily maximum 1-hr ozone at Fresno-Drummond Street

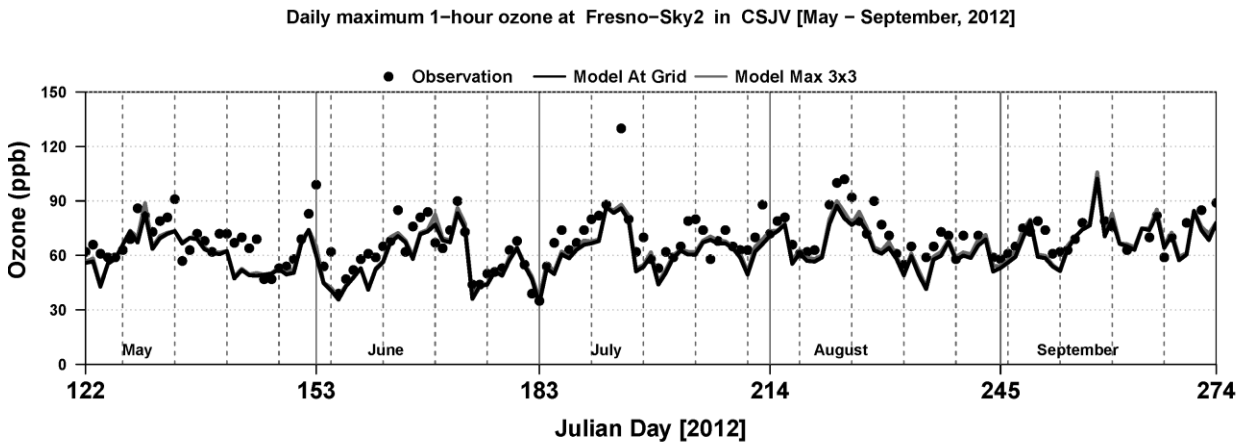

Figure S. 66 Time-series of daily maximum 1-hr ozone at Fresno-Sierra Skypark #2

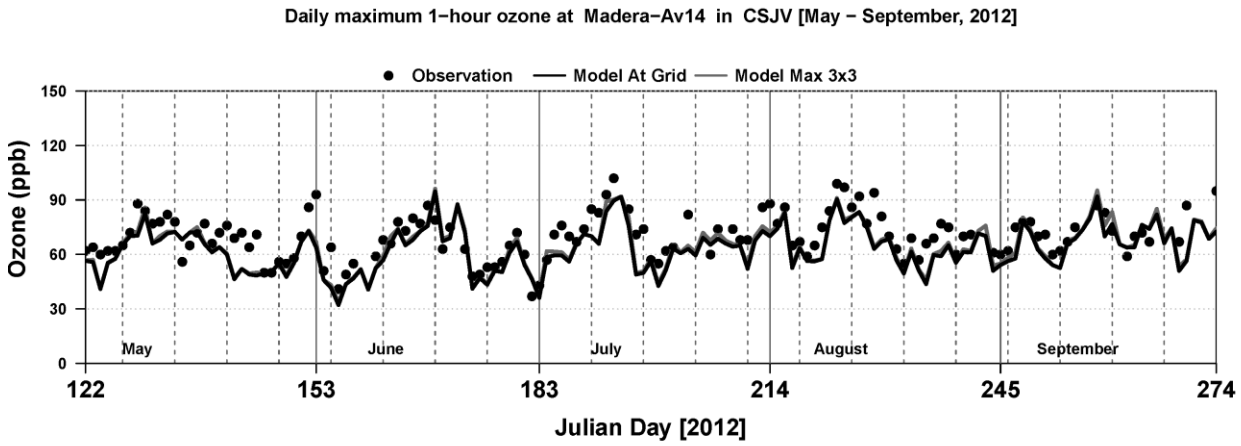

Figure S. 67 Time-series of daily maximum 1-hr ozone at Madera-28261 Avenue 14

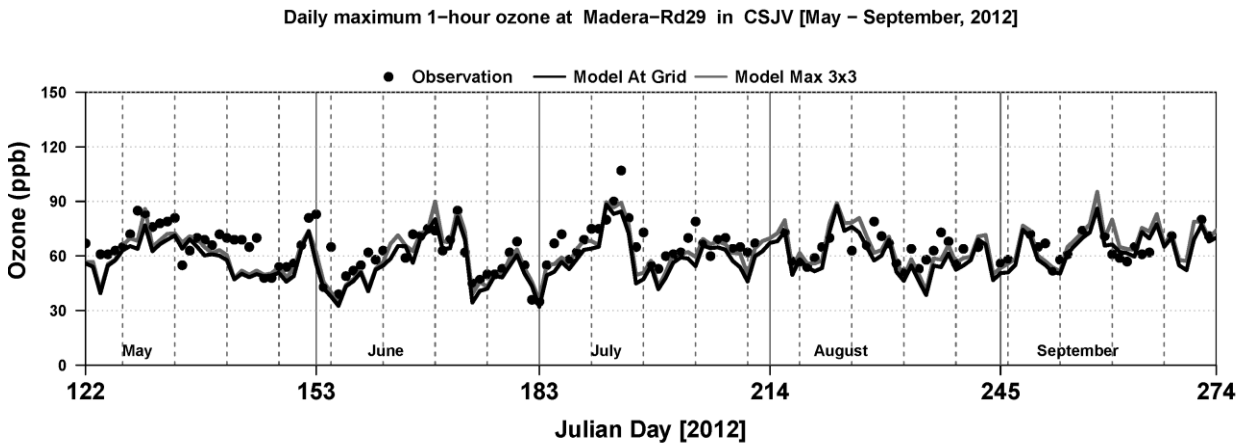

Figure S. 68 Time-series of daily maximum 1-hr ozone at Madera-Pump Yard

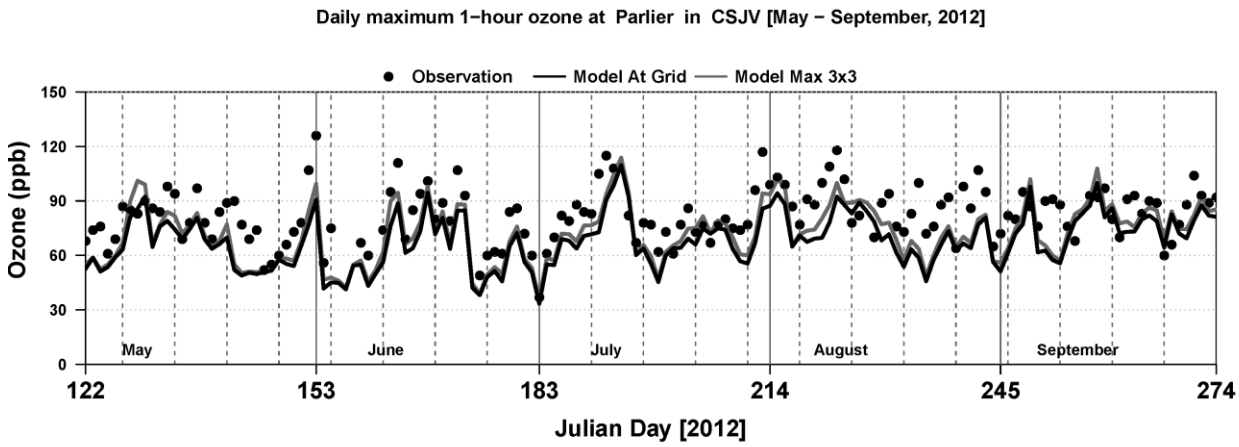

Figure S. 69 Time-series of daily maximum 1-hr ozone at Parlier

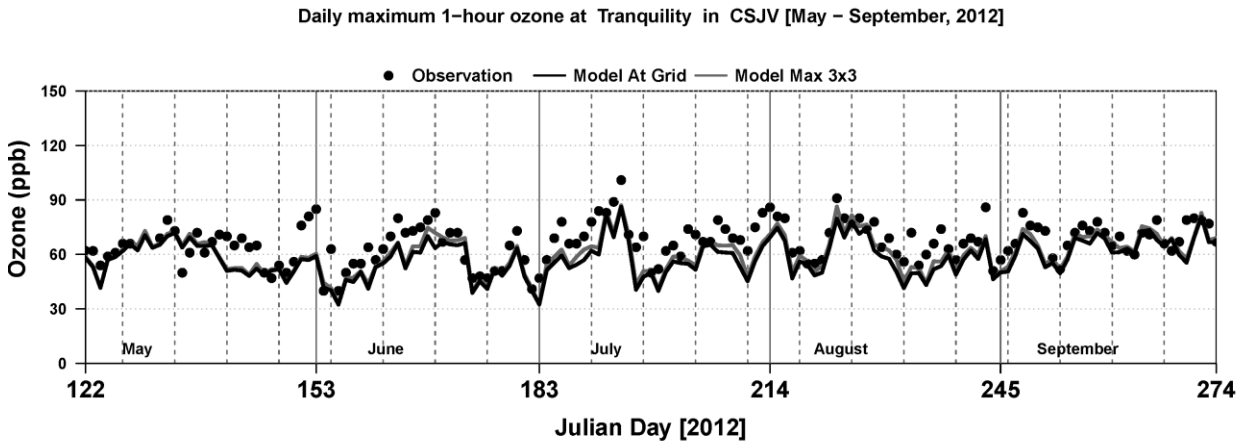

Figure S. 70 Time-series of daily maximum 1-hr ozone at Tranquility-32650 West Adams Avenue

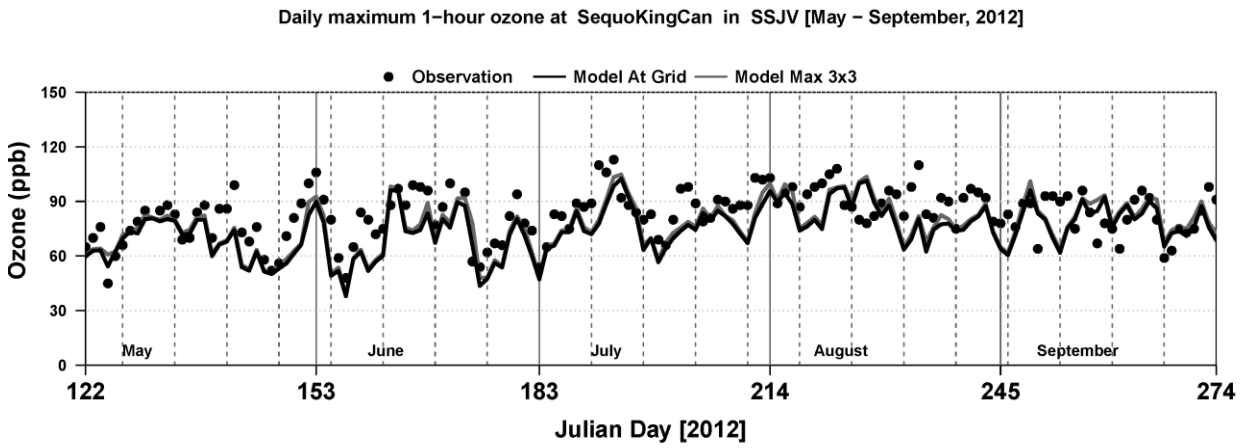

Figure S. 71 Time-series of daily maximum 1-hr ozone at Sequoia and Kings Canyon Natl Park

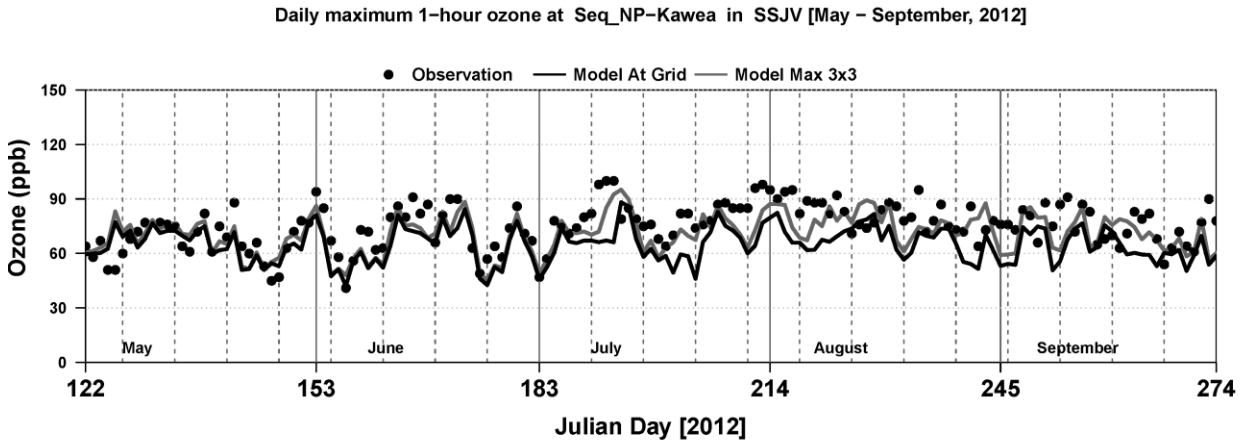

Figure S. 72 Time-series of daily maximum 1-hr ozone at Sequoia Natl Park-Lower Kaweah

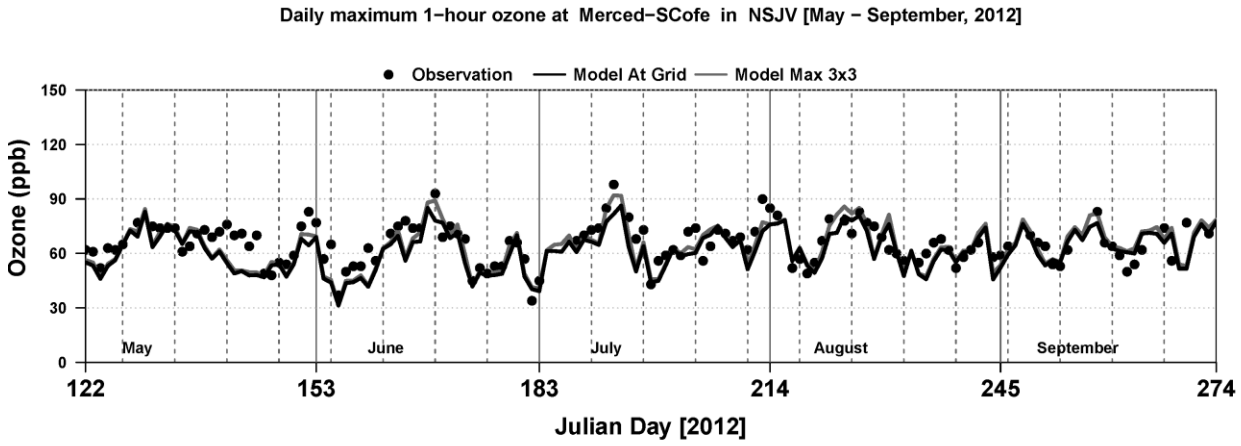

Figure S. 73 Time-series of daily maximum 1-hr ozone at Merced-S Coffee Avenue

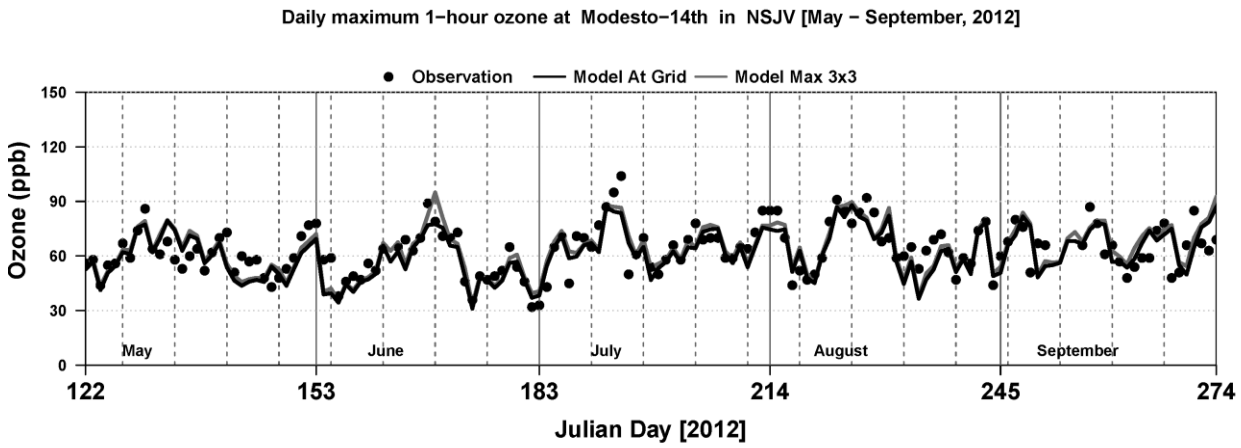

Figure S. 74 Time-series of daily maximum 1-hr ozone at Modesto-14th Street

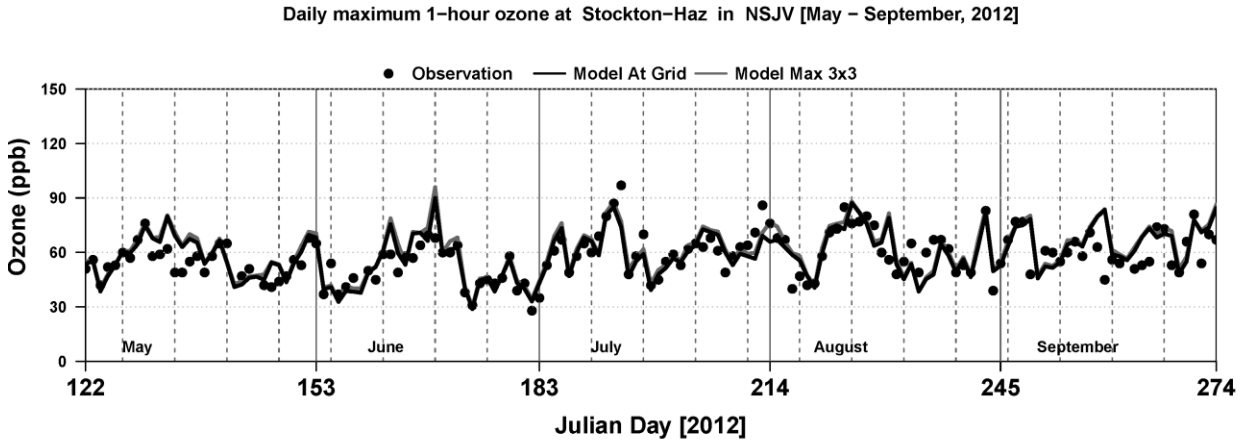

Figure S. 75 Time-series of daily maximum 1-hr ozone at Stockton-Hazelton Street

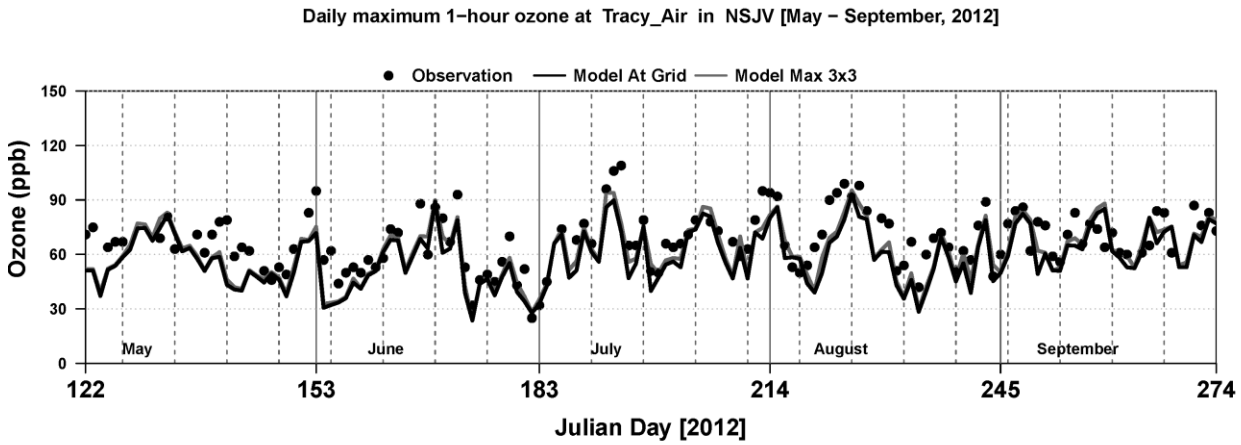

Figure S. 76 Time-series of daily maximum 1-hr ozone at Tracy-Airport

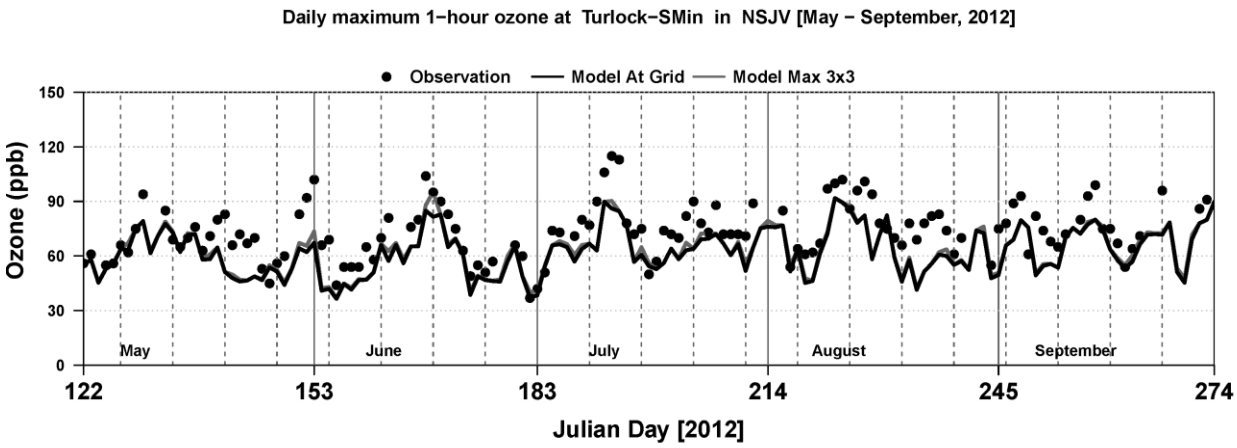

Figure S. 77 Time-series of daily maximum 1-hr ozone at Turlock-S Minaret Street

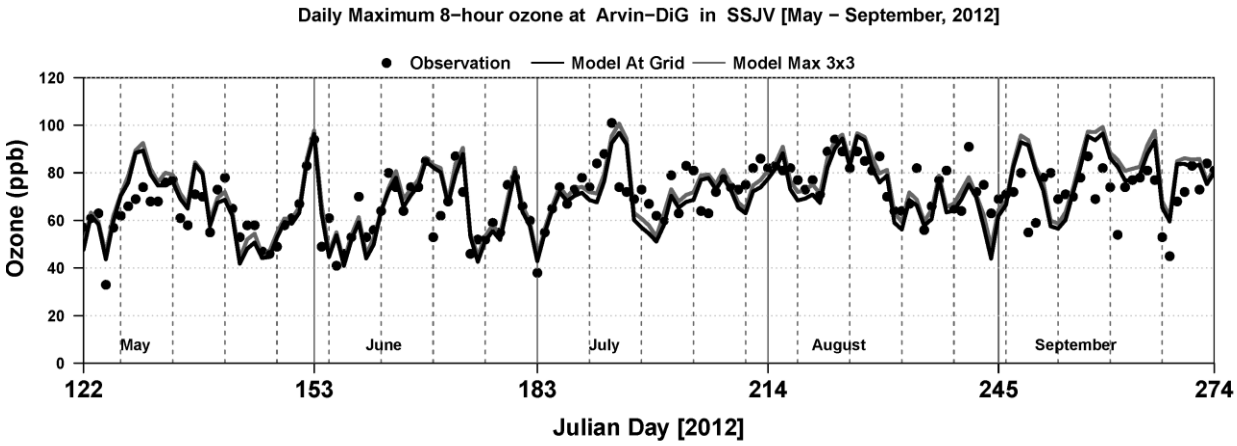

Figure S. 78 Time-series of daily maximum average 8-hr ozone at Arvin-Di Giorgio

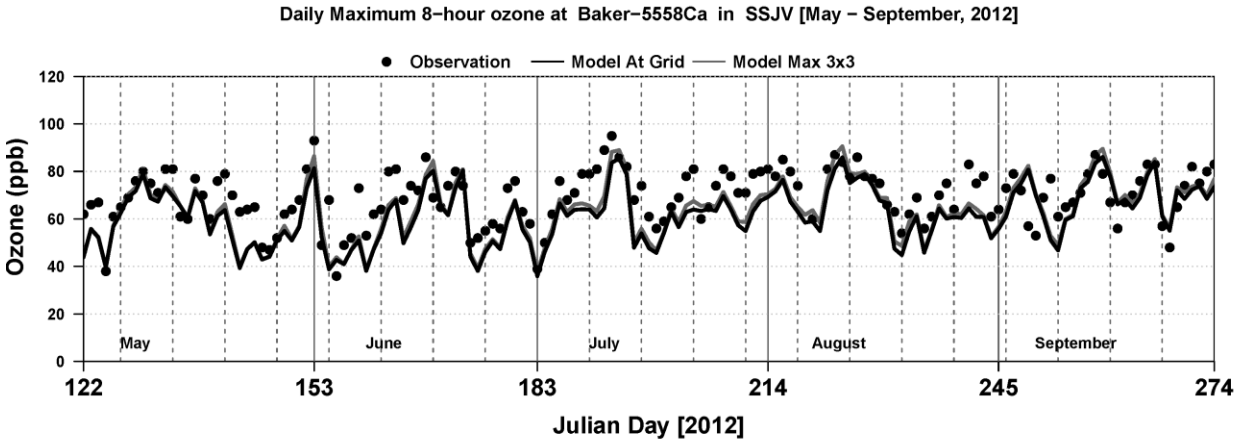

Figure S. 79 Time-series of daily maximum average 8-hr ozone at Bakersfield-5558 California Avenue

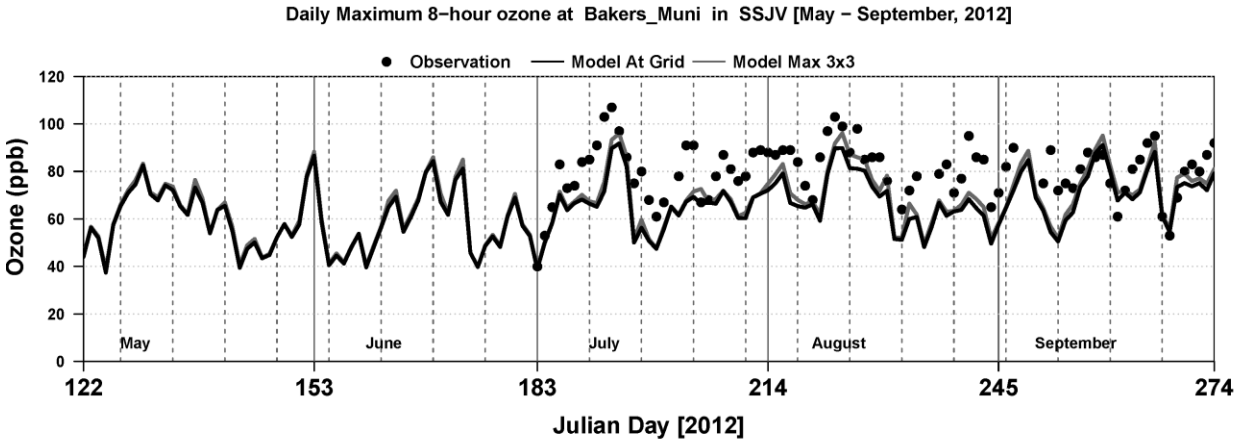

Figure S. 80 Time-series of daily maximum average 8-hr ozone at Bakersfield-Municipal Airport

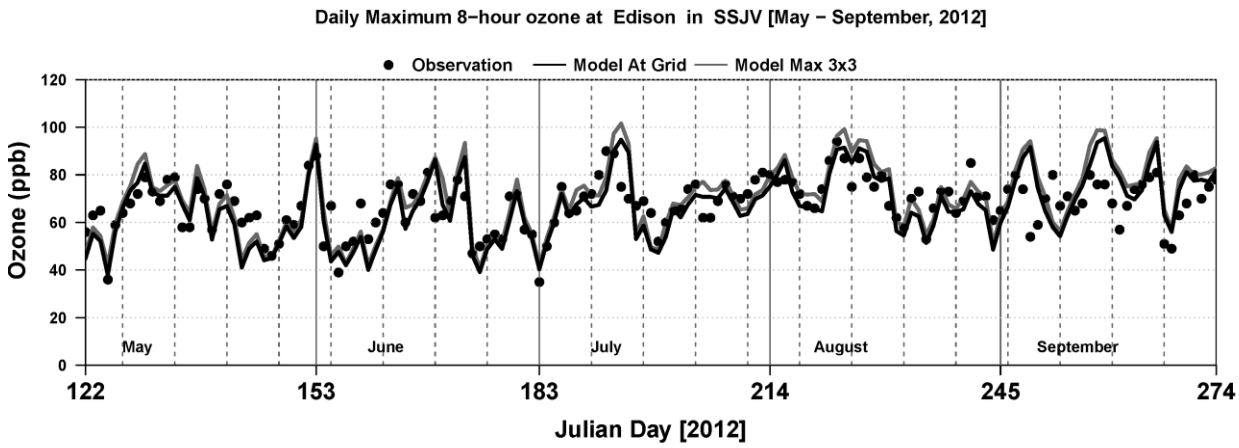

Figure S. 81 Time-series of daily maximum average 8-hr ozone at Edison

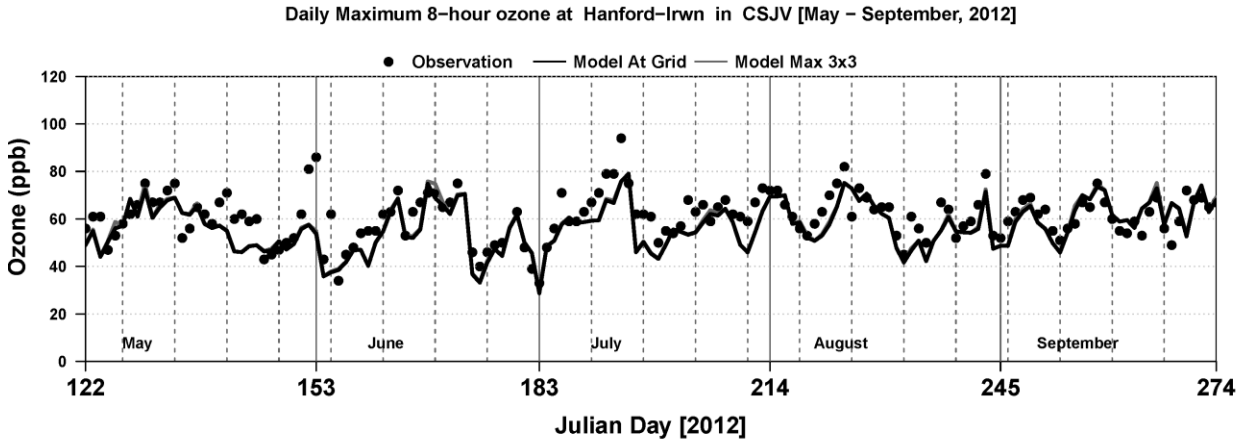

Figure S. 82 Time-series of daily maximum average 8-hr ozone at Hanford-S Irwin Street

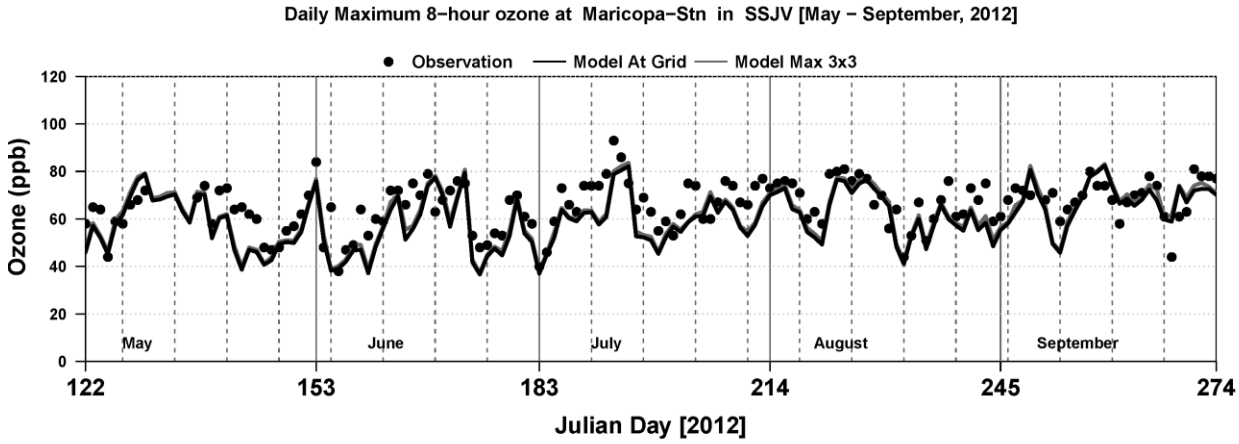

Figure S. 83 Time-series of daily maximum average 8-hr ozone at Maricopa-Stanislaus Street

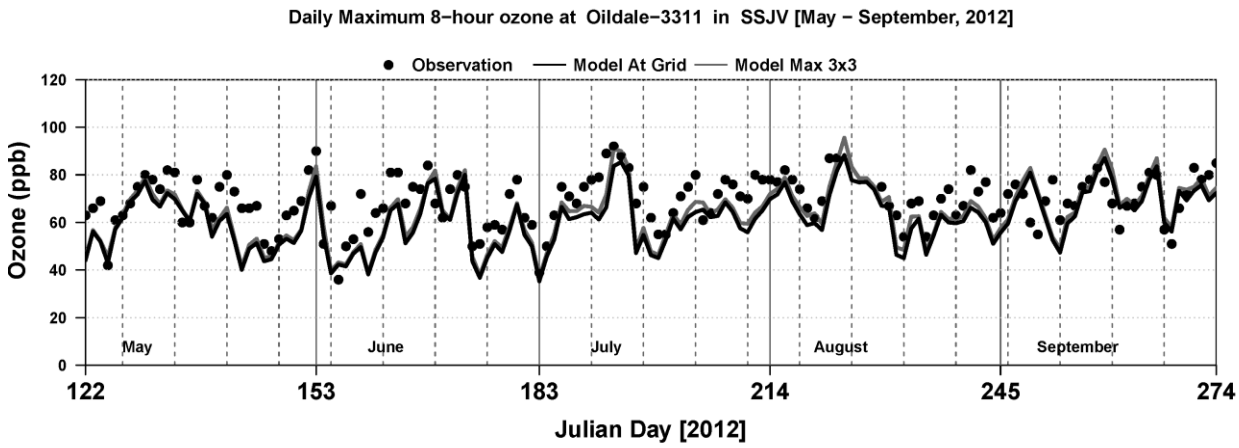

Figure S. 84 Time-series of daily maximum average 8-hr ozone at Oildale-3311 Manor Street

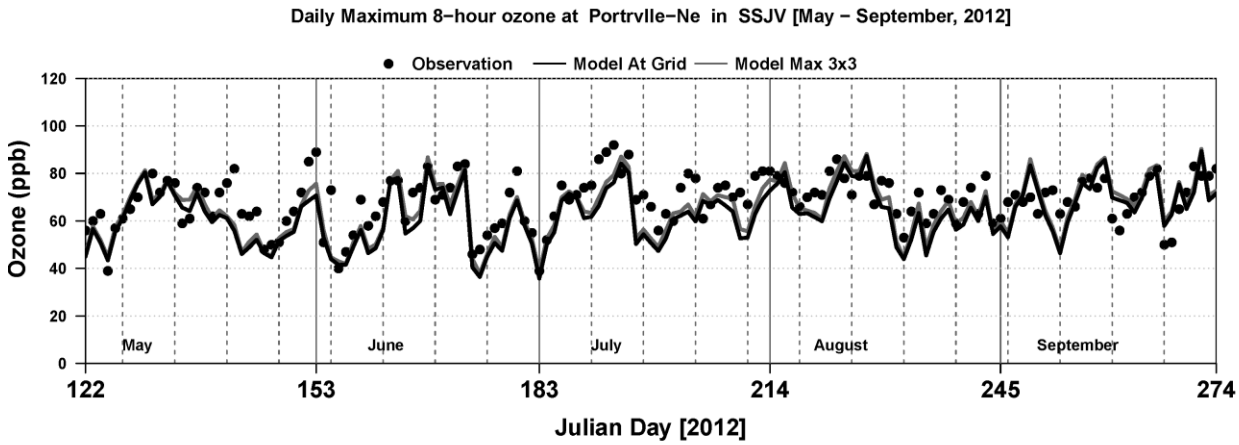

Figure S. 85 Time-series of daily maximum average 8-hr ozone at Porterville-1839 Newcomb Street

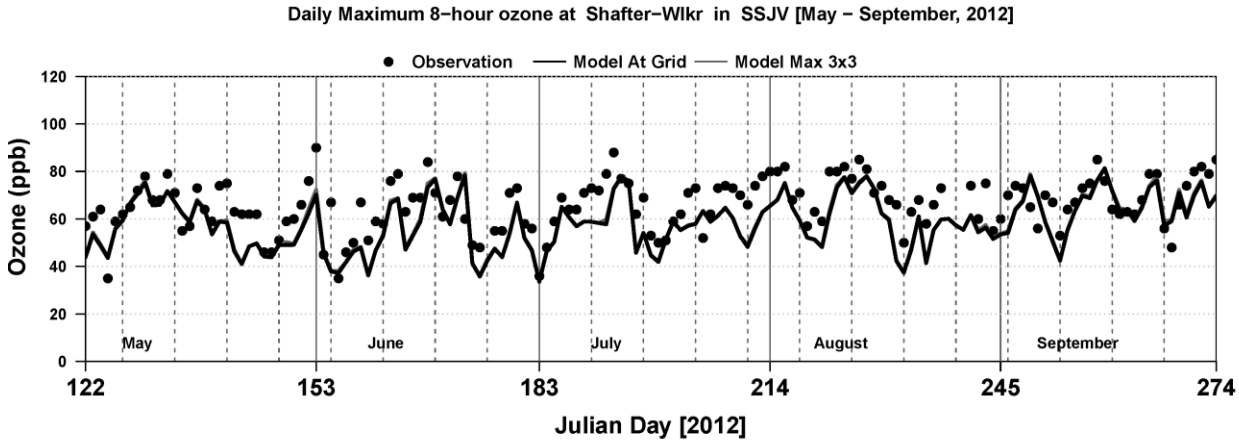

Figure S. 86 Time-series of daily maximum average 8-hr ozone at Shafter-Walker Street

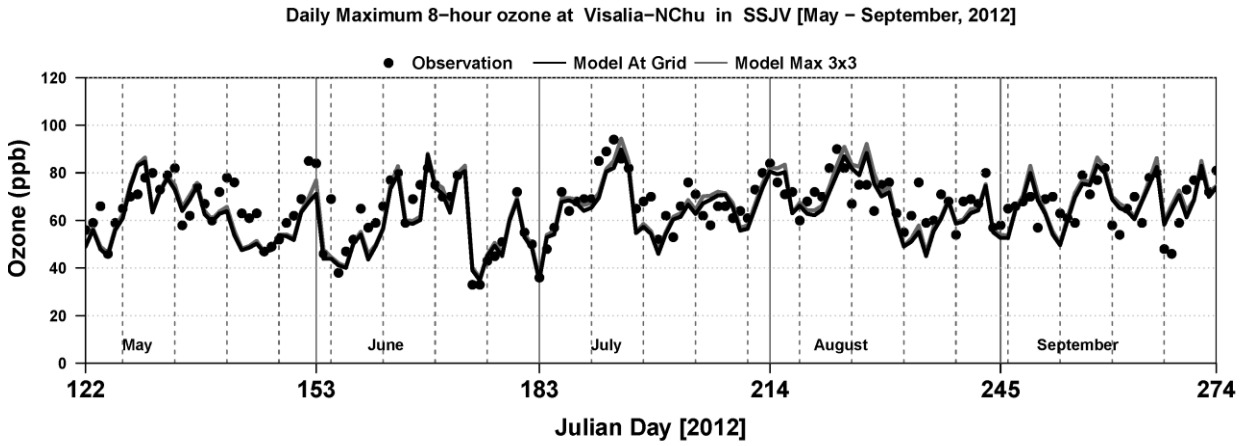

Figure S. 87 Time-series of daily maximum average 8-hr ozone at Visalia-N Church Street

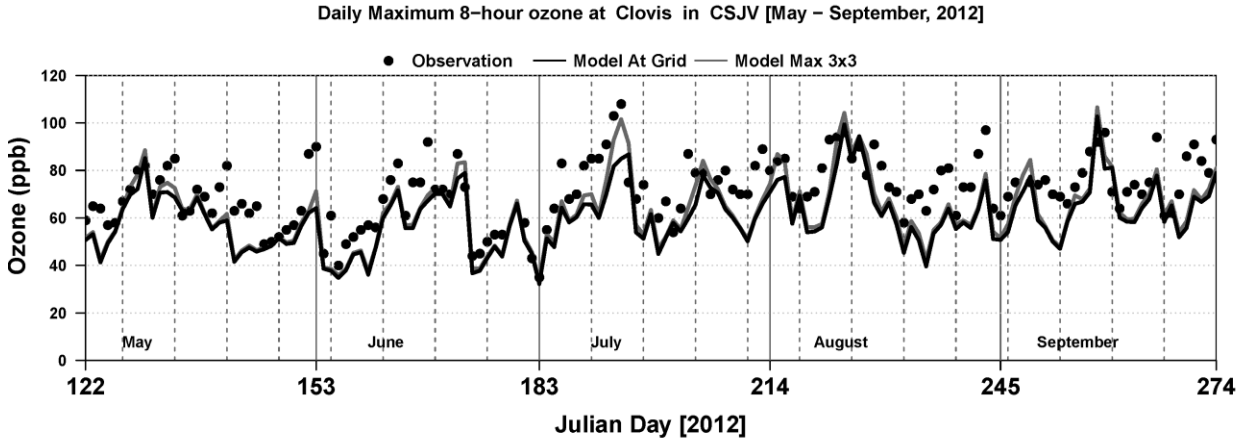

Figure S. 88 Time-series of daily maximum average 8-hr ozone at Clovis-N Villa Avenue

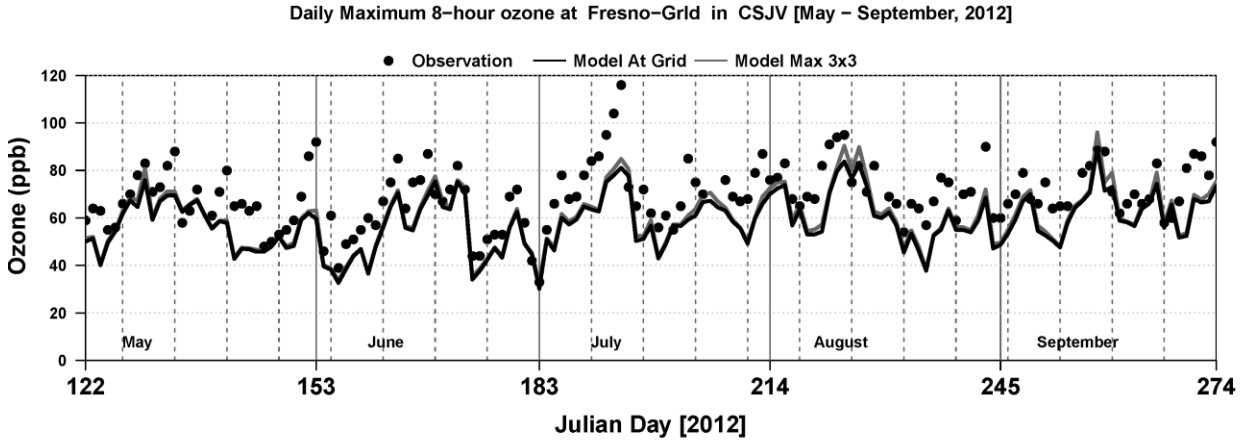

Figure S. 89 Time-series of daily maximum average 8-hr ozone at Fresno-Garland

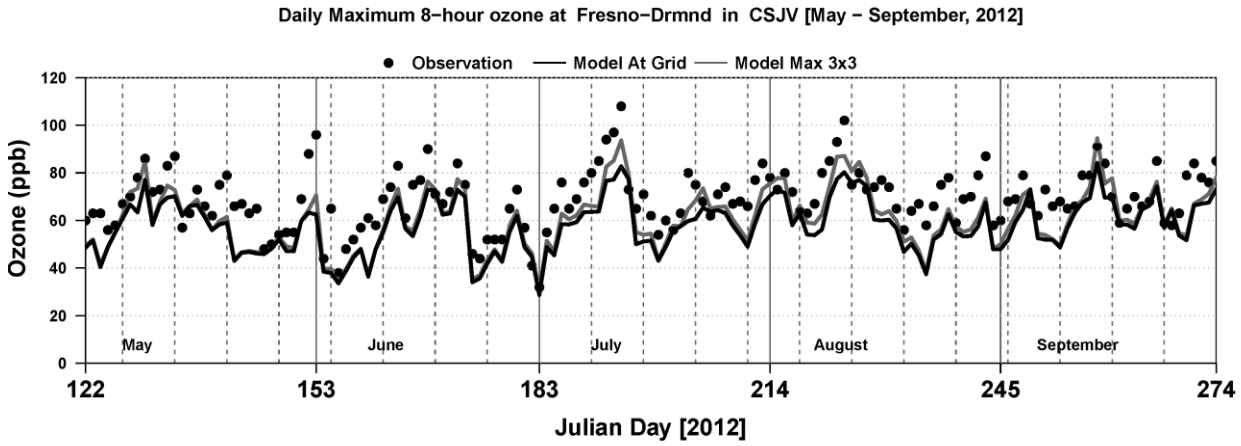

Figure S. 90 Time-series of daily maximum average 8-hr ozone at Fresno-Drummond Street

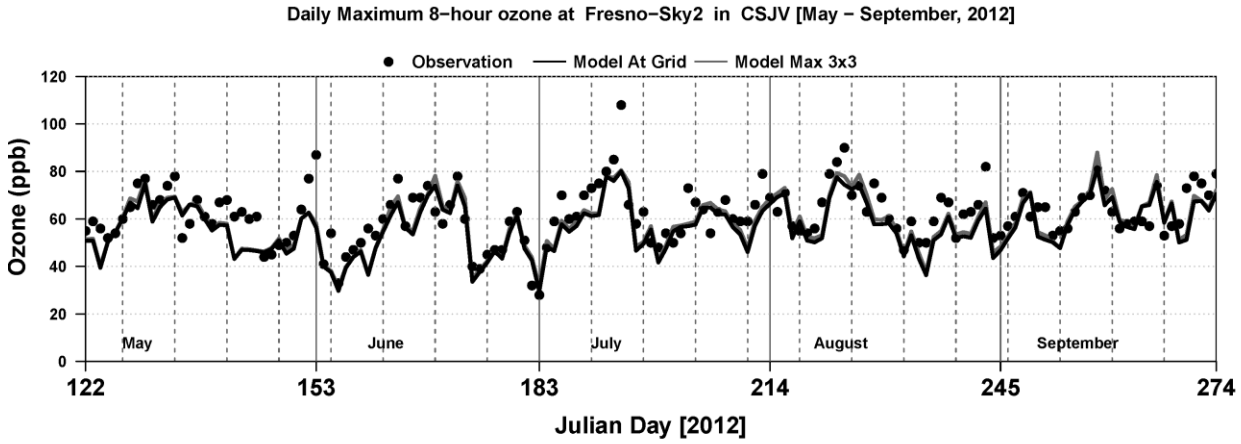

Figure S. 91 Time-series of daily maximum average 8-hr ozone at Fresno-Sierra Skypark #2

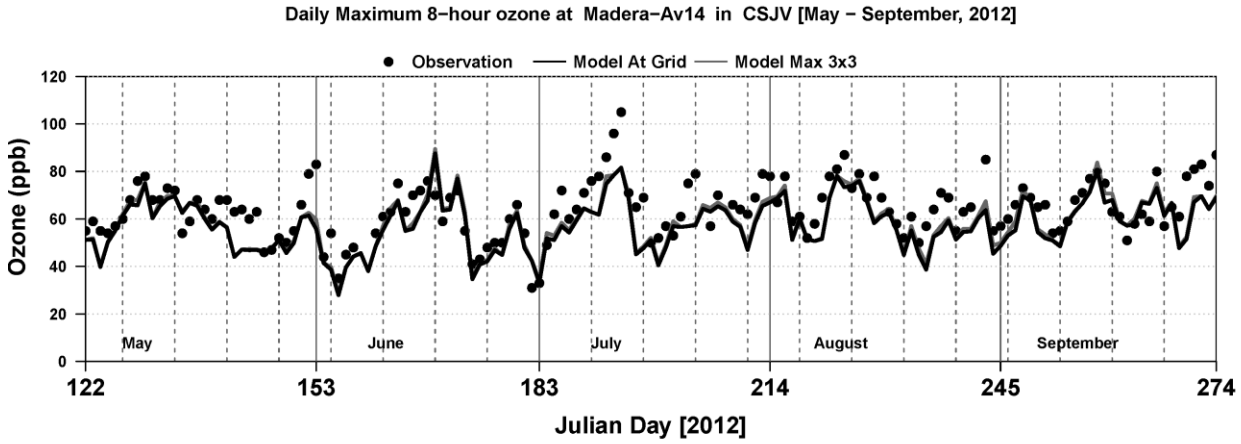

Figure S. 92 Time-series of daily maximum average 8-hr ozone at Madera-28261 Avenue 14

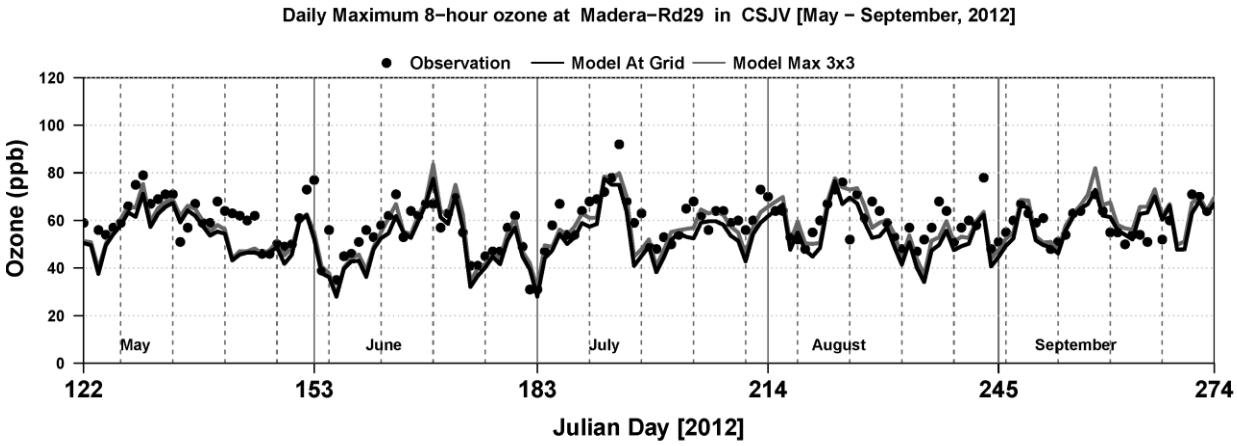

Figure S. 93 Time-series of daily maximum average 8-hr ozone at Madera-Pump Yard

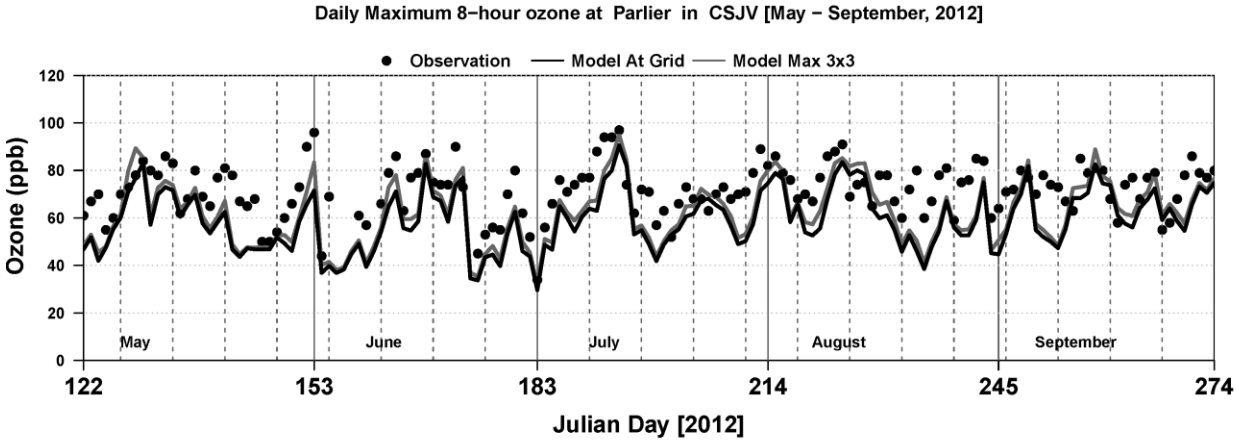

Figure S. 94 Time-series of daily maximum average 8-hr ozone at

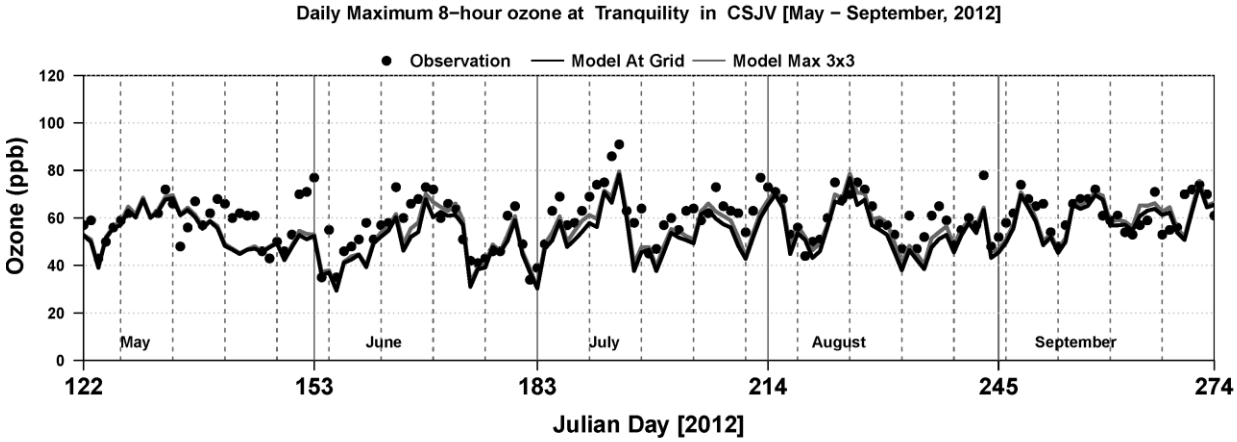

Figure S. 95 Time-series of daily maximum average 8-hr ozone at Parlier

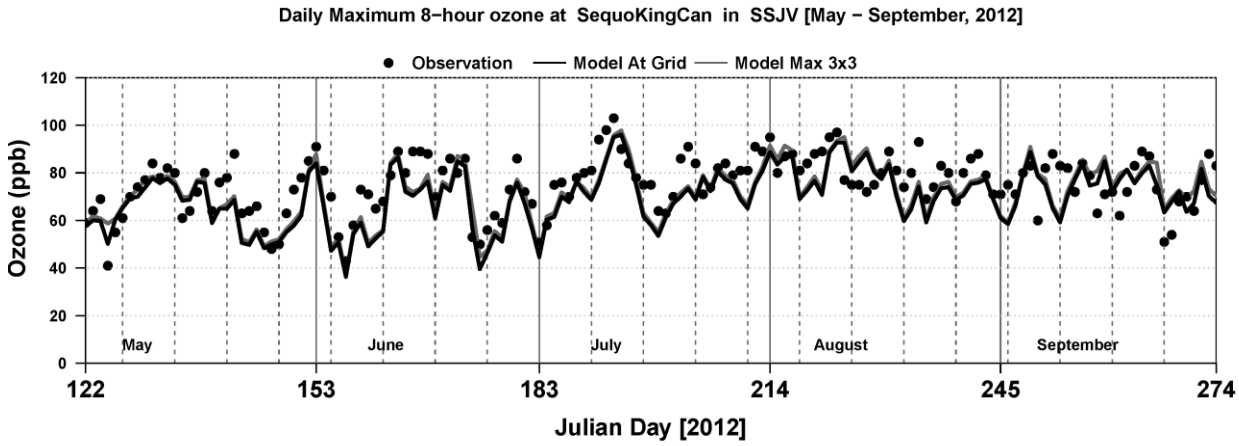

Figure S. 96 Time-series of daily maximum average 8-hr ozone at Sequoia and Kings Canyon Natl Park

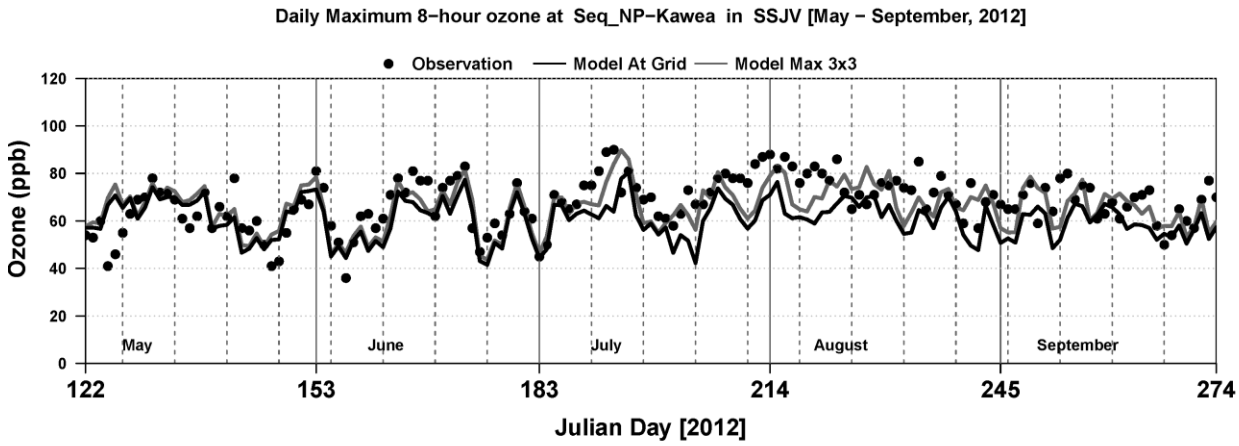

Figure S. 97 Time-series of daily maximum average 8-hr ozone at Sequoia Natl Park-Lower Kaweah

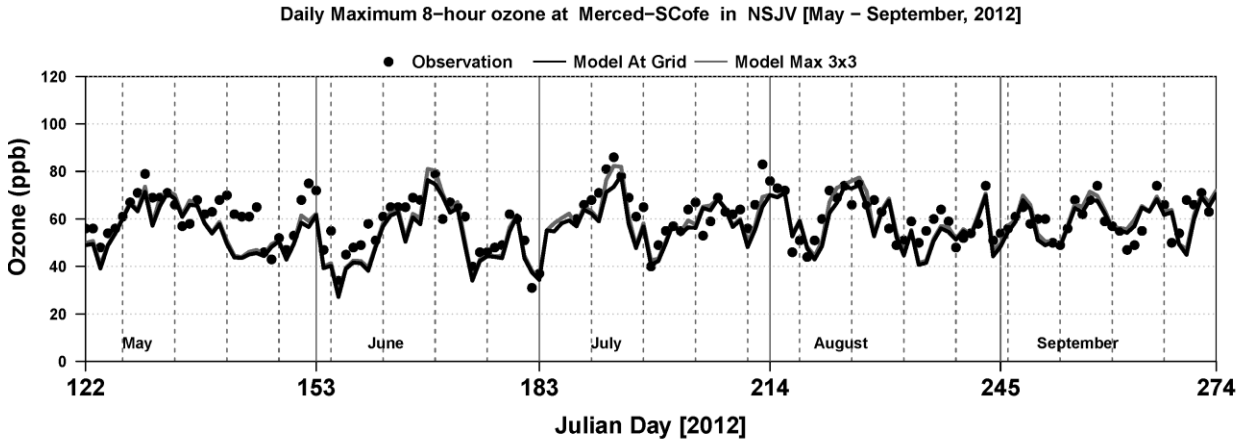

Figure S. 98 Time-series of daily maximum average 8-hr ozone at Merced-S Coffee Avenue

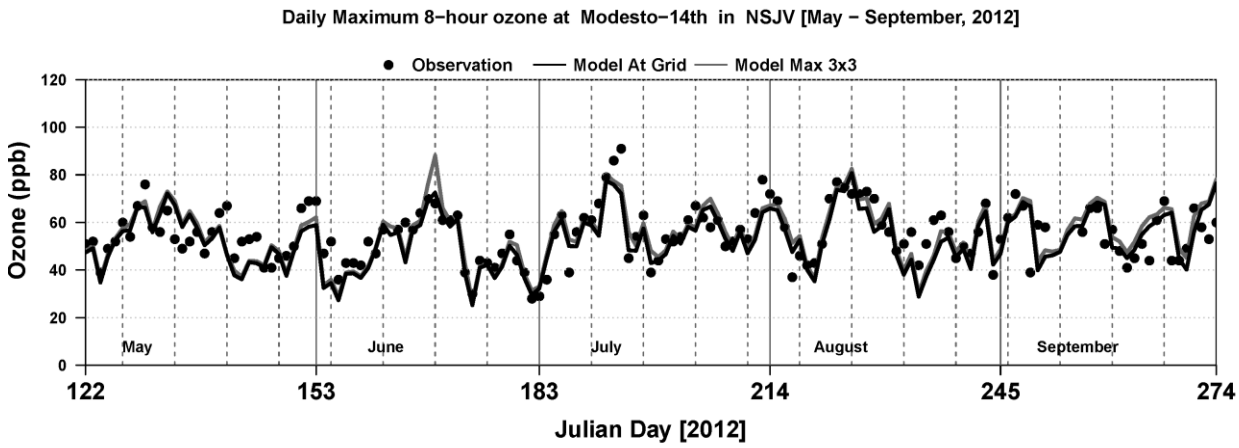

Figure S. 99 Time-series of daily maximum average 8-hr ozone at Modesto-14th Street

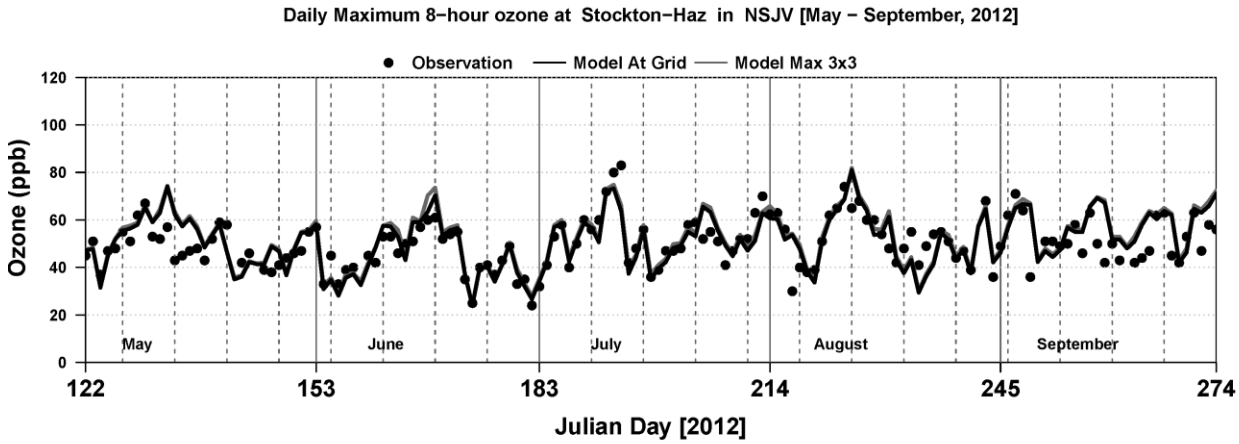

Figure S. 100 Time-series of daily maximum average 8-hr ozone at Stockton-Hazelton Street

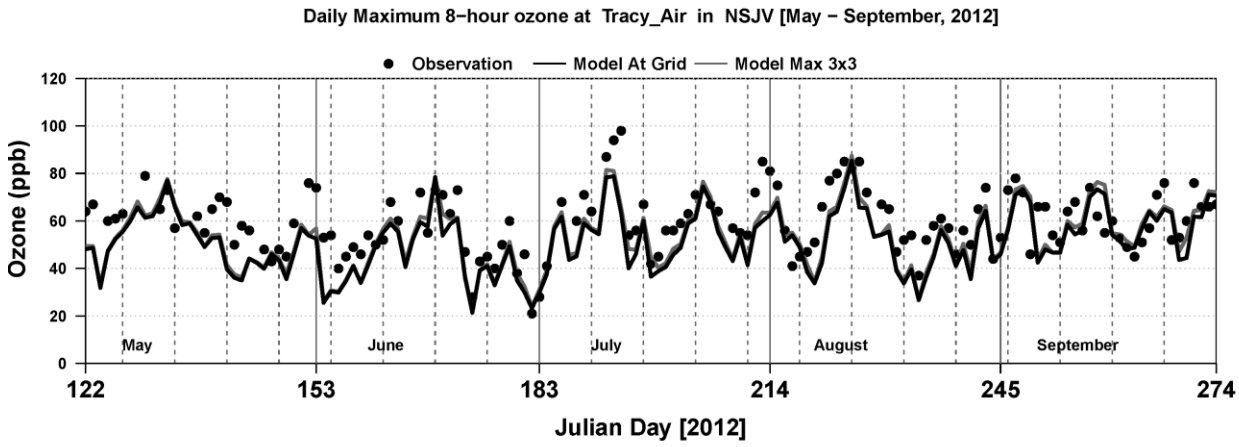

Figure S. 101 Time-series of daily maximum average 8-hr ozone at Tracy-Airport

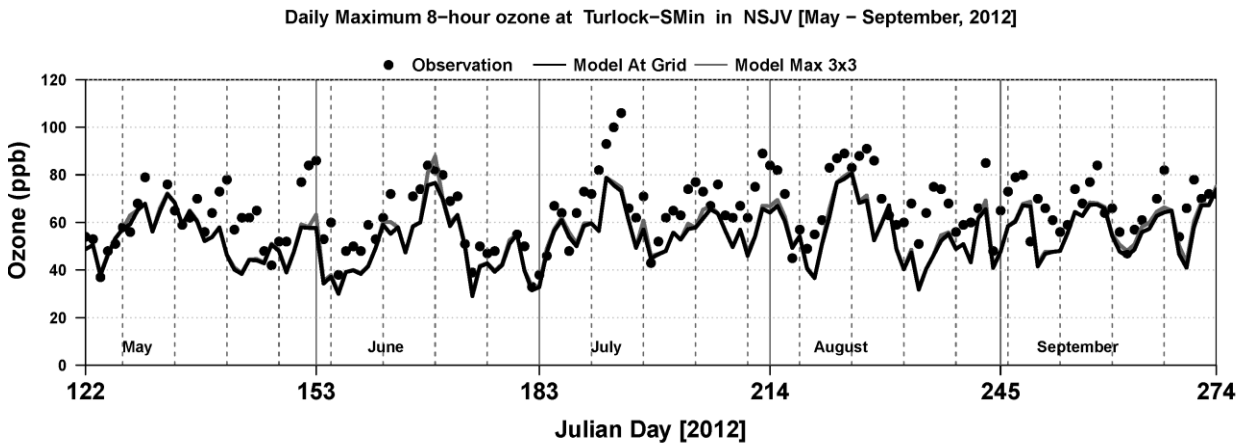

Figure S. 102 Time-series of daily maximum average 8-hr ozone at Turlock-S Minaret Street